Deliverable D3.32
Converter designs based on new components and modular multilevel topologies

Aalborg University (AAU), Denmark

Leibniz University Hannover (LUH), Germany

University of Strathclyde (USTRAT), United Kingdom

Agreement n.:	308974
Duration	November 2012 – October 2017
Co-ordinator:	DTU Wind

The research leading to these results has received funding from the European Community's Seventh Framework Programme FP7-ENERGY-2012-1-2STAGE under grant agreement No. 308974 (INNWIND.EU).

Document information

Document Name:	Converter Designs based on New Components and Modular Multilevel Topologies
Document Number:	Deliverable D 3.32
Author:	Dr. Fujin Deng, Prof. Zhe Chen, Aalborg University (AAU), Denmark, Mr. Dennis Karwatzki, Prof. Dr. –ing Axel Mertens, Leibniz University Hannover (LUH), Germany, Dr. Max Parker, Prof. Stephen Finney, University of Strathclyde (USTRAT), United Kingdom
Document Type	Report
Dissemination level	PU
Review:	Henk Polinder and Asger Bech Abrahamsen
Date:	2014/9/29
WP:	WP 3
Task:	Task 3.3
Approval:	Approved by WP Leader

Preface

This report is prepared for Deliverable D3.32 “Converter Design Based on New Components and Modular Multilevel Topologies” of the Task 3.3 Power Electronics in the WP 3 “Electro-Mechanical Conversion” of EU INNWIND project (FP7 “Innovative Wind Conversion System (10-20 MW) for Offshore Applications”).

The members of Task 3.3 Power Electronics team include:

Dr. Fujin Deng, Prof. Zhe Chen, Aalborg University (AAU), Denmark; Mr Dennis Karwatzki, Prof., Dr. -Ing. Axel Mertens, Leibniz University Hannover (LUH), Germany; Dr. Max Parker, Prof. Stephen Finney, University of Strathclyde (USTRAT), United Kingdom.

The contributions to the project report are made as follows:

- Chapter 1: AAU
- Chapter 2: AAU
- Chapter 3: LUH
- Chapter 4: USTRAT
- Chapter 5: AAU, LUH, and USTRAT

The Task 3.3 Power Electronics team wishes to thank Henk Polinder, Asger Bech Abrahamsen, other WP3 colleagues and partners of EU INNWIND, for their discussions, suggestions and comments, data contributions.

Contents

1 INTRODUCTION

1.1 Introduction

Over the last twenty years, renewable energy sources have been attracting great attention due to the cost increase, limited reserves, and adverse environmental impact of fossil fuels. In the meantime, technological advancements, cost reduction, and governmental incentives have made some renewable energy sources more competitive. Among them, wind energy is one of the fastest growing renewable energy sources [1-1~1-9].

So far, a variety of wind power technologies have been developed, which have improved the conversion efficiency and reduced the costs for wind energy production. The size of wind turbines has increased from a few kilowatts to several megawatts each [1-1~1-3]. The most recent finding of the wind energy development is that the high-power wind turbine provides some key innovations. Larger wind turbines often result in reduced cost since their production, installation, and maintenance costs are lower than the sum of smaller wind turbines achieving the same power output [1-4~1-6]. Today, multi-MW size wind turbines are being developed and installed. The steady growth of installed wind power together with the upscaling of the wind turbine power capability has pushed the research and development of wind turbine systems.

Power electronic converter is an enabling technology for renewable energy power generation system, which is used to convert electrical power from one form into another so as to efficiently match the application characteristics. In the wind turbine system, the power electronic converter is used to provide the connection/conversion between the generator and the grid to achieve high efficiency and meet the grid requirements, including frequency, voltage, active and reactive power, flickers, harmonics, and ride-through capabilities, etc. On the generator side, the ideal conversion system would enable the optimal energy to be captured, reducing the system power loss and stress; on the grid side, it would convert the power into the required frequency and voltage with the desired waveform. Power electronic converters are playing an increasingly significant role in the development of modern wind turbines and wind farms [1-2~1-9].

In recent years, power electronic technology, including semiconductor devices, circuit topologies, modulation, and control methods, has been rapid developed. The performances of the power electronic converters are continuously being improved and more and more power electronics have been incorporated into wind turbine systems to improve wind turbine control and to improve the interconnection to the grid system [1-2], [1-3].

The objective of this report is to evaluate the performance of the various power electronic converters for the 10 MW and 20 MW INNWIND. EU reference wind turbines, respectively. In this report, the power electronics converters will be assessed in view of costs, size, efficiency, reliability, and so on. In addition, the applications of new SiC semiconductors are also considered and the possible impacts are analyzed as well. Finally, the possible power converter configurations for 10 MW and 20 MW wind turbines are preliminarily compared in view of cost, size, efficiency, and reliability. In this preliminary comparison, the related grid code requirements such as reactive power regulation, voltage regulation, etc. are not involved, which has no impact on this report and will be considered in the next delivery report.

1.2 Power Converters

Power converters are widely used in wind energy conversion system. To date, a variety of power converters with different topologies and characteristics are developed for variable-speed wind turbine systems [1-10], [1-11]. Fig. 1-1 illustrates three types of wind energy conversion systems using different power converter configurations. Fig. 1-1(a) shows the wind energy conversion system based on a back-to-back (BTB) voltage source converters (VSCs). Fig. 1-1(b) shows a wind turbine system based diode rectifier, current source, and hybrid VSC-current source

converter (CSC). Fig. 1-1(c) shows a wind turbine system with a VSC AC/AC power electronic converter.

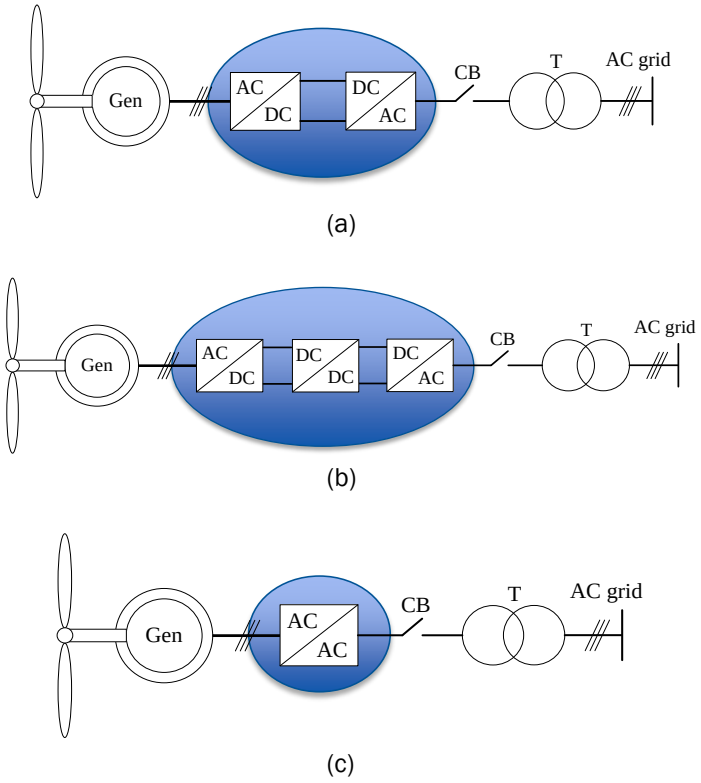

Fig. 1-1. The wind energy conversion system investigated is based on (a) Back-to-back converters. (b) Current source converter. (c) AC/AC converter.

In this report, various power converter topologies for the above three main types of wind energy conversion systems are discussed. These configurations includes two level (2L) configuration, three-level (3L) neutral point clamped (NPC) configuration, modular multilevel converters (MMCs) configurations, diode rectifier and thyristor configurations, etc. Their costs, size, efficiency, reliability, and impacts with new silicon carbide (SiC) semiconductors, etc. are presented for the studied 10 MW and 20 MW wind turbines.

1.3 References

[1-1] B. Wu, Y. Lang, N. Zargari, and S. Kouro, *Power Conversion and Control of Wind Energy System*, Wiley 2011.

[1-2] Z. Chen, "An overview of power electronic converter technology for renewable energy systems," in *Direct-Drive Wind and Marine Energy Systems, Edited by Markus Mueller,* Woodhead Publishing Ltd. 2013

[1-3] Z. Chen, "Power electronic converter systems for direct drive renewable energy applications," in *Direct-Drive Wind and Marine Energy Systems, Edited by Markus Mueller,* Woodhead Publishing Ltd. 2013.

[1-4] Z. Chen, "Advanced Wind Energy Converters Using Electronic Power Conversion," Durham, PhD Thesis, 1997.

[1-5] Z. Chen, E. Spooner, "Grid Interface Options for Variable-Speed, Permanent-Magnet Generators", *IEE Proc. -Electr. Power Applications*, Vol. 145, No. 4, July 1998, pp. 273-283.

[1-6] Z. Chen, E. Spooner, "Grid Power Quality with Variable-Speed Wind Turbines", *IEEE Transactions on Energy Conversion*, Vol. 16, No.2, June 2001, pp. 148-154.

[1-7] Z. Chen, E. Spooner, "Voltage Source Inverters for High-Power, Variable-Voltage DC Power Sources", *IEE Proc. –Generation, Transmission and Distributions*, Vol. 148, No. 5, September 2001, pp. 439-447.

[1-8] Z. Chen, E. Spooner, "Current Source Thyristor Inverter And Its Active Compensation System," *IEE Proc. –Generation, Transmission and Distributions*, Vol. 150, No. 4, July 2003, pp. 447-454.

[1-9] Z. Chen, "Compensation Schemes for A SCR Converter in Variable Speed Wind Power Systems," *IEEE Transactions on Power Delivery*, Vol. 19, No 2, April 2004, pp. 813-821.

[1-10] Z. Chen. "An introduction of power electronic technology", in *Direct-Drive Wind and Marine Energy Systems, Edited by Markus Mueller,* Woodhead Publishing Ltd. 2013.

[1-11] Z. Chen. "Power electronic converter systems for direct drive renewable energy applications," in *Direct-Drive Wind and Marine Energy Systems, Edited by Markus Mueller,* Woodhead Publishing Ltd. 2013.

2 BACK-TO-BACK VOLTAGE SOUSRCE CONVERTERS

2.1 Introduction

This chapter mainly investigates power converters for six sets of 10 and 20 MW wind turbine conditions as shown in Table 2-1. For the 10 MW and 20 MW power converters, the ac line-to-line voltage V_{ll} is 3.3 kV and 6.6 kV respectively, which results in the same ac current peak value I_m as 2.47 kA. The same voltage is used for both generator and grid side, the grid-side frequency of the power converter is 50 Hz because the power converter is connected to the grid with the frequency of 50 Hz. The frequencies at the generator side of the power converter are considered as 2.5 Hz, 25 Hz, and 50 Hz, respectively, where the nominal electric frequency of 2.5 Hz represents a superconducting direct drive generator in wind turbine systems and 50 Hz represents a pseudo direct drive generator in wind turbine systems.

Table 2-1
Investigated Power Converters

Converter capacity P_n (MW)	AC voltage V_{ll} (kV)	AC current peak value I_m (kA)	Generator-side nominal AC frequency (Hz)	Grid-side nominal AC frequency (Hz)
10	3.3	2.47	2.5	50
20	6.6			
10	3.3		25	
20	6.6			
10	3.3		50	
20	6.6			

Fig. 2-1 shows the studied back-to-back (BTB) voltage source converters (VSCs) configurations for wind turbine systems.

Fig. 2-1(a) shows the block diagram of a wind energy conversion system based on two-level VSCs, which has been widely used in wind power industry. The two-level VSC is composed of six switches, and the voltage applied on each switch is the dc-link voltage [2-1].

Fig. 2-1(b) shows the block diagram of a wind energy conversion system based on 3-level (3L) neutral point clamped (NPC) converters. The three-level NPC converter is composed with 12 switches, and the voltage applied on each switch is only half of the dc-link voltage. The three-level NPC converter is widely used for medium-voltage applications. In comparison with two-level VSC, the three-level NPC converter has lower *dv/dt* and smaller total harmonic distortion (THD) in its ac output voltages under the same switching frequency [2-1].

Fig. 2-1(c) shows the block diagram of a wind energy conversion system based on a configuration with parallel 3-level (P3L) converters, where a few converters are connected in parallel for one wind turbine. The rating of each converter can be a fraction of the power rating of the wind turbine. In addition, the paralleled converter system may also improve the system reliability [2-1].

Fig. 2-1(d) shows the block diagram of a wind energy conversion system based on a modular multilevel converter (MMC). The MMC becomes attractive in recent year for high-power and high-voltage applications. The MMC consists of a number of series-connected submodule (SM) converters, it can be used for high-voltage level and produce small THD in its ac output voltage. Each SM can be built with a small voltage rating, and the low-voltage level power semiconductor can then be used for the high voltage and high power system. In addition, the series-connected

arm inductor in each arm can limit the current and protect the system during short-circuit faults [2-2~2-5].

From Fig. 2-1, it can be seen that the BTB power converter is composed with the generator-side converter and the grid-side converter. The generator is connected to the grid via the BTB power converter and a transformer. Normally, the generator-side converter is used to control the generator for optimal power capture and the grid-side converter is used to keep the dc-link voltage constant. In order to reduce the current THD at the generator and grid side, the filter is also equipped.

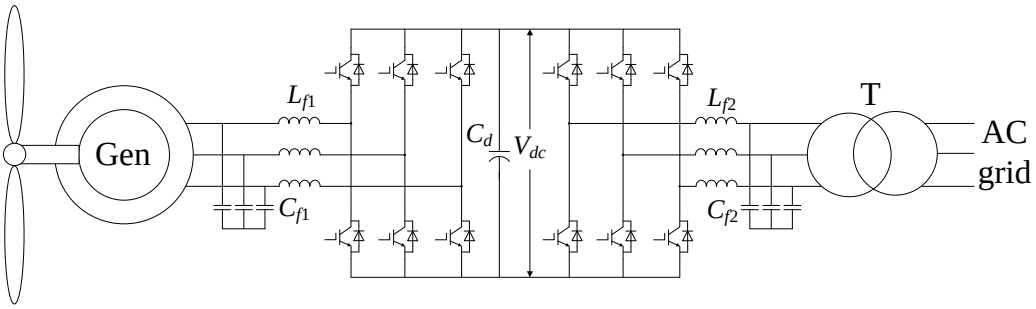

(a)

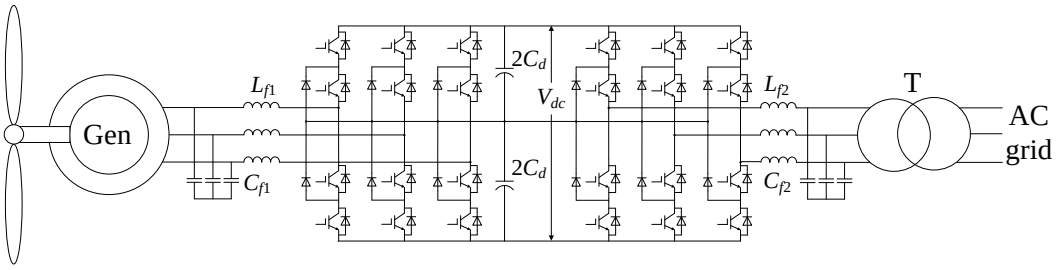

(b)

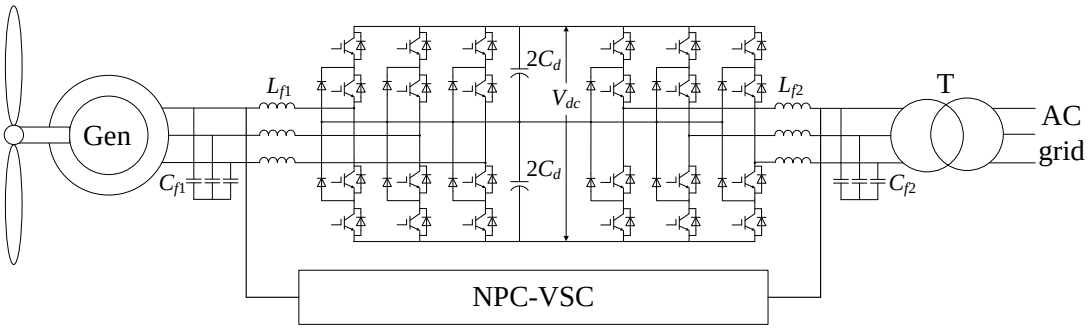

(c)

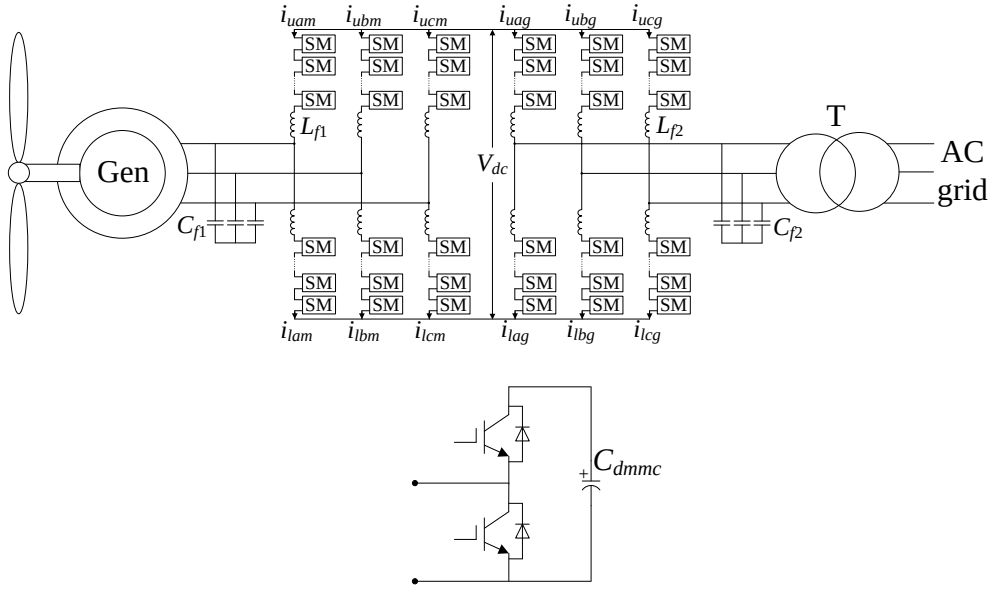

(d)

Fig. 2-1. Wind energy conversion system based on (a) 2-level voltage source converters. (b) 3-level (3L) neutral point clamped (NPC) converters. (c) Parallel 3-level (P3L) NPC converters. (d) Modular multilevel converters (MMCs).

The 2L power converter is widely used for low-voltage (e.g. 690 V) wind turbine system [2-1]. In this report, the ac voltage of the power converter is medium voltages of 3.3 and 6.6 kV, because using a low voltagw would cause unrealistic high current ratings. Thus the 2L configuration is not suitable for the medium voltage power converter and is not considered in this report any further. The 3L, P3L, and MMCs-based power converters are suitable for the medium voltage power converter configurations, which are mainly considered in this report. Therefore, the mainly investigated power converters in this chapter are listed below

Table 2-2
Investigated Power Converter Configurations

Generator-side rated frequency (Hz)	Rated power (MW)	Converter configuration
2.5	10	3L
		P3L
		MMC
	20	3L
		P3L
		MMC
25	10	3L
		P3L
		MMC
	20	3L
		P3L
		MMC
50	10	3L
		P3L
		MMC

	20	3L
		P3L
		MMC

This chapter investigates the above various power converter configurations in view of costs, size, efficiency, and reliability for applications in 2.5, 25 & 50 Hz - 10 & 20 MW wind turbine systems.

2.2 Costs

The main costs of the power converters include:

- Semiconductors Costs
- Passive components (inductor & capacitor) Costs
- Cooling Systems Costs
- Mechanical Systems Costs

The costs of the power converter for 2.5, 25 & 50 Hz - 10 & 20 MW wind turbine systems are investigated below.

2.2.1 Semiconductors Costs

Tables 2-3 lists the semiconductor costs for the power converters in the 2.5, 25 & 50 Hz - 10 & 20 MW wind turbine systems, where the different power converter configurations including 3L, P3L, and MMCs are considered.

According to [2-6], the dc-link voltage of the BTB converters can be designed as

$$V_{dc} = V_{ll} \times \sqrt{2} \times 1.15$$

As to the 10 and 20 MW power converters, their ac voltages V_{ll} are 3.3 and 6.6 kV, respectively. Hence, the dc-link voltages of the 10 and 20 MW power converters can be designed as 5.4 and 10.8 kV, respectively. Each switch in the 3L and P3L configuration takes half of the dc-link voltage.

According to [2-6], in the 3L and P3L configurations, the required peak repetitive voltage rating for each switch/diode and clamping diode is

$$V_v = \frac{V_{dc}}{2} \times 1.6$$

Hence, the preferred repetitive blocking voltage for each switch in the 3L and P3L configurations can be calculated as 4.5 kV and 9 kV in the 10 MW and 20 MW systems, respectively.

In the 10 MW and 20 MW 3L configurations, the switch current is the same to the ac current, which is 2.47 kA. In the 10 MW and 20 MW P3L configurations composed of two 3L converters connected in parallel, the switch current is half of the ac current, which is 1.23 kA. In order to protect the switch, a 2.5 times margin of the RMS current is selected. As a consequence, the required current peak for each switch in the 10 and 20 MW - 3L configuration is 4.45 kA and the required current peak for each switch in the 10 and 20 MW - P3L configuration is 2.22 kA.

In this report, suppose the 1700 V Infineon semiconductors are used to construct the different configurations for the cost comparisons. Based on the required voltage and current for

each switch shown in Table 2-3, the IGBT/Diode module FZ2400R17HP4 1700V/2400A connected in parallel/series is used for the switch 3L and P3L configuration, the Diode DZ800S17K3 1700V/800A connected in parallel/series is used for the clamping diode in the 3L and P3L configurations. In the 3L and P3L configurations shown in Fig. 2-1, the required IGBT/Diode and clamped Diode number is

$$n_{igbt} = ceil(\frac{V_v}{1700}) \cdot ceil(\frac{I_{swm}}{2400}) \cdot 24$$
$$n_{cdiode} = ceil(\frac{V_v}{1700}) \cdot ceil(\frac{I_{swm}}{800}) \cdot 12$$

where V_v and I_{swm} is the required peak repetitive voltage rating and required current peak for each semiconductor such as the IGBT and the Diode, respectively.

Owing to the multiple module configuration of the MMCs, the dc-link voltage V_{smdc} in each SM can be reduced to a small value as

$$V_{smdc} = \frac{V_{dc}}{n}$$

where V_{dc} is the dc-link voltage of the BTB converter and n is the SM number in each arm of the MMCs. As to the 5.4 and 10.8 kV dc-link voltage V_{dc}, the number of SM can be selected as 6 and 12 per arm, where the preferred repetitive blocking voltage of each switch is 1700 V. Suppose that the circulating current is eliminated in the MMC, the arm current peak value can be calculated as [2-2~2-5]

$$I_{armm} = I_m + \frac{P_n}{3V_{dc}}$$

In order to protect the MMCs configurations, the required switch current is set with 2.5 times of the RMS current. Therefore, the required switch current is 5.56 kA for both of the 10 and 20 MW MMC configurations.

In this report, the IGBT/Diode module FZ1800R17HP4 1700V/1800A connected in parallel/series is used for the switch in the MMC configurations. From Fig. 2-1, the required IGBT/Diode number for the 10 and 20 MW MMC configurations, respectively, is

$$n_{igbt\_10mw} = ceil(\frac{V_{smdc}}{1700}) \cdot ceil(\frac{I_{armm}}{1800}) \cdot 144$$

$$n_{igbt\_20mw} = ceil(\frac{V_{smdc}}{1700}) \cdot ceil(\frac{I_{armm}}{1800}) \cdot 288$$

From Table 2-3, it can be seen that the semiconductor number of the 3L and P3L configuration is the same in the 10 and 20 MW systems, respectively, and the semiconductor number of the 20 MW - 3L and P3L configurations is double of that in the 10 MW - 3L and P3L configurations. The cost of the Infineon semiconductors are listed in Table 2-4 as well, from which the total cost of the semiconductors can be calculated, as shown in Table 2-3. Fig. 2-2 shows the total semiconductor costs for the studied 10 and 20 MW configurations. It can be seen that in both the 10 and 20 MW systems, the 2L and P3L configuration have the same semiconductor costs, which is a little lower than MMCs-based configurations. In addition, the semiconductor costs of the 20 MW systems are double of the 10 MW systems.

Table 2-3
Costs of Semiconductors

Wind turbine power (MW)		10			20		
Converter configuration		3L	P3L	MMC	3L	P3L	MMC
AC voltage (kV)		3.3			6.6		
AC current peak value (kA)		2.47					
Generator-side AC frequency (Hz)		2.5, 25 & 50					
Grid-side AC frequency (Hz)		50					
DC-link voltage V_{dc} (kV)		5.4			10.8		
Switch	Switch voltage (kV)	2.7		0.96	5.4		0.96
	preferred repetitive blocking voltage (kV)	4.5		1.7	9		1.7
	Switch current peak (kA)	2.47	1.23	3.09	2.47	1.23	3.09
	Switch current peak value with 2.5 times RMS margin (kA)	4.4	2.2	5.5	4.4	2.2	5.5
	Switch type	FZ2400R17HP4		FZ1800 R17HP4	FZ2400R17HP4		FZ1800 R17HP4
IGBT/DIODE number		144		432	288		864
Clamping diode number (DZ800S17K3)		216		-	432		-
Total Semiconductor costs (k€)		181		372	362		744

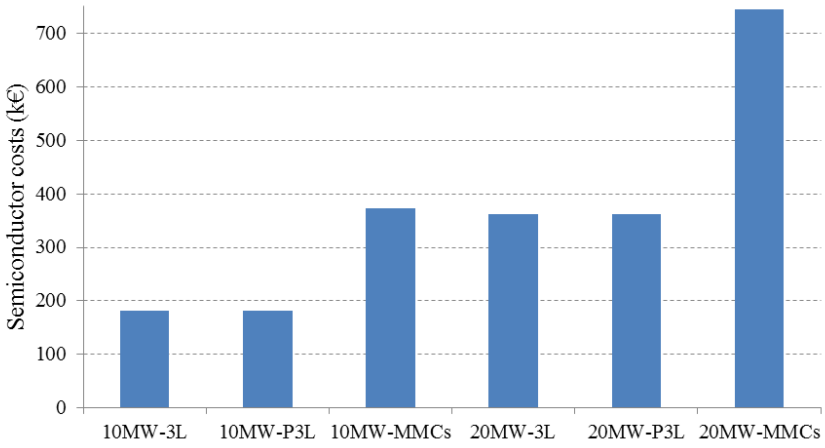

Fig. 2-2. Semiconductor costs for 10 & 20 MW - 3L, P3L, and MMCs configurations based BTB power converters.

Table 2-4
Semiconductors (referring Fig. 3-16 in Section 3.4)

Semiconductors	Peak repetitive voltage (V)	DC voltage (V)	Peak current (A)	Price (€)
FZ1800R17HP4	1700	900	1800	860.75
FZ2400R17HP4			2400	1055.68
DZ800S17K3			800	133.83

2.2.2 Passive Components Costs

The costs of the passive components in the configurations of the BTB power converters are investigated and compared. The passive component mainly includes the filter inductor, filter capacitor, and the dc-link capacitor.

The filter is usually adopted in industry to reduce the harmonics around the switching frequency and multiples of the switching frequency at the generator side and the grid side of the BTB power converter. The design of the filter is closely related to switching frequency. Suppose the switching frequency f_{sw} for the 3L, P3L, and MMC based configurations are all selected as 600 Hz for filter design and cost comparisons.

During the design of the filter, some design criteria should be specified to meet the generator-side and grid-side requirements. Here, the THD of the generator-side current is limited less than 3.5% and the grid-side current is limited less than 5% [2-7]. The filter capacitor value is limited by the decrease of the power factor at the rated power, which is generally less than 5%. According to [2-8], the filter capacitor can be obtained as

$$C_f = k\frac{P_n}{6\pi f U_g^2}$$

where k is the coefficient and k<5%. P_n is the rated power of the converter. U_g is the ac phase voltage. f is the ac source frequency.

The filter is normally used at the ac side, the filter design is carried out by setting the resonance frequency f_{res} of the filter below the switching frequency f_{sw}, generally around $0.5f_{sw}$ but often lower than this value due to the effect of the sub-harmonics of switching frequency [2-7], [2-8]. The resonance frequency of the LC filter is calculated by

$$f_{res} = \frac{\sqrt{L_f + L_m}}{2\pi\sqrt{C_f L_f L_m}}$$

where L_f is the filter inductance, C_f is the filter capacitance, L_m is the generator leakage inductance on the generator side or the combination of the grid inductance and transformer leakage inductance on the grid side. The damping resistance R_f (series-connected in the filter capacitor branch C_{f1} and C_{f2} in Fig. 2-1) are essential to suppress resonance. According to [2-8], the value of damping resistance can be design as

$$R_f = \frac{1}{6\pi f_{res} C_f}$$

According to [2-8], the dc-link capacitor of the 3L and P3L configurations of Fig. 2-1 can be designed as

$$C_d = \frac{P_n}{2 f_{sw} V_{dc} \Delta u}$$

where P_n is rated power of converter. Δu is voltage ripple, V_{dc} is dc-link voltage. The capacitor voltage ripple in the 3L and P3L is limited under 1%.

As to the MMCs-based configuration, the capacitor current $i_{cs}(t)$ in each SM of the upper arm can be expressed as [2-9]

$$i_{cs}(t) = [\frac{1}{2} - \frac{1}{2} m \sin(\omega t)] \cdot i_u(t)$$

where m is modulation index. ω is angular frequency. $i_u(t)$ is upper arm current in Fig. 2-1(d), which can be described as [2-2~2-5]

$$i_u(t) = \frac{P_n}{3V_{dc}} + \frac{1}{2} I_m \sin(\omega t + \theta)$$

where I_m is current peak value. θ is current phase angle. To simplify the design, the fundamental current component in the capacitor current is considered, which causes a corresponding voltage ripple and its time-varying function $\Delta_{uc}(t)$ can be expressed as

$$\Delta u_c(t) = \frac{i_{cs}(t)}{j\omega C_{dmmc}}$$

where C_{dmmc} is capacitance in each SM of the MMC, as shown in Fig. 2-1. In this report, the capacitor voltage ripple Δ_{uc} is selected as 10 % to design the capacitance C_{dmmc} in the MMC.

After the design of these passive components, the designed inductance and capacitance are used in the simulation, as shown in Tables 2-5, 2-6, and 2-7. The capacitor AVX FFLI6B3007KJE (3000uF/800V) is selected for 3L and P3L configurations [2-10]. The price of the capacitor AVX FFLI6B3007KJE is 288.4 €/unit, as shown in Table 2-8. The capacitor AVX FFLI6U1607KJE (1600uF/1150V) is selected for MMC-based configuration. The price of the capacitor AVX FFLI6U1607KJE is 217.49 €/unit, as shown in Table 2-8. The reference prices for the filter inductor and capacitor are listed in Table 2-9, which are used for the filter price calculation. Fig. 2-3 to Fig. 2-5 show the costs of the passive components for 2.5, 25, and 50 Hz power converters. The dc-link capacitor is the most expensive component and the filter capacitors are relatively cheap among the passive components. The cost of the MMCs configuration is much bigger than that in the other configurations. Owing to the very low ac frequency, the 2.5 Hz - MMCs configuration require a bigger capacitance than that required at the 25 and 50 Hz - MMCs configurations. In each ac frequency, the passive components costs of the 10 MW - 3L and P3L are almost the same, further, the passive components costs of the 20 MW - 3L and P3L are also almost the same, where the passive components costs of the 20 MW - 3L and P3L configurations is almost the double costs of the passive components of the 10 MW - 3L and P3L configurations.

Table 2-5
Costs of passive components for 2.5 Hz systems

Wind turbine power (MW)		10			20		
Converter configuration		3L	P3L	MMC	3L	P3L	MMC
Average switching frequency for each switch (Hz)		600					
Generator-side filter	Inductor (mH)	0.6	1	0.26	1.4	2.3	0.45
	Capacitor (mF)	0.8	0.8	0.2	0.45	0.45	0.1
Grid-side filter	Inductor (mH)	1.8	2.2	0.4	2.9	3.5	0.66
	Capacitor (mF)	0.15	0.15	0.1	0.07	0.07	0.05
DC-link capacitor	Capacitor (C_d, C_{dmmc}) (mF)	25	12.5	660* & 33#	12.5	6.25	660* & 33#
Total cost of inductor (k€)		116	115	114	208	209	192
Total cost of filter capacitor (k€)		11	11	4	25	25	7

Total cost of DC-link capacitor (k€)	152		3391	234		6782
Total passive components costs (k€)	279	278	3509	467	468	6981

660 mF* is for the generator-side MMCs converter and 33 mF# is for the grid-side MMCs converter.

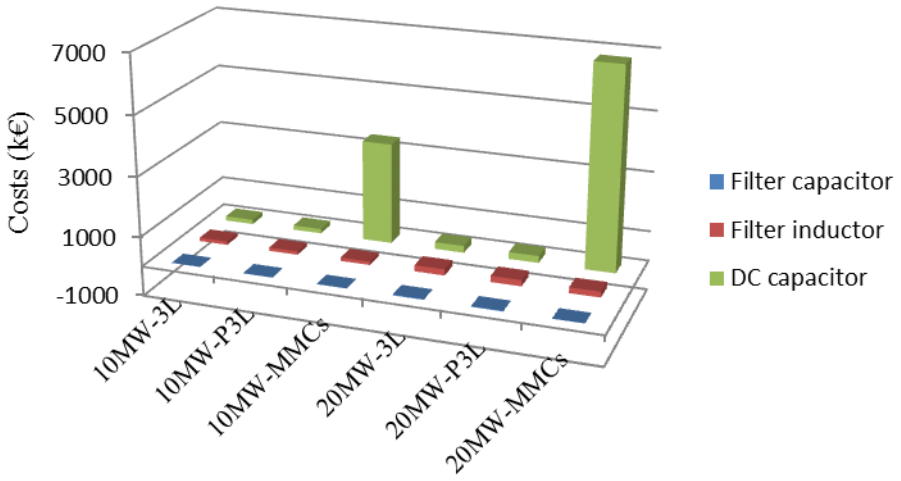

(a)

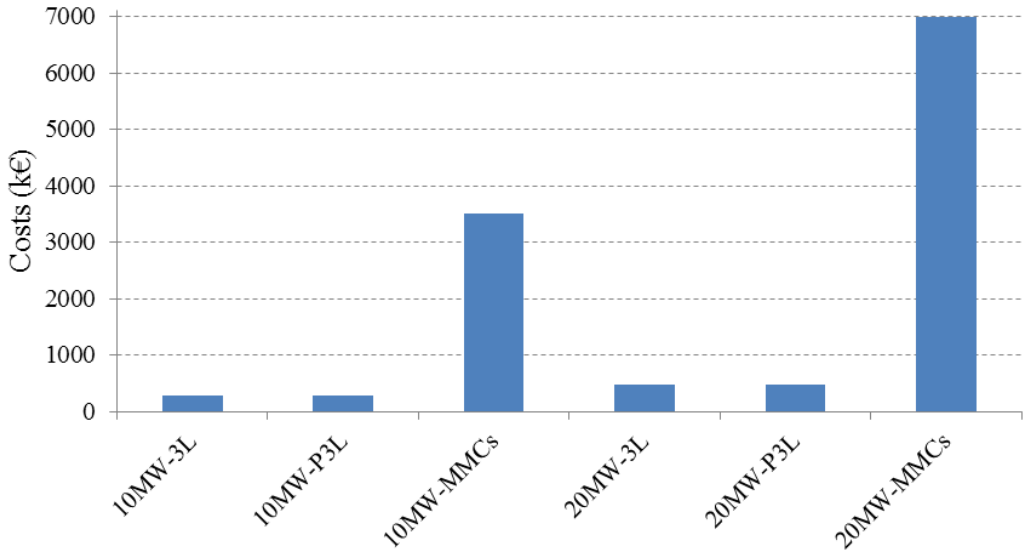

(b)

Fig. 2-3. (a) Costs of the filter inductor, filter capacitor, and DC capacitor for various configurations in 2.5 Hz systems. (b) Costs of the total passive components for various configurations in 2.5 Hz systems.

Table 2-6
Costs of passive components for 25 Hz systems

Wind turbine power (MW)		10			20		
Converter configuration		3L	P3L	MMC	3L	P3L	MMC
Average switching frequency for each switch (Hz)		600					
Generator-side filter	Inductor (mH)	1.2	1.5	0.26	1.9	2.3	0.44
	Capacitor (mF)	0.3	0.3	0.2	0.15	0.15	0.1
Grid-side filter	Inductor (mH)	1.8	2.2	0.4	2.9	3.5	0.66
	Capacitor (mF)	0.15	0.15	0.1	0.07	0.07	0.05
DC-link capacitor	Capacitor (C_d, C_{dmmc}) (mF)	25	12.5	66* & 33#	12.5	6.25	66* & 33#
Total cost of inductor (k€)		146	133	114	232	209	192
Total cost of filter capacitor (k€)		5	5	4	11	11	7
Total cost of DC-link capacitor (k€)		152		484	234		968
Total passive components costs (k€)		303	290	602	477	454	1167

66 mF* is for the generator-side MMCs converter and 33 mF# is for the grid-side MMCs converter.

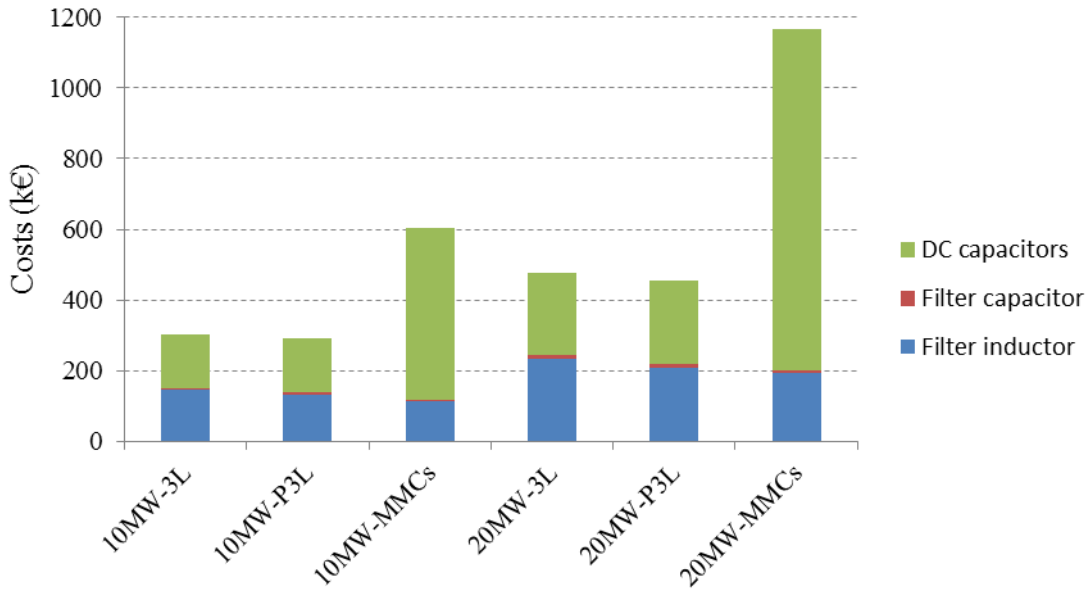

Fig. 2-4. Costs of the passive components for various configurations in 25 Hz systems.

Table 2-7
Costs of passive components for 50 Hz systems

Wind turbine power (MW)		10			20		
Converter configuration		3L	P3L	MMC	3L	P3L	MMC
Average switching frequency for each switch (Hz)		600					
Generator-side filter	Inductor (mH)	1.8	2.2	0.4	2.9	3.5	0.66
	Capacitor (mF)	0.15	0.15	0.1	0.07	0.07	0.05
Grid-side filter	Inductor (mH)	1.8	2.2	0.4	2.9	3.5	0.66
	Capacitor (mF)	0.15	0.15	0.1	0.07	0.07	0.05
DC-link capacitor	Capacitor (C_d, C_{dmmc}) (mF)	25	12.5	33	12.5	6.25	33
Total cost of inductor (k€)		175	158	138	282	252	228
Total cost of filter capacitor (k€)		4	4	3	7	7	5
Total cost of DC-link capacitor (k€)		152		323	234		646
Total passive components costs (k€)		331	314	464	523	493	879

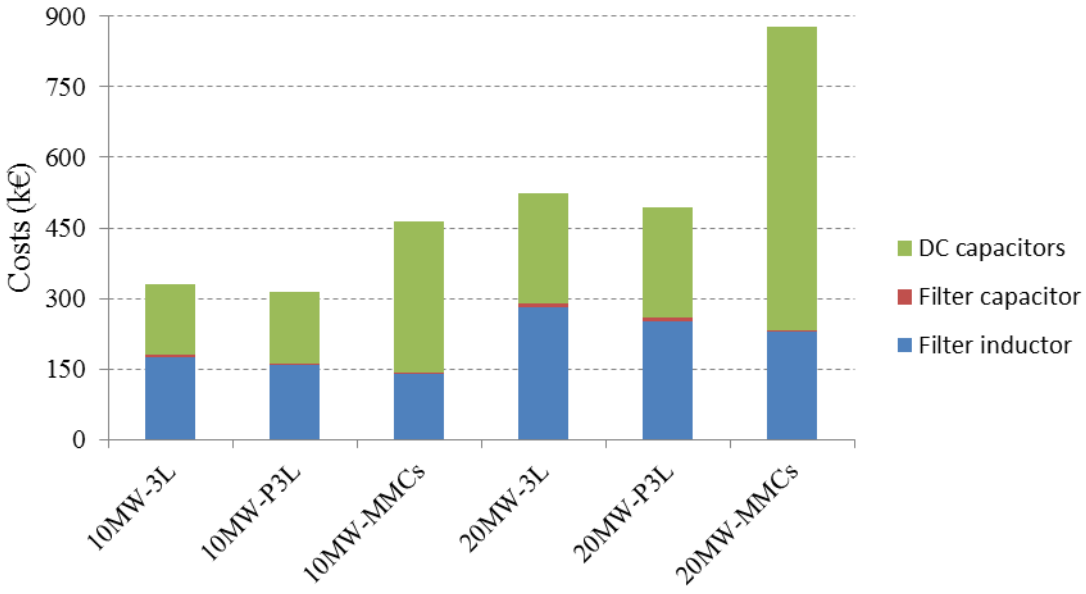

Fig. 2-5. Costs of the passive components for various configurations in 50 Hz systems.

Table 2-8
DC Capacitors [2-10]

Type	Capacitance (uF)	Voltage (kV)	Price (€)
AVX FFLI6B3007KJE	3000	0.8	288.4
AVX FFLI6U1607KJE	1600	1150	217.49

(INNWIND. EU. Deliverable 3.32, Converter designs based on new components and modular multilevel topologies)

Table 2-9
Reference Price for Filter [2-11]

Filter	Type	Price (k€)
Three-phase filter inductor	0.33 mH/2.4 kA	16
	0.50 mH/1.2 kA	9
	0.26 mH/3.2 kA	22
Three-phase filter capacitor	150 uF/3 kV	1.8
	75 uF/6 kV	3.6

2.2.3 Cooling System Costs

The cost of the cooling system is estimated based on the maximum power loss of the power converter. The cooling system cost for per loss is assumed as 800 €/kW (see the Appendix. A). Based on the power converter efficiency shown in Figs. 2-11 to Fig. 2-13 (see Section 2.4), Table 2-10 lists the costs of the cooling system for the power converters in 2.5, 25 & 50 Hz - 10 & 20 MW wind turbine systems. Fig. 2-6 illustrates the cooling system costs for 2.5, 25 and 50 Hz system, respectively. In the 2.5 Hz system, the cooling system costs for 10 MW 3L and P3L are almost the same and the cooling system costs for 20 MW 3L and P3L are almost the same, where the cooling system costs in the 20 MW systems are nearly double of that in the 10 MW systems. The 25 and 50 Hz systems have the nearly same results.

Table 2-10
Costs of Cooling System

Power converters		Cost (k€)
2.5 Hz system	10MW-3L	148
	10MW-P3L	143
	10MW-MMC	158
	20MW-3L	320
	20MW-P3L	306
	20MW-MMC	336
25 Hz system	10MW-3L	152
	10MW-P3L	144
	10MW-MMC	164
	20MW-3L	320
	20MW-P3L	317
	20MW-MMC	342
50 Hz system	10MW-3L	156
	10MW-P3L	147
	10MW-MMC	164
	20MW-3L	320
	20MW-P3L	304
	20MW-MMC	336

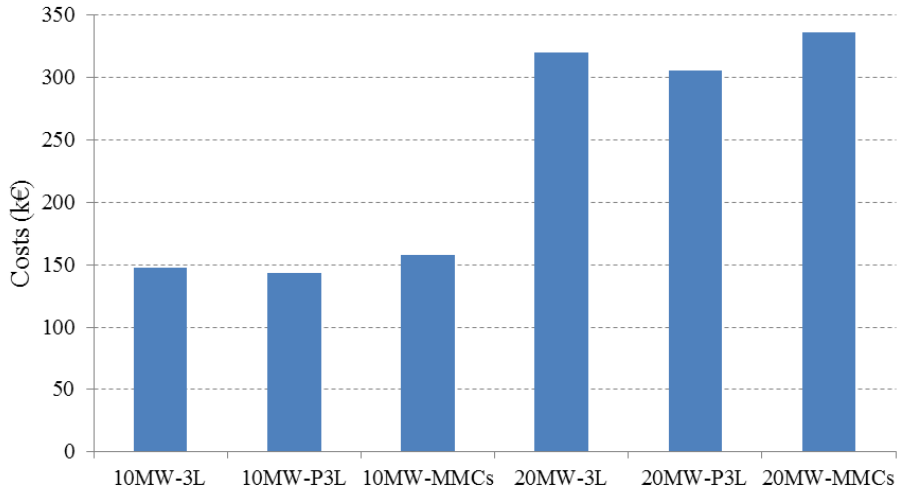
350
300
250
200
150
100
50
0
Costs (k€)
10MW-3L
10MW-P3L
10MW-MMCs
20MW-3L
20MW-P3L
20MW-MMCs

(a)

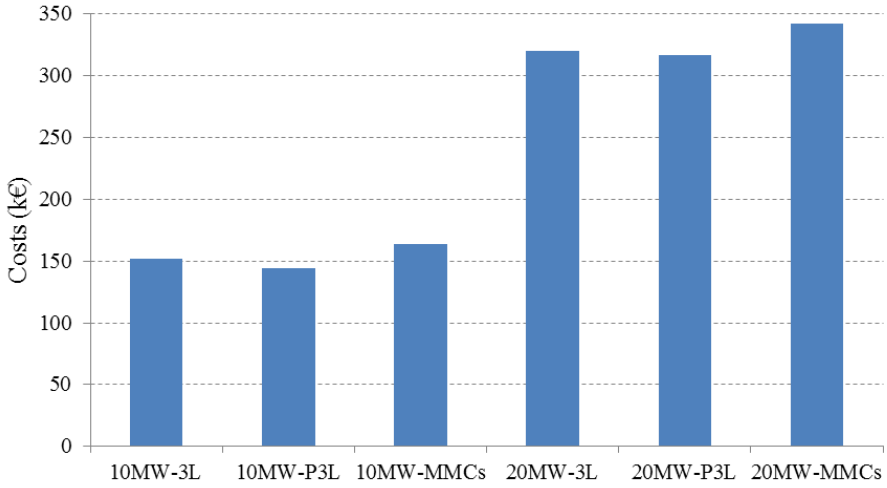
350
300
250
200
150
100
50
0
Costs (k€)
10MW-3L
10MW-P3L
10MW-MMCs
20MW-3L
20MW-P3L
20MW-MMCs

(b)

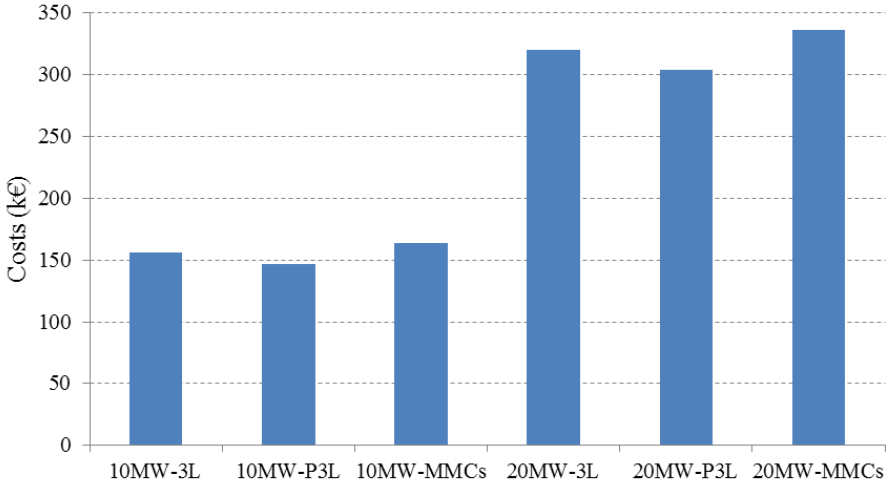
350
300
250
200
150
100
50
0
Costs (k€)
10MW-3L
10MW-P3L
10MW-MMCs
20MW-3L
20MW-P3L
20MW-MMCs

(c)

Fig. 2-6. (a) Cooling system costs of the 2.5 Hz system with various configurations. (b) Cooling system costs of the 25 Hz system with various configurations. (b) Cooling system costs of the 50 Hz system with various configurations.

2.2.4 Conclusions

Table 2-11 lists the total power converter costs including semiconductor cost, passive components cost, cooling system cost, and mechanical system cost, where the mechanical system cost is about 40% of the total cost excluding the cooling system.

Fig. 2-7 ~ Fig. 2-9 illustrate the 2.5, 25, and 50 Hz power converter costs with various configurations. It can be seen that the MMC configurations have the highest cost, where the dc capacitor in the passive components cost accounts for a high cost. The 3L and P3L configurations almost need the same cost in the 10 MW and 20 MW systems, respectively, and the cost for the 20 MW system is almost double of that for the 10 MW system. In addition, along with the increase of the generator-side frequency from 2.5 Hz to 50 Hz, the passive components cost in the MMC configuration is gradually reduced, which results in the reduction of the system total cost. From Fig. 2-7 ~ Fig. 2-9, it can be seen that the 3L and P3L have the lower costs in comparison with the MMC configurations in the 2.5, 25 and 50 Hz systems.

Table 2-11
Costs of Different Power Converter Configurations

Power converters		Semiconductor cost (k€)	Passive components costs			Cooling system cost (k€)	Mechanical cost (k€)	Total cost (k€)
			Filter inductor cost (k€)	Filter capacitor cost (k€)	DC-link capacitor cost (k€)			
2.5 Hz-system	10MW-3L	181	116	11	152	148	184	792
	10MW-P3L	181	115	11	152	143	184	786
	10MW-MMC	372	114	4	3391	158	1552	5591
	20MW-3L	362	208	25	234	320	332	1481
	20MW-P3L	362	209	25	234	306	332	1468
	20MW-MMC	744	192	7	6782	336	3090	11151
25 Hz-system	10MW-3L	181	146	5	152	152	194	830
	10MW-P3L	181	133	5	152	144	188	803
	10MW-MMC	372	114	4	484	164	390	1528
	20MW-3L	362	232	11	234	320	336	1495
	20MW-P3L	362	209	11	234	317	326	1459

(INNWIND. EU. Deliverable 3.32, Converter designs based on new components and modular multilevel topologies)

	20MW-MMC	744	192	7	968	342	764	3017
50 Hz-system	10MW-3L	181	175	4	152	156	205	873
	10MW-P3L	181	158	4	152	147	198	840
	10MW-MMC	372	138	3	323	164	334	1334
	20MW-3L	362	282	7	234	320	354	1559
	20MW-P3L	362	252	7	234	304	342	1501
	20MW-MMC	744	228	5	646	336	649	2608

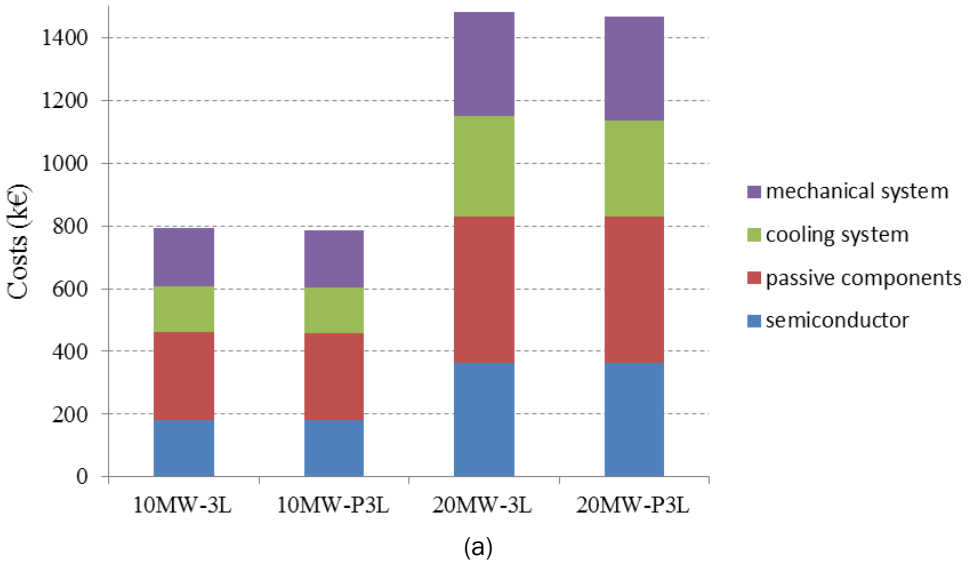

(a)

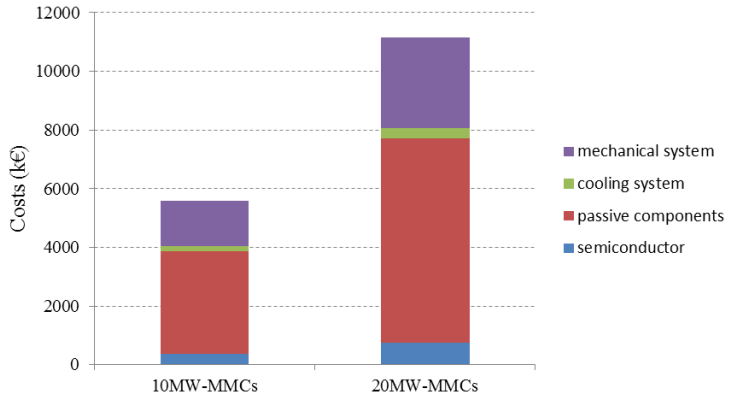

(b)

Fig. 2-7. Costs for power converters with various configurations in 2.5 Hz systems. (a) Costs of 3L and P3L configurations. (b) Costs of MMCs configuration.

(INNWIND. EU. Deliverable 3.32, Converter designs based on new components and modular multilevel topologies)

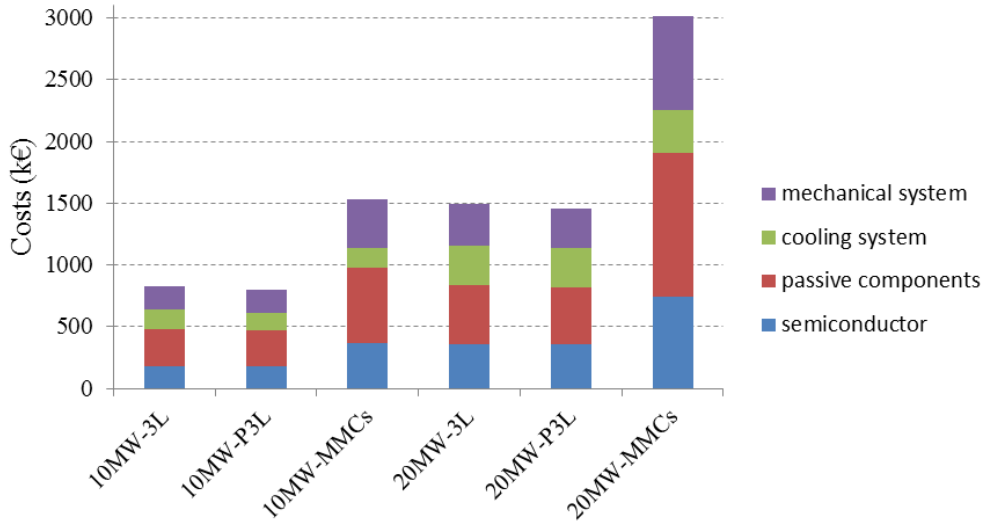

Fig. 2-8. Costs for power converters with various configurations in 25 Hz systems.

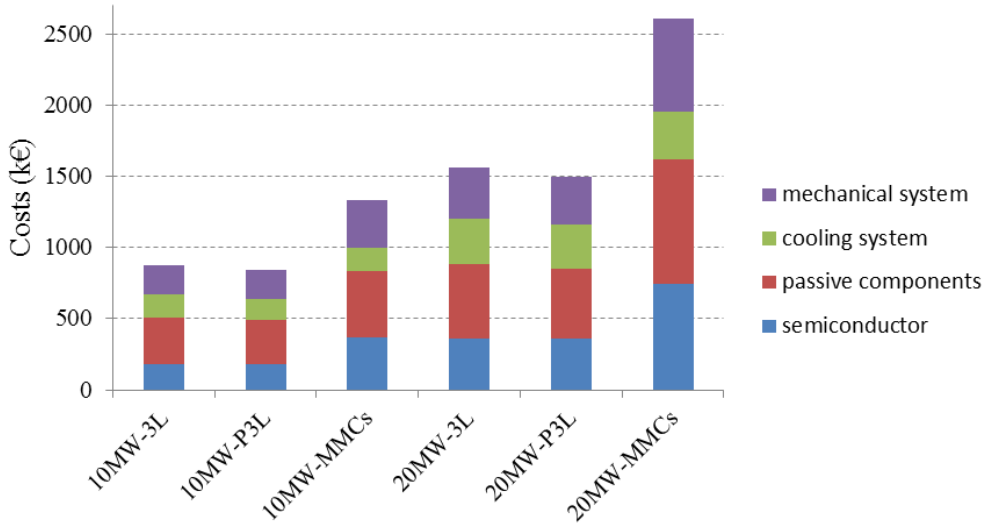

Fig. 2-9. Costs for power converters with various configurations in 50 Hz systems.

2.3 Size and Weight

2.3.1 Converter Size

The size of power converters are roughly estimated here, as shown in Table 2-12, where the size of active rectifier unit, inverter unit, control unit, and cooling unit, etc, are considered. Fig. 2-10 illustrates the size of the power converter with different configurations.

The ABB 4.5 MVA and 9 MVA - PCS 6000 BTB power converters with the size of 5100×1200×2450 (L×W×H mm) and 5700×1200×2450 (L×W×H mm) [2-12] are referred here for the size estimation of 3L and P3L power converters. Suppose the linear relationship between the converter power and converter size, the size of the 10 MW 3L and P3L power converter can be considered the same as approximate 5833×1200×2450 (L×W×H mm); the size of the 20 MW 3L

and P3L power converter is approximately 7167×1200×2450 (L×W×H mm), which has been listed in Table 2-12.

The sizes of the 8.3 MVA and 13.3 MVA - SIEMENS' cell-based SINAMICS PERFECT HARMONYGH150 [2-13] are referred here for the size estimation of the MMC-based power converters. The GH150 contains two parts. One part is the diode rectifier and the other part is the MMC inverter. Only considering a MMC inverter in the GH150, the sizes of the 8.3 MVA and 13.3 MVA MMC inverters are approximately 4800*1275*2810 (L×W×H mm) and 5700*1275*2810 (L×W×H mm). Suppose the linear relationship between the converter power and converter size, the size of a 10 MW and 20 MW MMC inverter can be approximately estimated as 5106*1275*2810 (L×W×H mm) and 6906*1275*2810 (L×W×H mm), respectively. The size of the 25 and 50 Hz - 10 MW BTB MMC configurations is approximately 10212*1275*2810 (L×W×H mm). The size of the 25 and 50 Hz - 20 MW BTB MMC configuration is approximately 13812*1275*2810 (L×W×H mm). The 2.5 Hz system based on MMCs configurations requires a bigger capacitance than 25 and 50 Hz systems as shown in Table 2-5. As a consequence, the size of the 2.5 Hz system based on MMCs configuration is the biggest among these different configurations, which is a little difficult to be estimated, but it does not affect the comparisons in this report.

Table 2-12
Size of Various Power Converters

Power converters		Cubic size (L*W*H mm)	Volume (m^3)
2.5 Hz-system	10MW-3L	5833*1200*2450	17.1
	10MW-P3L	5833*1200*2450	17.1
	10MW-MMC	-	-
	20MW-3L	7167*1200*2450	21.1
	20MW-P3L	7167*1200*2450	21.1
	20MW-MMC	-	-
25 Hz-system	10MW-3L	5833*1200*2450	17.1
	10MW-P3L	5833*1200*2450	17.1
	10MW-MMC	10212*1275*2810	36.6
	20MW-3L	7167*1200*2450	21.1
	20MW-P3L	7167*1200*2450	21.1
	20MW-MMC	13812*1275*2810	49.5
50 Hz-system	10MW-3L	5833*1200*2450	17.1
	10MW-P3L	5833*1200*2450	17.1
	10MW-MMC	10212*1275*2810	36.6
	20MW-3L	7167*1200*2450	21.1
	20MW-P3L	7167*1200*2450	21.1
	20MW-MMC	13812*1275*2810	49.5

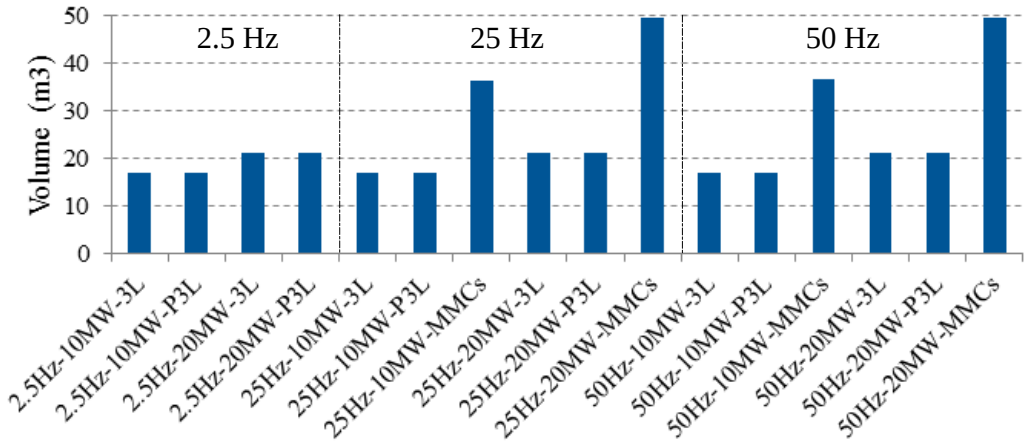

Fig. 2-10. Power converter sizes of 2.5, 25 and 50 Hz systems with various configurations.

2.3.2 Converter Weight

The weight of power converters are roughly estimated here, as shown in Table 2-13. Fig. 2-11 illustrates the weight of the power converter with different configurations.

The ABB 4.5 MVA and 9 MVA - PCS 6000 BTB power converters with the weight of approximately 5250 kg and 6200 kg [2-12] are referred here for the weight estimation of 3L and P3L power converters. Suppose the linear relationship between the converter power and the converter weight, the weight of the 10 MW 3L and P3L power converters can be considered the same as approximate 6400 kg; the weight of the 20 MW 3L and P3L power converters can be considered the same as approximate 8522 kg, which has been listed in Table 2-13.

The sizes of the 8.3 MVA and 13.3 MVA - SIEMENS' cell-based SINAMICS PERFECT HARMONYGH150 [2-13] are referred here for the weight estimation of the MMC-based power converters. The GH150 contains two parts. One part is the diode rectifier and the other part is the MMC inverter. Only considering a MMC inverter in the GH150, the weight of the 8.3 MVA and 13.3 MVA MMC inverters are approximately 6310 kg and 8440 kg. Suppose the linear relationship between the converter power and converter weight, the weight of a 10 MW and 20 MW MMC inverter can be approximately estimated as 5458 kg and 6736 kg, respectively. The weight of the 25 and 50 Hz - 10 MW BTB MMC configurations is approximately 11785 kg; the weight of the 25 and 50 Hz - 20 MW BTB MMC configuration is approximately 16897 kg. The 2.5 Hz system based on MMCs configurations requires a bigger capacitance than 25 and 50 Hz systems as shown in Table 2-5. As a consequence, the weight of the 2.5 Hz system based on MMCs configuration is the heaviest among these different configurations, which is a little difficult to be estimated, but it does not affect the comparisons in this report

Table 2-13
Weight of Various Power Converters

Power converters		Weight (kg)
2.5 Hz-system	10MW-3L	6411
	10MW-P3L	6411
	10MW-MMC	-
	20MW-3L	8522

	20MW-P3L	8522
	20MW-MMC	-
25 Hz-system	10MW-3L	6411
	10MW-P3L	6411
	10MW-MMC	11785
	20MW-3L	8522
	20MW-P3L	8522
	20MW-MMC	16897
50 Hz-system	10MW-3L	6411
	10MW-P3L	6411
	10MW-MMC	11785
	20MW-3L	8522
	20MW-P3L	8522
	20MW-MMC	16897

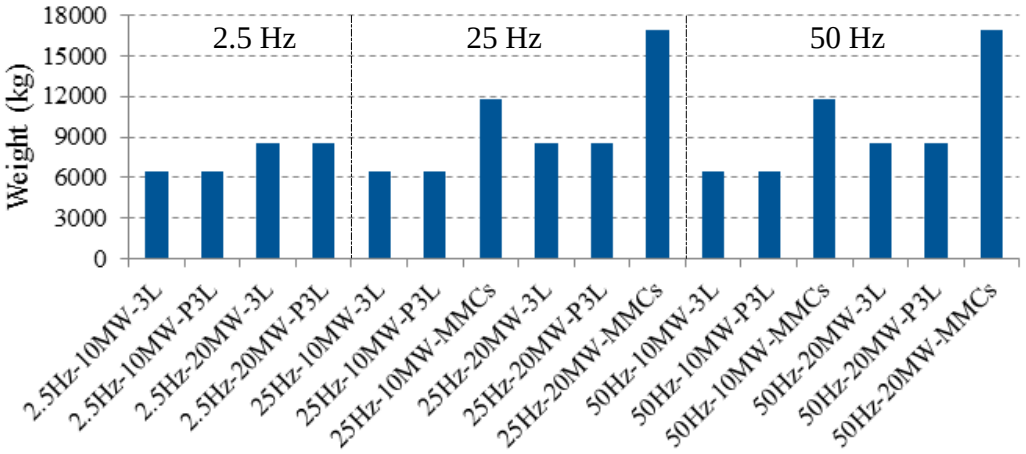

Fig. 2-11. Power converter weights of 2.5, 25 and 50 Hz systems with various configurations.

2.4 Efficiency

The 10 MW and 20 MW wind power system based on the various power converter configurations are modeled and simulated with the professional time-domain simulation tool PSCAD/EMTDC [2-14]. The system parameters are shown in the Appendix. A and the relationships between the wind speed and the power for the 10 MW and 20 MW wind turbine system are also shown in the Appendix. A. The simulation result semiconductor current (IGBT and Diode current) is obtained and used for power losses calculation with the IGBT and Diode data-sheet. The conduction losses and switching losses of the semiconductors (IGBT and Diode) are mainly considered here.

The semiconductor conduction losses can be calculated using a semiconductor approximation with a series connection of DC voltage source u_{vo} representing semiconductor on-state zero-current collector-emitter voltage and a collector emitter on-state resistance r_c as [2-15]

$$u_v(i_c) = u_{v0} + r_c \bullet i_c$$

where i_c is semiconductor current. These important parameters (u_{v0} and r_c) can be read directly from the semiconductor (IGBT and Diode in Table 2-4) datasheet. The instantaneous value of the semiconductor conduction losses can be expressed as

$$P_{ce}(t) = u_v(t) \bullet i_c(t)$$

The average conduction losses can be obtained as

$$P_{ceav} = \frac{1}{T_{sw}} \int_0^{T_{sw}} P_{ce}(t)dt$$

where $T_{sw}=1/f_{sw}$.

The switching losses in the semiconductor are the product of switching energies and the switching frequency f_{sw} as

$$P_{sw}(t) = (E_{on} + E_{off}) \bullet f_{sw}$$

where E_{on} and E_{off} is the turn-on and turn-off energy losses in the semiconductor, which can be read directly from the semiconductor datasheet. As a consequence, the semiconductor losses can be calculated as

$$P_{loss} = P_{ceav} + P_{sw}$$

2.4.1 Efficiency for 2.5 Hz - 10 & 20 MW Power Converters

The efficiency for the 10 and 20 MW - 2.5 Hz power converters are shown in Fig. 2-12. It can be observed that the P3L configurations have a high efficiency. The efficiency of the MMC configuration is a little low, because more semiconductors are used in the MMCs.

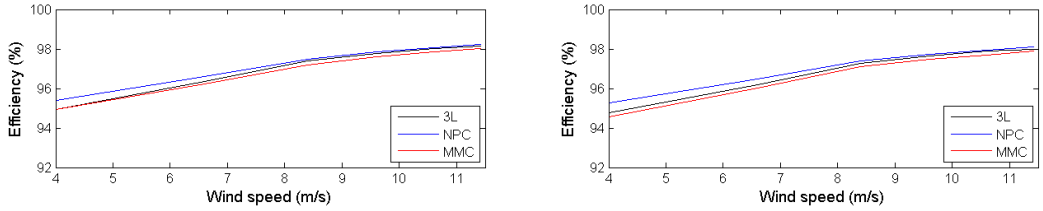

(a) (b)

Fig. 2-12. Efficiency for 2.5 Hz system (a) 10 MW power converters. (b) 20MW power converters.

2.4.2 Efficiency for 25 Hz - 10 & 20 MW Power Converters

The efficiency for the 10 and 20 MW - 25 Hz power converters are shown in Fig. 2-13. It can be observed that the P3L configurations have a high efficiency. The efficiency of the MMC configuration is a little low, because more semiconductors are used in the MMCs.

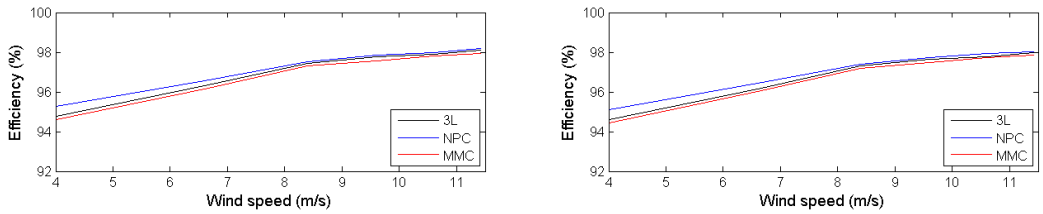

(INNWIND. EU. Deliverable 3.32, Converter designs based on new components and modular multilevel topologies)

(a) (b)

Fig. 2-13. Efficiency for 25 Hz system (a) 10 MW power converters. (b) 20MW power converters.

2.4.3 Efficiency for 50 Hz - 10 & 20 MW Power Converters

The efficiency for the 10 and 20 MW - 50 Hz power converters are shown in Fig. 2-14. It can be observed that the P3L configurations have a high efficiency. The efficiency of the MMC configuration is a little low, because more semiconductors are used in the MMCs.

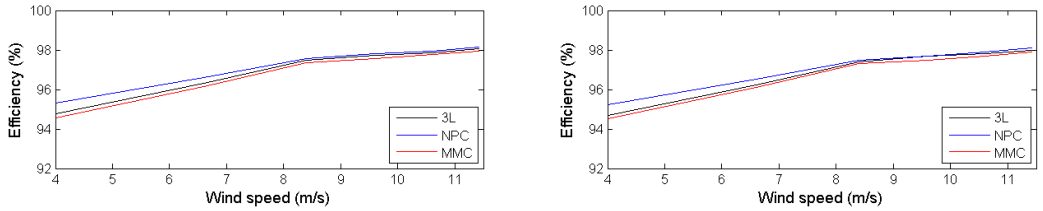

(a) (b)

Fig. 2-14. Efficiency for 50 Hz system (a) 10 MW power converters. (b) 20MW power converters.

2.5 Silicon Carbide (SiC) Semiconductor Consideration

Power electronics has experienced revolutionary changes during the last three or four decades, and one of the important development areas is in semiconductor devices. The SiC semiconductor is considered to be used to replace the Si semiconductor in the above power converter configurations to study the impacts of the low switching losses and high switching frequency characteristics of SiC devices. Although the development of the SiC semiconductor is actively conducted recently, there is still no commercial SiC product for high voltage and current available on market. In this investigation, suppose the current SiC-based switch CAS300M12BM2 (1200V/300A) is considered in series and parallel for the construction of different power converter configurations.

Suppose the losses of the SiC-based system is kept almost the same as the Si-based system, the switching frequency of the SiC semiconductor is selected as 20 kHz, where the efficiency of the Si -based system is similar to that of the Si-based system, as shown in Fig. 2-15 ~ Fig. 17. Tables 2-14 ~ Table 2-16 show the passive components for 2.5, 25, and 50 Hz power converter configurations. From these Tables, it can be seen that, the application of the SiC-based semiconductor can make a high switching frequency and result in small passive components and therefore reduce the costs.

Table 2-14
Inductors and Capacitors for 2.5 Hz Systems

Wind turbine power (MW)		10			20		
Converter configuration		3L	P3L	MMC	3L	P3L	MMC
Average switching frequency for each switch (kHz)		20					
Generator-side filter	Inductor (uH)	3.3	6.6	26	7.3	14.6	45
	Capacitor (mF)	0.6	0.6	0.06	0.3	0.3	0.04
Grid-side filter	Inductor (uH)	130	230	16	270	490	26

(INNWIND. EU. Deliverable 3.32, Converter designs based on new components and modular multilevel topologies)

	Capacitor (mF)	0.1	0.1	0.06	0.06	0.06	0.03
DC-link capacitor	Capacitor (mF)	25	12.5	660 * & 33#	12.5	6.5	660* & 33#

660 mF* is for the generator-side MMCs converter and 33 mF# is for the grid-side MMCs converter.

Table 2-15
Inductors and Capacitors for 25 Hz System

Wind turbine power (MW)		10			20		
Converter configuration		3L	P3L	MMC	3L	P3L	MMC
Average switching frequency for each switch (kHz)		20					
Generator-side filter	Inductor (uH)	50	105	11	130	322	18
	Capacitor (mF)	0.2	0.2	0.12	0.12	0.12	0.06
Grid-side filter	Inductor (uH)	130	230	16	270	490	26
	Capacitor (mF)	0.1	0.1	0.06	0.06	0.06	0.03
DC-link capacitor	Capacitor (mF)	25	12.5	66* & 33#	12.5	6.5	66* & 33#

66 mF* is for the generator-side MMCs converter and 33 mF# is for the grid-side MMCs converter.

Table 2-16
Inductors and Capacitors for 50 Hz System

Wind turbine power (MW)		10			20		
Converter configuration		3L	P3L	MMC	3L	P3L	MMC
Average switching frequency for each switch (kHz)		20					
Generator-side filter	Inductor (uH)	130	230	16	270	490	26
	Capacitor (mF)	0.1	0.1	0.06	0.06	0.06	0.03
Grid-side filter	Inductor (uH)	130	230	16	270	490	26
	Capacitor (mF)	0.1	0.1	0.06	0.06	0.06	0.03
DC-link capacitor	Capacitor (mF)	25	12.5	33	12.5	6.5	33

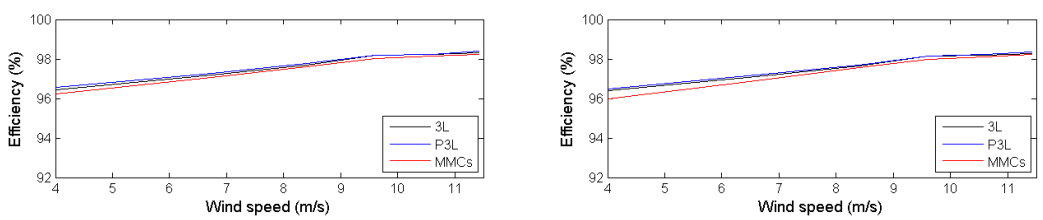

Fig. 2-15. Efficiency for 2.5 Hz systems. (a) 10 MW power converters. (b) 20MW power converters.

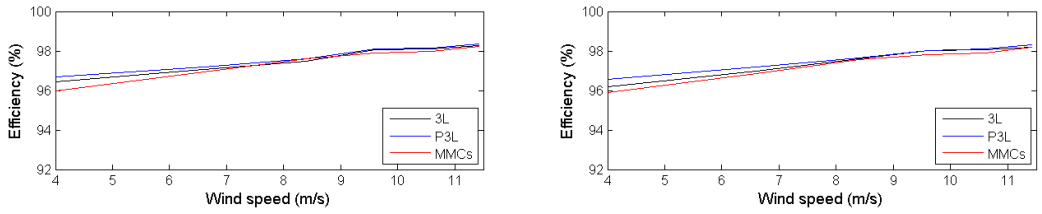

(a) (b)

Fig. 2-16. Efficiency for 25 Hz systems. (a) 10 MW power converters. (b) 20MW power converters.

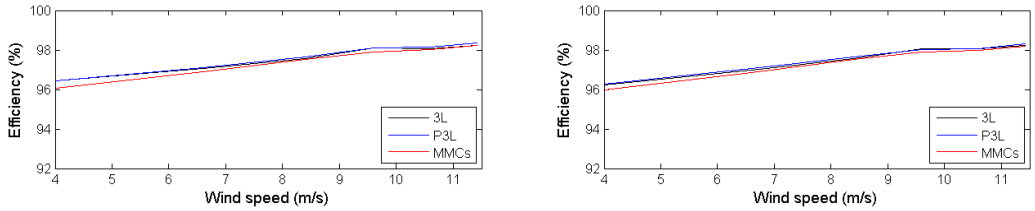

(a) (b)

Fig. 2-17. Efficiency for 50 Hz systems. (a) 10 MW power converters. (b) 20MW power converters.

2.6 Reliability

Fig. 2-1 shows the different power converter configurations. Among them, it can be seen that the P3L and MMCs configurations have a high reliability in comparison with the 3L configurations. As to the P3L configuration, it has several 3L converter units to be connected in parallel. If some faults occur to any 3L unit, the faulty 3L unit will be isolated from the system. The left healthy 3L converter unit can still work to keep a part of the system in continuous operation, as shown in Fig. 2-18. As to the MMC based wind turbine system, some extra SMs are equipped for the redundancy operation, as shown in Fig. 2-19. If some SMs are broken in the arm, the extra SMs in the same arm will be able to keep the wind turbine to be continuous operated. As a consequence, the redundancy operation of the P3L and MMC configurations increase the reliability of the power electronic system in the wind turbine.

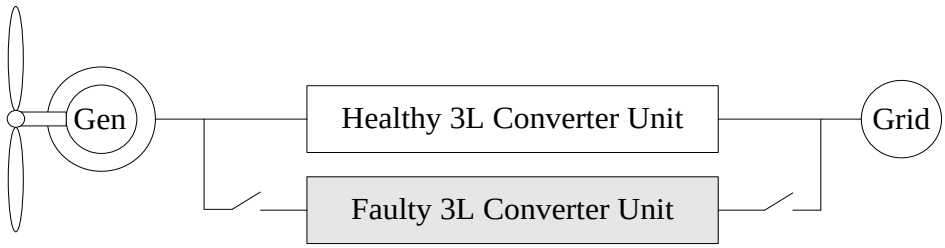

Fig. 2-18. Redundancy for the P3L configuration-based wind turbine.

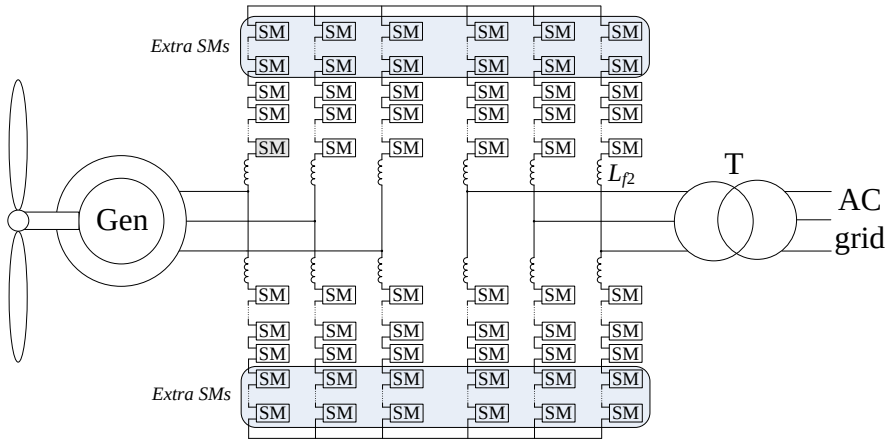

Fig. 2-19. Redundancy for the MMC configuration-based wind turbine.

2.7 Conclusions

In this Section, the cost, size, efficiency, and reliability of the power converters with different configurations (including 3L, P3L, MMCs) are discussed. The 3L and P3L configurations not only have the low costs but also the small size in comparison with the MMCs-based configuration, because the MMCs-based configuration requires larger number of capacitors. In addition, the efficiency of the 3L and P3L configuration is a little higher than that of the MMC configuration, because more semiconductors are used in the MMC configuration. On the other hand, the P3L and the MMC configuration have a higher reliability in comparison with the 3L configuration. As a consequence, the P3L configuration is the best configuration among these BTB configurations.

2.8 Simulation Studies

Owing to the excellent performance of the P3L configuration, the simulation waveforms of P3L converters are presented in this section.

Fig. 2-20 and Fig. 2-21 show the simulation waveforms of the 10 & 20 MW - 2.5 Hz wind turbine system based on P3L configuration, respectively, where the wind turbines are operated at rated power. The generator-side and the grid-side current waveforms are shows in Fig. 2-20 and Fig. 2-21.

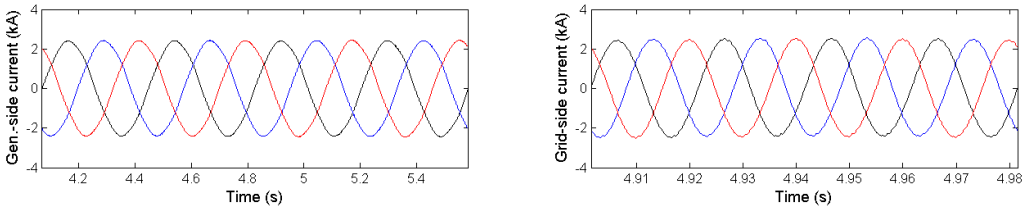

(a) (b)

Fig. 2-20. Simulation waveform of 10 MW - 2.5 Hz wind turbine system. (a) Generator-side current. (b) Grid-side current.

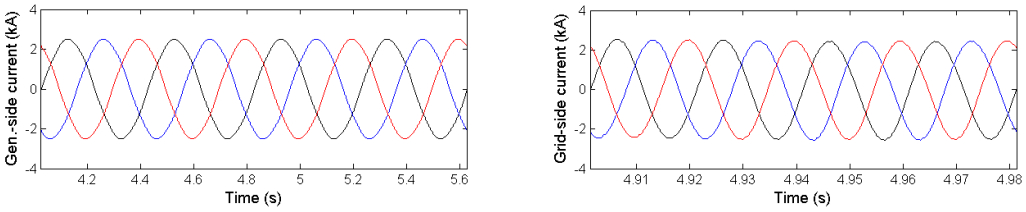

(a) (b)

Fig. 2-21. Simulation waveform of 20 MW - 2.5 Hz wind turbine system. (a) Generator-side current. (b) Grid-side current.

Fig. 2-22 and Fig. 2-23 show the simulation waveforms of the 10 & 20 MW - 25 Hz wind turbine system based on P3L configuration, respectively, where the wind turbines are operated at rated power. The generator-side and the grid-side current waveforms are shows in Fig. 2-22 and Fig. 2-23.

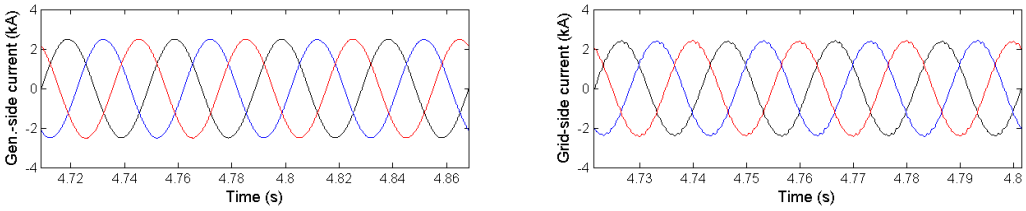

(a) (b)

Fig. 2-22. Simulation waveform of 10 MW - 25 Hz wind turbine system. (a) Generator-side current. (b) Grid-side current.

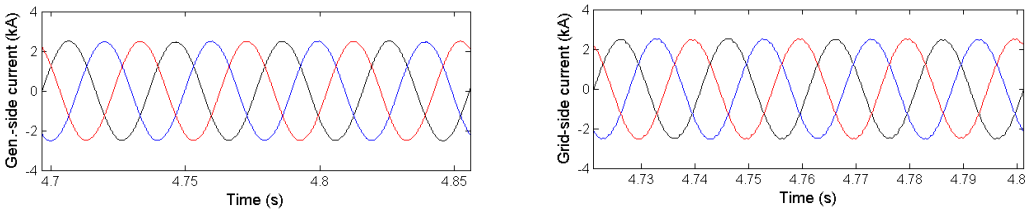

(a) (b)

Fig. 2-23. Simulation waveform of 20 MW - 25 Hz wind turbine system. (a) Generator-side current. (b) Grid-side current.

Fig. 2-24 and Fig. 2-25 show the simulation waveforms of the 10 & 20 MW - 50 Hz wind turbine system based on P3L configuration, respectively, where the wind turbines are operated at rated power. The generator-side and the grid-side current waveforms are shows in Fig. 2-24 and Fig. 2-25.

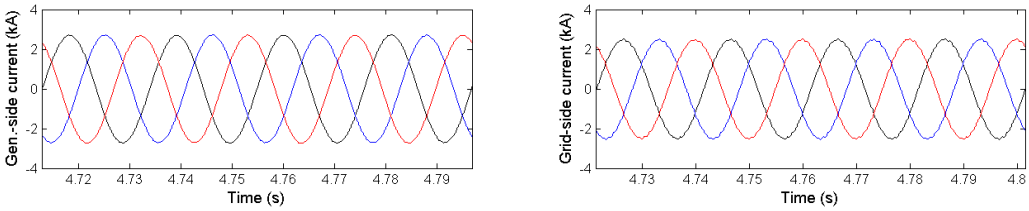

(a) (b)

Fig. 2-24. Simulation waveform of 10 MW - 50 Hz wind turbine system. (a) Generator-side current. (b) Grid-side current.

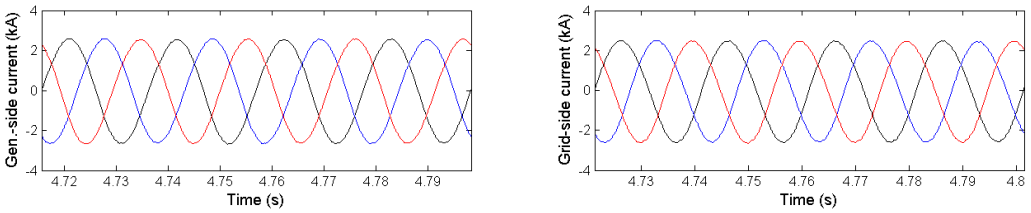

(a) (b)

Fig. 2-25. Simulation waveform of 20 MW - 50 Hz wind turbine system. (a) Generator-side current. (b) Grid-side current.

2.9 Appendix

A. Cooling System Cost Calculation

The cost of 10 MW power converter is about 80 k€/MW [2-16] and its efficiency is about 98% [2-12]. Normally, the cooling system cost is approximate 10% ~ 20% of converter cost, where the bigger of the converter capacity, the higher of the percentage of the cooling system cost. As to the 10 & 20 MW wind turbine system, the cooling system cost is selected approximately 20% of converter cost. As a result, the cooling system cost for per MW power loss can be calculated as

$$\frac{\text{Cooling system cost}}{\text{Power losses}} = \frac{10\text{MW} \times 80\text{k€/MW} \times 20\%}{10\text{MW} \times (1-98\%)} = 800\ \text{k€/MW}$$

B. 10 & 20 MW Wind Turbine System Parameters

The 2.5. 25 and 50 Hz – 10 and 20 MW wind turbine system parameters for simulation studies are shown in Table 2-17 ~ Table 2-20.

Table 2-17
10 and 20 MW Wind Turbine Parameters for Simulations [17]

Wind turbine parameter	Value	Value
Wind turbine rated power (MW)	10	20
Rotor diameter (m)	178	252
Hub height	119	153
Cut in wind speed (m/s)	4	4
Nominal wind speed (m/s)	11.4	11.4
Cut out wind speed (m/s)	25	25

Table 2-18
10 and 20 MW - 2.5 Hz System Parameters for Simulations

2.5 Hz generator parameter	Value	Value
Rated power (MW)	10	20
Number of phase	3	3
Rated line-to-line voltage (kV)	3.3	6.6
Rated frequency (Hz)	2.5	2.5
Number of pole pairs	16	23
Induction in d-axis X_d (p.u.)	0.3	0.2
Induction in q-axis X_q (p.u.)	0.3	0.2
Moment of inertia H (s)	8	16

Table 2-19
10 and 20 MW - 25 Hz System Parameters for Simulations

PDDG parameter	Value	Value
Rated power (MW)	10	20
Number of phase	3	3
Rated line-to-line voltage (kV)	3.3	6.6
Rated frequency (Hz)	25	25
Number of pole pairs	160	230
Induction in d-axis X_d (p.u.)	0.3	0.2
Induction in q-axis X_q (p.u.)	0.3	0.2
Moment of inertia H (s)	8	16

Table 2-20
10 and 20 MW - 50 Hz System Parameters for Simulations

PDDG parameter	Value	Value
Rated power (MW)	10	20
Number of phase	3	3
Rated line-to-line voltage (kV)	3.3	6.6
Rated frequency (Hz)	50	50
Number of pole pairs	320	460
Induction in d-axis X_d (p.u.)	0.3	0.2
Induction in q-axis X_q (p.u.)	0.3	0.2
Moment of inertia H (s)	8	16

The relationships between the wind speed and the power for 10 MW and 20 MW wind turbine system are

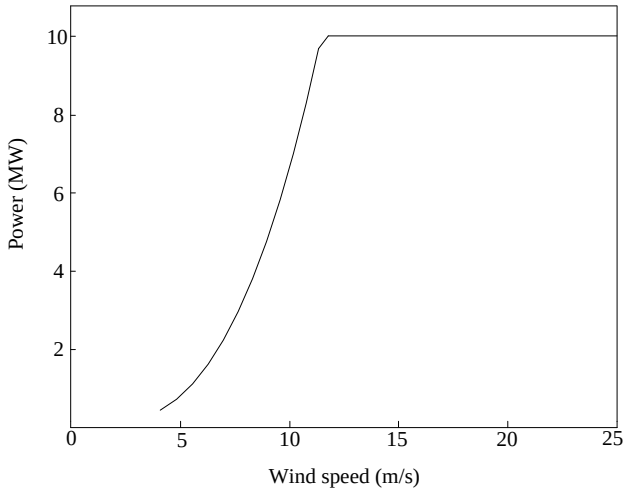

(a)

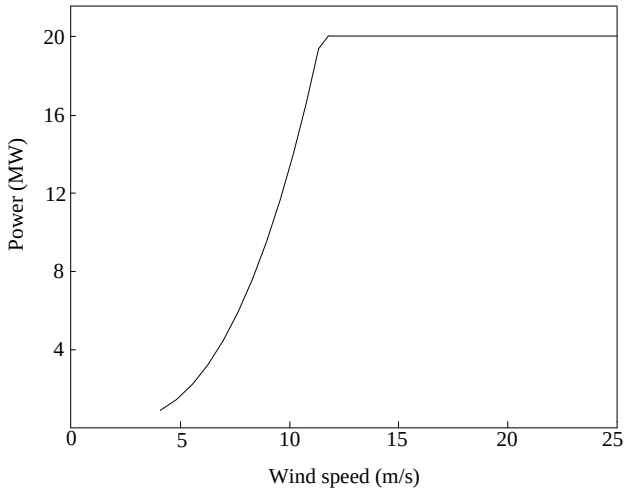

(b)

Fig. 2-26. Relationship between wind speed and power. (a) 10 MW wind turbine system. (b) 20 MW wind turbine system.

2.10 References

[2-1] B. Wu, Y. Lang, N. Zargari, and S. Kouro, *Power Conversion and Control of Wind Energy System*, Wiley 2011.

[2-2] F. Deng and Z. Chen, "A control method for voltage balancing in modular multilevel converters," *IEEE Transactions on Power Electronics*, Vol. 29, no. 1, pp. 66-76, Jan. 2014.

[2-3] F. Deng and Z. Chen, "Elimination of DC-link current ripple for modular multilevel converters with capacitor voltage-balancing pulse-shifted carrier PWM," *IEEE Transactions on Power Electronics*, vol. 30, no. 1, pp. 284-296, Jan. 2015.

[2-4] F. Deng and Z. Chen, "Fault Detection and Localization Method for Modular Multilevel Converters," *IEEE Transactions on Power Electronics*, In Press, 2015.

[2-5] F. Deng and Z. Chen, "Voltage-Balancing Method for Modular Multilevel Converters Switched at Grid Frequency," *IEEE Transactions on Industrial Electronics*, In Press, 2015.

[2-6] B. Backlund, M. Rahimo, S. Klaka, J. Siefken, "Topologies, voltage ratings and state of the art high power semiconductor devices for medium voltage wind energy conversion," in *proceeding on PEMWA*, 2009, pp. 1-6.

[2-7] X. Zeng, Z. Chen, and F. Blaabjerg, "Design and comparison of full-size converters for large variable-speed wind turbines," in *proceeding on European Conference on Power Electronics and Applications 2007,* pp. 1-10.

[2-8] X. Wei, L. Xiao, Z. Yao, and C. Gong, "Design of LCL filter for wind power inverter," in *proceeding on WNWEC*, 2010, pp. 1-6.

[2-9] Q. Song, W. Liu, X. Li, H. Rao, S. Xu, and L. Li, "A steady-state analysis method for a modular multilevel converter," *IEEE Transactions on Power Electronics*, vol. 28, no. 8, pp.3702-3713, Aug. 2013.

[2-10] AVX Capacitors for Power Electronics

[2-11] Communication with industry.

[2-12] ABB. PCS 6000 for large wind turbines medium voltage, full power converters up to 9 MVA

[2-13] SIEMENS, The next level of versatility for cell-based medium-voltage drives SINAMICS PERFECT HARMONY GH150

[2-14] PSCAD, [Online available] https://hvdc.ca/pscad/

[2-15] D. Graovac and M. Purschel, *IGBT Power Losses Calcuation Using the Data-sheet Parameters*, Infineon Technologies AG, 2009.

[2-16] Communication with DTU, Denmark.

[2-17] INNWIND D1.21 report. Reference Wind Turbine Report.

3 MODULAR MULTILEVEL DIRECT AC/AC VOLTAGE SOURCE CONVERTERS

This chapter focuses on modular multilevel direct AC/AC converters and their possible application for wind turbine systems. Modular multilevel direct AC/AC converters are an emerging alternative to the "Modular Multilvel Converter" (M²LC). The main difference to the M²LC is the missing central DC-link and the use of H-bridge modules. Besides, the basic building blocks are the same.

3.1 Topologies

There are two known modular multilevel direct AC/AC converters, namely the so-called "Hexverter" topology and the "Modular Multilevel Matrix Converter" (MMMC). There are only a few publications addressing these two rather new topologies. This is why the basic concept of the topologies is explained in this section.

3.1.1 Hexverter

The Hexverter topology (Fig. 3-1) belongs to the family of modular multilevel converters. It consists of six so-called branches (or: clusters, arms) and connects two three-phase systems directly without a central DC-link. The six branches comprise series-connected H-bridge modules and an inductor. Each phase of each system is connected to two phases of the other system.

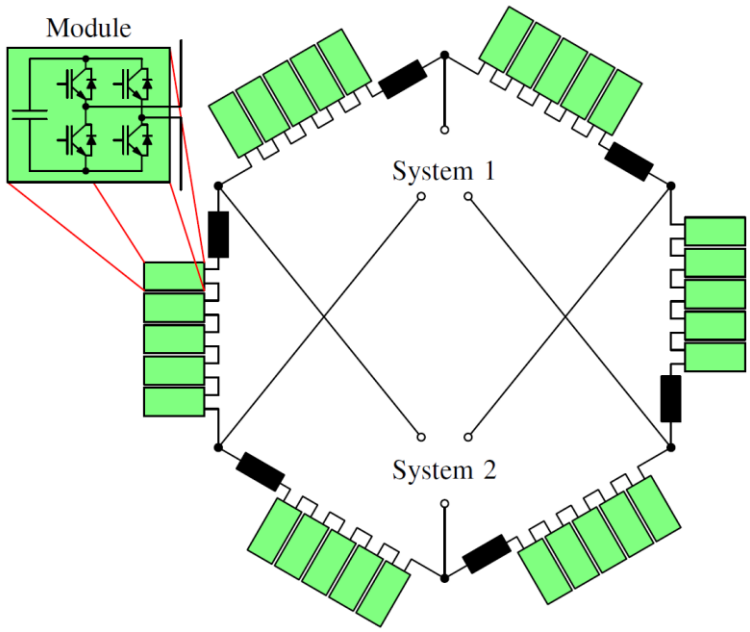

Fig. 3-1. Schematic of the Hexverter topology.

For connecting the two systems, the voltages of the branches and the branch currents must have components of both system frequencies. An example for the branch voltages and branch currents is given in Fig. 3-2. The curves shown in Fig. 3-2 are the result of the simulation of an arbitrarily chosen scenario.

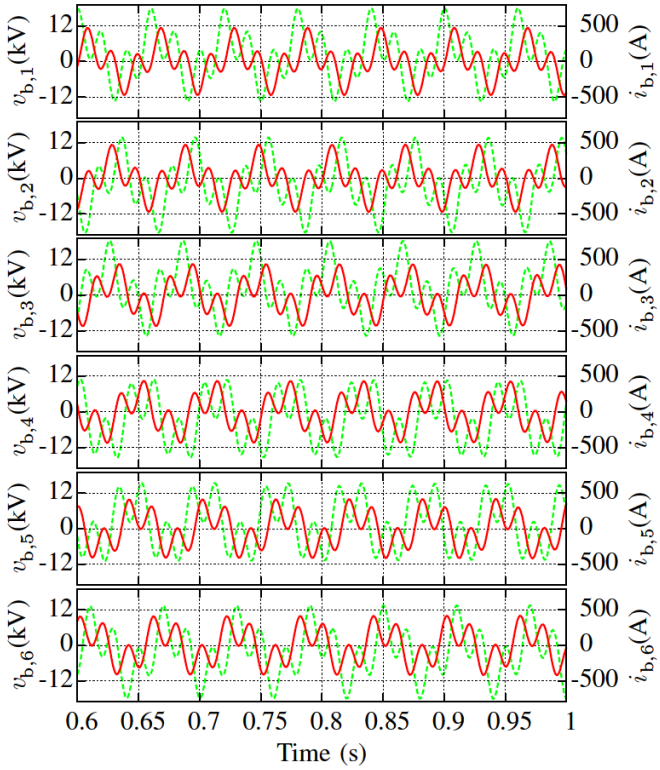

Fig. 3-2. Simulation results: Branch voltages in dashed green lines and branch currents in continuous red lines.

The shown branch voltages and currents consist of frequency components of both system frequencies. On the one hand, the current and voltage components with the lower frequency are in phase. On the other hand, the current and voltage components with the higher frequency are in phase opposition. The active branch powers resulting from the different frequencies have opposite signs and power is transferred from one system to the other. Furthermore, with the same absolute values for these powers, the DC-link capacitors of the modules are not charged or discharged and the system remains stable.

The system description of the Hexverter is based on an equivalent circuit, shown in Fig. 3-3. In this equivalent circuit, the series-connected submodules in each branch are replaced by controlled voltage sources. Additionally a resistor represents the losses in each branch. The electric network (converter and both systems) in Fig. 3-3 has twelve branches and eight nodes. According to Kirchhoff's law, these numbers of branches and nodes lead to five independent currents. Five independent currents mean five state-space variables for the describing state-space representation.

With the neutral points of the systems not connected, it is sufficient to describe the system currents in αβ-components. The two αβ-components of the currents for each system are used as the first four state-space variables. As a fifth state-space variable a so-called circulating current is defined:

$$i_{\mathrm{cir}} = \frac{1}{6} \cdot \sum_{n=1}^{6} i_{\mathrm{b},n}$$

The circulating current is an inner converter current, flowing through all six Hexverter branches without influencing the system currents. The vector of all the chosen state-space variables is:

$$\mathbf{x} = \begin{bmatrix} i_{\omega 1,\alpha} & i_{\omega 1,\beta} & i_{\omega 2,\alpha} & i_{\omega 2,\beta} & i_{\mathrm{cir}} \end{bmatrix}^T \quad .$$

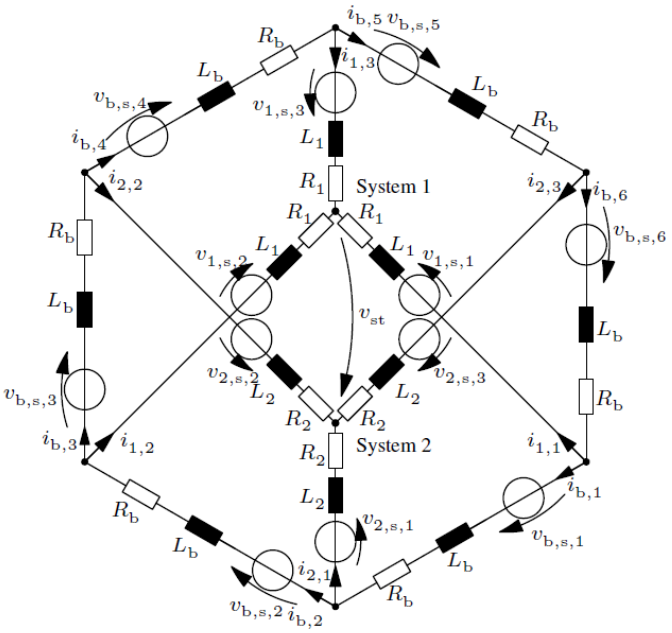

Fig. 3-3. Equivalent circuit of the Hexverter topology.

With the mesh and node equations from the equivalent circuit in Fig. 3-3 and with the chosen state-space variables, the resulting state-space representation is:

$$\frac{\partial}{\partial t}\begin{bmatrix} i_{1,\alpha}(t) \\ i_{1,\beta}(t) \\ i_{2,\alpha}(t) \\ i_{2,\beta}(t) \\ i_{\mathrm{cir}}(t) \end{bmatrix} = \boldsymbol{A}\cdot\begin{bmatrix} i_{1,\alpha}(t) \\ i_{1,\beta}(t) \\ i_{2,\alpha}(t) \\ i_{2,\beta}(t) \\ i_{\mathrm{cir}}(t) \end{bmatrix} + \boldsymbol{B}\cdot\begin{bmatrix} v_{\mathrm{b,s,1}}(t) \\ v_{\mathrm{b,s,2}}(t) \\ v_{\mathrm{b,s,3}}(t) \\ v_{\mathrm{b,s,4}}(t) \\ v_{\mathrm{b,s,5}}(t) \\ v_{\mathrm{b,s,6}}(t) \end{bmatrix} + \boldsymbol{E}\cdot\begin{bmatrix} v_{1,\mathrm{s},\alpha}(t) \\ v_{1,\mathrm{s},\beta}(t) \\ v_{1,\mathrm{s},0}(t) \\ v_{2,\mathrm{s},\alpha}(t) \\ v_{2,\mathrm{s},\beta}(t) \\ v_{2,\mathrm{s},0}(t) \end{bmatrix}.$$

The matrices **A**, **B** and **E** are

$$\boldsymbol{A} = \begin{bmatrix} k_{1,2} & 0 & l_2 & -\sqrt{3}\cdot l_2 & 0 \\ 0 & k_{1,2} & -\sqrt{3}\cdot l_2 & l_2 & 0 \\ l_1 & -\sqrt{3}\cdot l_1 & k_{2,1} & 0 & 0 \\ -\sqrt{3}\cdot l_1 & l_1 & 0 & k_{2,1} & 0 \\ 0 & 0 & 0 & 0 & -\frac{R_\mathrm{b}}{L_\mathrm{b}} \end{bmatrix},$$

$$\boldsymbol{B} = \begin{bmatrix} \frac{2\cdot L_\mathrm{b}+3\cdot L_2}{3\cdot d} & \frac{3\cdot L_2+L_\mathrm{b}}{3\cdot d} & -\frac{L_\mathrm{b}}{3\cdot d} & \frac{L_\mathrm{b}}{3\cdot d} & -\frac{3\dot{L}_2+L_\mathrm{b}}{3\cdot d} & -\frac{3\cdot L_2+2\cdot L_\mathrm{b}}{3\cdot d} \\ -\frac{L_2}{\sqrt{3}\cdot d} & -\frac{L_2+L_\mathrm{b}}{\sqrt{3}\cdot d} & \frac{2\cdot L_2+L_\mathrm{b}}{\sqrt{3}\cdot d} & \frac{2\cdot L_2+L_\mathrm{b}}{\sqrt{3}\cdot d} & \frac{L_2+L_\mathrm{b}}{\sqrt{3}\cdot d} & \frac{L_2}{\sqrt{3}\cdot d} \\ -\frac{3\cdot L_1+2\cdot L_\mathrm{b}}{3\cdot d} & \frac{3\cdot L_1+2\cdot L_\mathrm{b}}{3\cdot d} & \frac{3\cdot L_1+L_\mathrm{b}}{3\cdot d} & -\frac{L_\mathrm{b}}{3\cdot d} & \frac{L_\mathrm{b}}{3\cdot d} & -\frac{3\cdot L_1+L_\mathrm{b}}{3\cdot d} \\ -\frac{L_1}{\sqrt{3}\cdot d} & -\frac{L_1}{\sqrt{3}\cdot d} & -\frac{L_1+L_\mathrm{b}}{\sqrt{3}\cdot d} & \frac{2\cdot L_1+L_\mathrm{b}}{\sqrt{3}\cdot d} & \frac{2\cdot L_1+L_\mathrm{b}}{\sqrt{3}\cdot d} & -\frac{L_1+L_\mathrm{b}}{\sqrt{3}\cdot d} \\ -\frac{1}{6\cdot L_\mathrm{b}} & -\frac{1}{6\cdot L_\mathrm{b}} & -\frac{1}{6\cdot L_\mathrm{b}} & -\frac{1}{6\cdot L_\mathrm{b}} & -\frac{1}{6\cdot L_\mathrm{b}} & -\frac{1}{6\cdot L_\mathrm{b}} \end{bmatrix},$$

$$\boldsymbol{E} = \begin{bmatrix} -\frac{2L_\mathrm{b}+3L_2}{d} & 0 & 0 & \frac{1}{2}\frac{L_\mathrm{b}}{d} & -\frac{\sqrt{3}}{2}\frac{L_\mathrm{b}}{d} & 0 \\ 0 & -\frac{2L_\mathrm{b}+3L_2}{d} & 0 & \frac{\sqrt{3}}{2}\frac{L_\mathrm{b}}{d} & \frac{1}{2}\frac{L_\mathrm{b}}{d} & 0 \\ \frac{1}{2}\frac{L_\mathrm{b}}{d} & \frac{\sqrt{3}}{2}\frac{L_\mathrm{b}}{d} & 0 & -\frac{2L_\mathrm{b}+3L_1}{d} & 0 & 0 \\ -\frac{\sqrt{3}}{2}\frac{L_\mathrm{b}}{d} & \frac{1}{2}\frac{L_\mathrm{b}}{d} & 0 & 0 & -\frac{2L_\mathrm{b}+3L_1}{d} & 0 \\ 0 & 0 & 0 & 0 & 0 & 0 \end{bmatrix}.$$

For a better readability, several abbreviations are used:

$$d = L_\mathrm{b} \cdot (L_\mathrm{b} + 2 \cdot L_1 + 2 \cdot L_2) + 3 \cdot L_1 \cdot L_2 \,,$$
$$k_{i,j} = -\frac{R_i \cdot (2 \cdot L_\mathrm{b} + 3 \cdot L_j) + R_\mathrm{b} \cdot (L_\mathrm{b} + 2 \cdot L_j)}{d} \,,$$
$$l_i = \frac{1}{2} \cdot \frac{L_\mathrm{b} \cdot R_i - L_i \cdot R_\mathrm{b}}{d} \quad .$$

For controlling the five state-space variables only five input variables are necessary. With the six controllable voltage sources as six inputs, there is one degree of freedom in choosing the input variables. This degree of freedom is used to control the so-called star point voltage. The star point voltage is the voltage between the neutral points of the systems and is defined by:

$$v_\mathrm{st}(t) = \frac{1}{6} \cdot \sum_{n=1}^{6} \left((-1)^{(n+1)} \cdot v_{\mathrm{b,s},n}(t) \right) - v_{1,s,0}(t) + v_{2,s,0}(t) \quad .$$

Besides the six controllable source voltages of the branches, the zero sequence components of both systems $v_{1,s,0}(t), v_{2,s,0}(t)$are part of the equation. All five state-space variables and the star point voltage are independently controllable with the six input variables.

A central problem of all modular multilevel converters is controlling the energies stored in the modules DC-link capacitors. Balancing the energies of the modules within one branch is a problem addressed e.g. with sorting-based modulation concepts. Such concepts are discussed in detail for the M²LC (for example in [1]) and can be adapted for the Hexverter.

Balancing the energies between the branches is a problem specific to all modular topologies. If the branch powers

$$p_{\mathrm{b},n}(t) = v_{\mathrm{b,s},n}(t) \cdot i_{\mathrm{b},n}(t)$$

have a constant part, the branch energies

$$e_{\mathrm{b},n}(t) = \int p_{\mathrm{b},n}(t) \partial t + c_n$$

would increase or decrease continuously, i.e. the DC-link capacitors would be charged or discharged continuously. This charging or discharging would lead to a system breakdown or insufficient branch voltage reserves for controlling the system currents and the circulating current. The constant part of the branch powers of the Hexverter is

$$P_\mathrm{b,n} = -\frac{P_1 + P_2}{6} + (-1)^n \cdot \left(\frac{Q_1 - Q_2}{\sqrt{3} \cdot 6} - V_\mathrm{st} \cdot I_\mathrm{cir} \right) \,,$$

with a constant circulating current I_cir, a constant star point voltage V_st, the active powers of the two systems P_1, P_2, the reactive powers of the two systems Q_1, Q_2, and neglecting the branch inductors. This equation consists of three parts. The first part describes the active power balance of the connected systems, which is equally split up between all branches. The second part depends on the reactive powers of the systems and has a different sign for adjacent branches. Thus, for $Q_1 \neq Q_2$ there a constant branch power with different sign for adjacent branches and energy is shifted between the branches. To assure a stable operation in such operating points, the third term of the equation is used. It is defined as so-called “adjacent compensating power”

$$P_\mathrm{adj,c} = V_\mathrm{st} \cdot I_\mathrm{cir}$$

and is used to compensate the energy shifts caused by reactive powers of the systems. The necessary maximum adjacent compensating power is relevant for designing the converter

components, because the needed circulating current and star point voltage increase the occurring branch voltages and currents.

In a real system, small differences in the used components can cause energy shifts between the branches of the Hexverter. For the compensation of these energy shifts, a complete branch energy control is necessary. The basic idea for controlling all the branch energies independently is the use of circulating current components (or star point voltage components) with the frequencies of the two systems. Such components cause constant branch powers, which can be used to balance the branch energies. With a circulating current

$$i_{\mathrm{cir}}(t) = I_{\mathrm{cir}} + \hat{i}_{\mathrm{cir},\omega 1,\alpha} \cdot \cos\left(\omega_1 \cdot t\right) + \hat{i}_{\mathrm{cir},\omega 1,\beta} \cdot \cos\left(\omega_1 \cdot t - \frac{\pi}{2}\right) \ldots$$
$$+ \hat{i}_{\mathrm{cir},\omega 2,\alpha} \cdot \cos\left(\omega_2 \cdot t + \psi'\right) + \hat{i}_{\mathrm{cir},\omega 2,\beta} \cdot \cos\left(\omega_2 \cdot t + \psi' - \frac{\pi}{2}\right) ,$$

with the phasing between the two systems' voltages ψ', the constant part of the branch powers (neglecting disturbances) for different system frequencies are

$$\begin{bmatrix} P_{\mathrm{b},1} \\ P_{\mathrm{b},2} \\ P_{\mathrm{b},3} \\ P_{\mathrm{b},4} \\ P_{\mathrm{b},5} \\ P_{\mathrm{b},6} \end{bmatrix} = \underbrace{\begin{bmatrix} 1 & \frac{\hat{v}_1}{2} & 0 & -\frac{\hat{v}_2}{2} & 0 & -\frac{1}{6} \\ -1 & \frac{\hat{v}_1}{4} & -\frac{\sqrt{3}\hat{v}_1}{4} & \frac{\hat{v}_2}{2} & 0 & -\frac{1}{6} \\ 1 & -\frac{\hat{v}_1}{4} & \frac{\sqrt{3}\hat{v}_1}{4} & \frac{\hat{v}_2}{4} & -\frac{\sqrt{3}\hat{v}_2}{4} & -\frac{1}{6} \\ -1 & \frac{\hat{v}_1}{4} & \frac{\sqrt{3}\hat{v}_1}{4} & -\frac{\hat{v}_2}{4} & \frac{\sqrt{3}\hat{v}_2}{4} & -\frac{1}{6} \\ 1 & -\frac{\hat{v}_1}{4} & -\frac{\sqrt{3}\hat{v}_1}{4} & \frac{\hat{v}_2}{4} & \frac{\sqrt{3}\hat{v}_2}{4} & -\frac{1}{6} \\ -1 & -\frac{\hat{v}_1}{2} & 0 & -\frac{\hat{v}_2}{4} & -\frac{\sqrt{3}\hat{v}_2}{4} & -\frac{1}{6} \end{bmatrix}}_{\boldsymbol{M}_{\mathrm{const}}} \cdot \begin{bmatrix} P_{\mathrm{adj,c}} \\ \hat{i}_{\mathrm{cir},\omega 1,\alpha} \\ \hat{i}_{\mathrm{cir},\omega 1,\beta} \\ \hat{i}_{\mathrm{cir},\omega 2,\alpha} \\ \hat{i}_{\mathrm{cir},\omega 2,\beta} \\ \Delta P \end{bmatrix} .$$

The matrix has a full rank and all constant branch powers can be controlled independently by using the adjacent compensating power, frequency components of the circulating current and the active power balance of the systems.

Altogether, the control concept for the Hexverter is illustrated in Fig. 3-4. The control concept can be divided in the state space variable control and the branch energy control. The state space variable controllers control the system currents and the circulating current. Their output is transformed to setpoint values for the branch source voltages with the matrix **B**, to which the star point voltage is added. For the simulations, the state space variable controllers are realised with P-Resonant controllers. The input for the state space variable controller is generated by a "setpoint value generation"-block. This block calculates the setpoint values for the state space variables based on the setpoint values for the active and reactive powers of the systems and the necessary circulating current, star point voltage and difference in the active powers that are needed for the branch energy control. The circulating current, star point voltage and difference in the active powers are the output of the branch energy controller. The input of the branch energy controller is the error of the mean module energy in each branch transformed with $\boldsymbol{M}_{\mathrm{const}}^{-1}$. The branch energy controllers are realised with PI controllers in the simulation model.

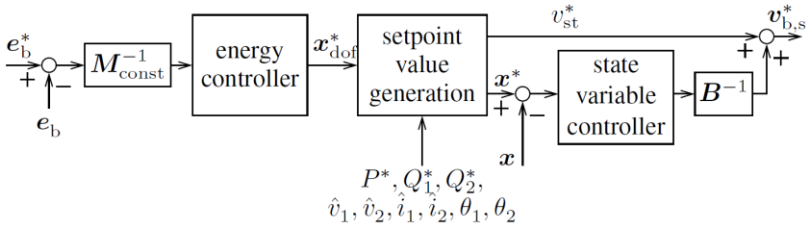

Fig. 3-4. Branch energy and state space variable control concept.

More details on the system description and the branch energy control can be found in [2], [3] and [4].

3.1.2 Modular Multilevel Matrix Converter

The second known modular multilevel direct AC/AC converter is the MMMC (Fig. 3-5). The basic building blocks (branches) of the MMMC are the same as for the Hexverter. The branches of the MMMC also consist of series-connected H-bridge modules and an inductor. In contrast to the Hexverter, the MMMC has nine branches. Accordingly, each phase of each system is connected to all phases of the other system.

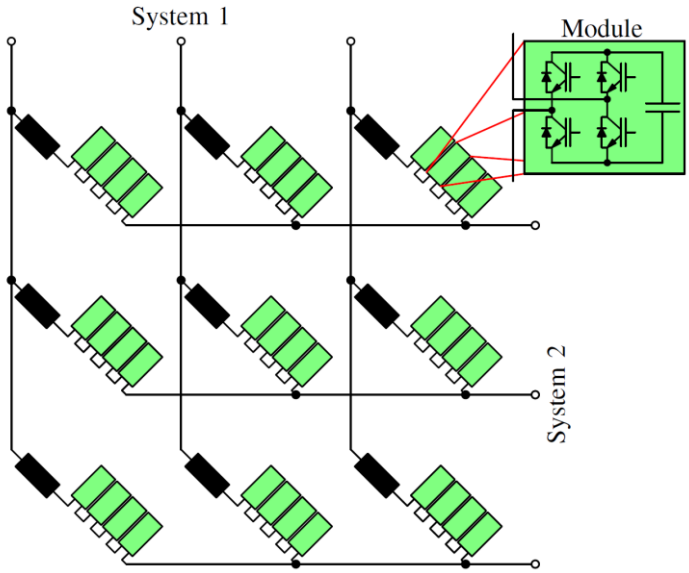

Fig. 3-5. Schematic of the Modular Multilevel Matrix Converter.

The basic concept of the MMMC is identical to the concept of the Hexverter. The branch voltages and branch currents consists of frequency components of both systems, similar to Fig. 3-2, only for nine branches.

For the system description of the MMMC an equivalent circuit is as well, Fig. 3-6. The series connected modules are replaced by controlled voltage sources and a resistor representing the losses is added.

With the higher number of branches, the electric network in Fig. 3-5 has eight independent currents. Besides the four system currents in αβ-components four circulating currents are used. The circulating currents are defined by

$$\begin{aligned} i_{\mathrm{cir},1} &= \frac{1}{4} \cdot (i_{\mathrm{b},1} - i_{\mathrm{b},2} + i_{\mathrm{b},5} - i_{\mathrm{b},4}) \\ i_{\mathrm{cir},2} &= \frac{1}{4} \cdot (i_{\mathrm{b},2} - i_{\mathrm{b},3} + i_{\mathrm{b},6} - i_{\mathrm{b},5}) \\ i_{\mathrm{cir},3} &= \frac{1}{4} \cdot (i_{\mathrm{b},4} - i_{\mathrm{b},5} + i_{\mathrm{b},8} - i_{\mathrm{b},7}) \\ i_{\mathrm{cir},4} &= \frac{1}{4} \cdot (i_{\mathrm{b},5} - i_{\mathrm{b},6} + i_{\mathrm{b},9} - i_{\mathrm{b},8}) \end{aligned} \quad ,$$

but other equivalent definitions are possible. The resulting state space representation with these circulating currents is

$$\dot{\mathbf{x}} = \mathbf{A} \cdot \mathbf{x} + \mathbf{B} \cdot \mathbf{u} + \mathbf{E} \cdot \mathbf{z} \quad .$$

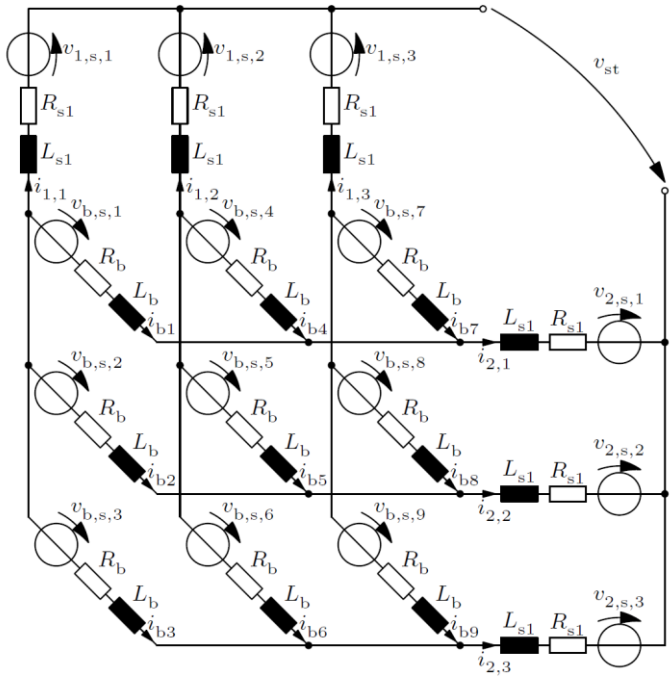

Fig. 3-6. Equivalent circuit of the Modular Multilevel Matrix Converter.

In this equation, the state vector **x**, the input vector **u** and the disturbance vector **z** are defined as

$$\mathbf{x} = \begin{bmatrix} i_{1,\alpha} & i_{1,\beta} & i_{2,\alpha} & i_{2,\beta} & i_{\mathrm{cir},1} & i_{\mathrm{cir},2} & i_{\mathrm{cir},3} & i_{\mathrm{cir},4} \end{bmatrix}^T$$
$$\mathbf{u} = \begin{bmatrix} v_{\mathrm{b,s},1} & \dots & v_{\mathrm{b,s},9} \end{bmatrix}^T$$
$$\mathbf{z} = \begin{bmatrix} v_{1,\mathrm{s},\alpha} & v_{1,\mathrm{s},\beta} & v_{1,\mathrm{s},0} & v_{2,\mathrm{s},\alpha} & v_{2,\mathrm{s},\beta} & v_{2,\mathrm{s},0} \end{bmatrix}^T .$$

The matrices **A**, **B** and **E** are

$$\mathbf{A} = \begin{bmatrix} -\frac{R_\mathrm{b}}{L_\mathrm{b}} & 0 & 0 & 0 & 0 & 0 & 0 & 0 \\ 0 & -\frac{R_\mathrm{b}}{L_\mathrm{b}} & 0 & 0 & 0 & 0 & 0 & 0 \\ 0 & 0 & -\frac{R_\mathrm{b}}{L_\mathrm{b}} & 0 & 0 & 0 & 0 & 0 \\ 0 & 0 & 0 & -\frac{R_\mathrm{b}}{L_\mathrm{b}} & 0 & 0 & 0 & 0 \\ 0 & 0 & 0 & 0 & -\frac{R_\mathrm{b}+3R_{\mathrm{s}1}}{r} & 0 & 0 & 0 \\ 0 & 0 & 0 & 0 & 0 & -\frac{R_\mathrm{b}+3R_{\mathrm{s}1}}{r} & 0 & 0 \\ 0 & 0 & 0 & 0 & 0 & 0 & -\frac{R_\mathrm{b}+3R_{\mathrm{s}2}}{q} & 0 \\ 0 & 0 & 0 & 0 & 0 & 0 & 0 & -\frac{R_\mathrm{b}+3R_{\mathrm{s}2}}{q} \end{bmatrix},$$

$$\mathbf{B} = \begin{bmatrix} -\frac{1}{4L_\mathrm{b}} & \frac{1}{4L_\mathrm{b}} & 0 & \frac{1}{4L_\mathrm{b}} & -\frac{1}{4L_\mathrm{b}} & 0 & 0 & 0 & 0 \\ 0 & -\frac{1}{4L_\mathrm{b}} & \frac{1}{4L_\mathrm{b}} & 0 & \frac{1}{4L_\mathrm{b}} & -\frac{1}{4L_\mathrm{b}} & 0 & 0 & 0 \\ 0 & 0 & 0 & -\frac{1}{4L_\mathrm{b}} & \frac{1}{4L_\mathrm{b}} & 0 & \frac{1}{4L_\mathrm{b}} & -\frac{1}{4L_\mathrm{b}} & 0 \\ 0 & 0 & 0 & 0 & -\frac{1}{4L_\mathrm{b}} & \frac{1}{4L_\mathrm{b}} & 0 & \frac{1}{4L_\mathrm{b}} & -\frac{1}{4L_\mathrm{b}} \\ \frac{2}{3r} & \frac{2}{3r} & \frac{2}{3r} & -\frac{1}{3r} & -\frac{1}{3r} & -\frac{1}{3r} & -\frac{1}{3r} & -\frac{1}{3r} & -\frac{1}{3r} \\ 0 & 0 & 0 & \frac{1}{\sqrt{3}r} & \frac{1}{\sqrt{3}r} & \frac{1}{\sqrt{3}r} & -\frac{1}{\sqrt{3}r} & -\frac{1}{\sqrt{3}r} & -\frac{1}{\sqrt{3}r} \\ -\frac{2}{3q} & \frac{1}{3q} & \frac{1}{3q} & -\frac{2}{3q} & \frac{1}{3q} & \frac{1}{3q} & -\frac{2}{3q} & \frac{1}{3q} & \frac{1}{3q} \\ 0 & -\frac{1}{\sqrt{3}q} & \frac{1}{\sqrt{3}q} & 0 & -\frac{1}{\sqrt{3}q} & \frac{1}{\sqrt{3}q} & 0 & -\frac{1}{\sqrt{3}q} & \frac{1}{\sqrt{3}q} \end{bmatrix},$$

$$\mathbf{E} = \begin{bmatrix} 0 & 0 & 0 & 0 & 0 & 0 \\ 0 & 0 & 0 & 0 & 0 & 0 \\ 0 & 0 & 0 & 0 & 0 & 0 \\ 0 & 0 & 0 & 0 & 0 & 0 \\ -\frac{3}{r} & 0 & 0 & 0 & 0 & 0 \\ 0 & -\frac{3}{r} & 0 & 0 & 0 & 0 \\ 0 & 0 & 0 & -\frac{3}{q} & 0 & 0 \\ 0 & 0 & 0 & 0 & -\frac{3}{q} & 0 \end{bmatrix}.$$

(INNWIND. EU. Deliverable 3.32, Converter designs based on new components and modular multilevel topologies)

In **A**, **B** and **E** the two abbreviations

$$r = L_{\mathrm{b}} + 3 \cdot L_{\mathrm{s1}}$$
$$q = L_{\mathrm{b}} + 3 \cdot L_{\mathrm{s2}}$$

are used. Equally to the Hexverter topology, there is one more controllable voltage source as input than there are independent currents in the system. This additional degree of freedom in choosing the input values is used to control the star point voltage, which is defined by:

$$v_{\mathrm{st}} = \left(\frac{1}{9} \cdot \sum_{n=1}^{9} v_{\mathrm{b,s},n} \right) - v_{1,\mathrm{s},0} + v_{2,\mathrm{s},0} \,.$$

All system currents, the four circulating currents and the star point voltage are independently controllable with the nine controlled voltage sources as input.

The main difference in the branch energy control of the MMMC compared to the Hexverter is that no adjacent compensating power is necessary. This fact can be seen in the constant part of the branch powers under neglection of the branch inductors and without circulating currents and star point voltage:

$$P_{\mathrm{b,n}} = -\frac{P_1 + P_2}{9} \,.$$

Only the active power balance influences the constant part of the branch powers, the reactive powers of the system have no influence. Hence no adjacent compensating power equivalent is necessary, which is advantageous for the components design.

Nevertheless, small differences in the used components can cause energy shifts between the branches, what must be handled with a complete branch energy control. The approach for the complete branch energy control is identical to the approach for the Hexverter. Components in the circulating current with the systems' frequencies are used as degrees of freedom for controlling the constant part of the branch energies. With the higher number of circulating currents different combinations of degrees of freedom are possible. The chosen combination for the simulation leads to the constant part of the branch powers:

$$\begin{bmatrix} P_{\mathrm{b},1} \\ P_{\mathrm{b},2} \\ P_{\mathrm{b},3} \\ P_{\mathrm{b},4} \\ P_{\mathrm{b},5} \\ P_{\mathrm{b},6} \\ P_{\mathrm{b},7} \\ P_{\mathrm{b},8} \\ P_{\mathrm{b},9} \end{bmatrix} = \underbrace{\frac{1}{9} \begin{bmatrix} -8\hat{v}_1 & 8\hat{v}_2 & -4\hat{v}_1 & 0 & -4\hat{v}_1 & 0 & -2\hat{v}_1 & 2\hat{v}_2 & 1 \\ 4\hat{v}_1 & 2\hat{v}_2 & -4\hat{v}_1 & 2\sqrt{3}\hat{v}_2 & 2\hat{v}_1 & -\sqrt{3}\hat{v}_2 & -2\hat{v}_1 & -\hat{v}_2 & 1 \\ 4\hat{v}_1 & 2\hat{v}_2 & 8\hat{v}_1 & 4\sqrt{3}\hat{v}_2 & 2\hat{v}_1 & \sqrt{3}\hat{v}_2 & 4\hat{v}_1 & 2\hat{v}_2 & 1 \\ -2\hat{v}_1 & -4\hat{v}_2 & -\hat{v}_1 & 0 & 2\hat{v}_1 & 0 & \hat{v}_1 & 2\hat{v}_2 & 1 \\ \hat{v}_1 & -\hat{v}_2 & -\hat{v}_1 & -\sqrt{3}\hat{v}_2 & -\hat{v}_1 & -\sqrt{3}\hat{v}_2 & \hat{v}_1 & -\hat{v}_2 & 1 \\ \hat{v}_1 & -\hat{v}_2 & 2\hat{v}_1 & -2\sqrt{3}\hat{v}_2 & -\hat{v}_1 & \sqrt{3}\hat{v}_2 & -2\hat{v}_1 & 2\hat{v}_2 & 1 \\ -2\hat{v}_1 & -4\hat{v}_2 & -\hat{v}_1 & 0 & -4\hat{v}_1 & 0 & -2\hat{v}_1 & -4\hat{v}_2 & 1 \\ \hat{v}_1 & -\hat{v}_2 & -\hat{v}_1 & -\sqrt{3}\hat{v}_2 & 2\hat{v}_1 & 2\sqrt{3}\hat{v}_2 & -2\hat{v}_1 & 2\hat{v}_2 & 1 \\ \hat{v}_1 & -\hat{v}_2 & 2\hat{v}_1 & -2\sqrt{3}\hat{v}_2 & 2\hat{v}_1 & -2\sqrt{3}\hat{v}_2 & 4\hat{v}_1 & -4\hat{v}_2 & 1 \end{bmatrix}}_{\boldsymbol{M}_{\mathrm{const}}} \cdot \begin{bmatrix} \hat{i}_{\mathrm{cir},1,\omega_1,\alpha} \\ \hat{i}_{\mathrm{cir},1,\omega_2,\alpha} \\ \hat{i}_{\mathrm{cir},2,\omega_1,\alpha} \\ \hat{i}_{\mathrm{cir},2,\omega_2,\beta} \\ \hat{i}_{\mathrm{cir},3,\omega_1,\alpha} \\ \hat{i}_{\mathrm{cir},3,\omega_2,\beta} \\ \hat{i}_{\mathrm{cir},4,\omega_1,\alpha} \\ \hat{i}_{\mathrm{cir},4,\omega_2,\alpha} \\ \Delta P \end{bmatrix} .$$

The matrix $\boldsymbol{M}_{\mathrm{const}}$ has full rank and all constant branch powers are independently controllable by using the chosen combination of frequency components of the circulating currents and the active power balance of the systems.

The control concept is based on Fig. 3-4 as well. It is similar to the one described for the Hexverter and is thus not explained in detail again. The only differences are the higher number of controllers due to the higher number of branches and state space variables; and the fact, that the star point voltage is always controlled to zero as no compensating adjacent power is needed. More information on the control of the MMMC is given in [5], [6] and [7].

Control methods for special operating points based on additional circulating currents are already investigated for the MMMC, [7, 8, 9]. These methods address operation at very low frequencies for one of the systems and for similar system frequencies. They aim to reduce the branch energy variation and to reduce the capacity demand by this. Fig. 3-7 shows the influence of the control methods on the maximum branch energy variation in principle. The reduction of the maximum branch energy variation comes along with the disadvantage of a higher maximum branch current. Nevertheless, for low nominal system frequencies in one system the reduced capacitor demand outweighs the increased semiconductor demand by far.

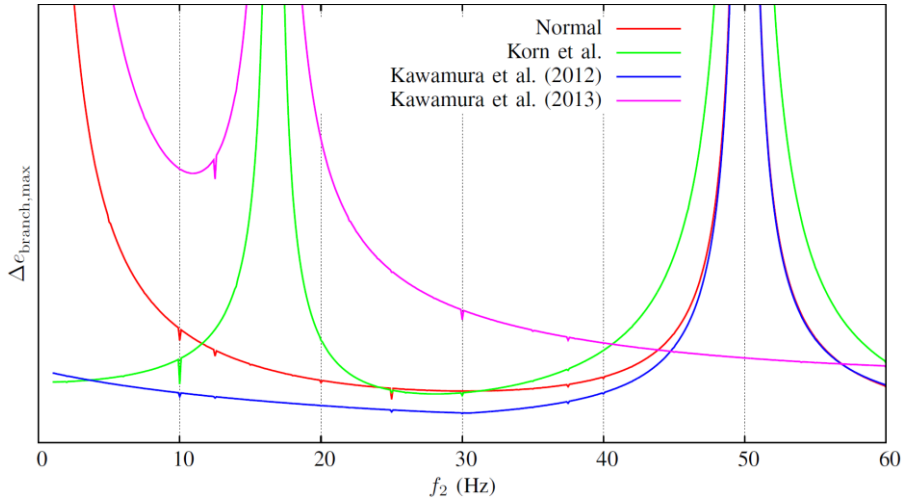

Fig. 3-7. Different control methods for the Modular Multilevel Matrix Converter, with f_1 = 50 Hz and varying f_2.

3.1.3 Operation with equal system frequencies

The operation of modular multilevel direct AC/AC converters with equal system frequencies is always problematic, because voltage and current components of different systems in the branch voltages cause additional constant parts in the branch powers. Additionally, the circulating current (and star point voltage) components for the two system frequencies influence the branch powers in the same way for equal frequencies, which reduces the number of degrees of freedom for the branch energy control.

This problem is described in [3] for the Hexverter topology. For the branch energy control, starpoint voltage and circulating current components are used. The resulting equation for the constant part of the branch powers (neglecting disturbances) is

$$\begin{bmatrix} P_{\mathrm{b},1} \\ P_{\mathrm{b},2} \\ P_{\mathrm{b},3} \\ P_{\mathrm{b},4} \\ P_{\mathrm{b},5} \\ P_{\mathrm{b},6} \end{bmatrix} = \begin{bmatrix} 1 & \frac{\hat{v}_1+\hat{v}_2\cos(\psi+\pi)}{2} & \frac{\hat{v}_2\cos(\psi-\frac{\pi}{2})}{2} \\ -1 & \frac{\hat{v}_1+2\hat{v}_2\cos(\psi)}{4} & \frac{-\sqrt{3}\hat{v}_1+2\hat{v}_2\cos(\psi+\frac{\pi}{2})}{4} \\ 1 & \frac{-\hat{v}_1+2\hat{v}_2\cos(\psi+\frac{\pi}{3})}{4} & \frac{\sqrt{3}\hat{v}_1+2\hat{v}_2\cos(\psi+\frac{5\pi}{6})}{4} \\ -1 & \frac{\hat{v}_1+2\hat{v}_2\cos(\psi-\frac{2\pi}{3})}{4} & \frac{\sqrt{3}\hat{v}_1+2\hat{v}_2\cos(\psi-\frac{\pi}{6})}{4} \\ 1 & \frac{-\hat{v}_1+2\hat{v}_2\cos(\psi-\frac{\pi}{3})}{4} & \frac{-\sqrt{3}\hat{v}_1+2\hat{v}_2\cos(\psi+\frac{\pi}{6})}{4} \\ -1 & \frac{-\hat{v}_1+\hat{v}_2\cos(\psi+\frac{2\pi}{3})}{2} & \frac{\hat{v}_2\cos(\psi-\frac{5\pi}{6})}{2} \end{bmatrix} \cdots$$

$$\begin{bmatrix} \frac{-3\hat{i}_1+2\sqrt{3}\hat{i}_2\cos(\psi+\varphi_1-\varphi_2-\frac{\pi}{6})}{12} & \frac{\sqrt{3}\hat{i}_1+2\sqrt{3}\hat{i}_2\cos(\psi+\varphi_1-\varphi_2+\frac{\pi}{3})}{12} & -\frac{1}{6} \\ \frac{3\hat{i}_1+2\sqrt{3}\hat{i}_2\cos(\psi+\varphi_1-\varphi_2+\frac{\pi}{6})}{12} & \frac{-\sqrt{3}\hat{i}_1+2\sqrt{3}\hat{i}_2\cos(\psi+\varphi_1-\varphi_2+\frac{2\pi}{3})}{12} & -\frac{1}{6} \\ \frac{\sqrt{3}\hat{i}_2\cos(\psi+\varphi_1-\varphi_2-\frac{5\pi}{6})}{6} & \frac{-\sqrt{3}\hat{i}_1+\sqrt{3}\hat{i}_2\cos(\psi+\varphi_1-\varphi_2-\frac{\pi}{3})}{6} & -\frac{1}{6} \\ \frac{\sqrt{3}\hat{i}_2\cos(\psi+\varphi_1-\varphi_2-\frac{\pi}{2})}{6} & \frac{\sqrt{3}\hat{i}_1+\sqrt{3}\hat{i}_2\cos(\psi+\varphi_1-\varphi_2)}{6} & -\frac{1}{6} \\ \frac{3\hat{i}_1+2\sqrt{3}\hat{i}_2\cos(\psi+\varphi_1-\varphi_2+\frac{\pi}{2})}{12} & \frac{\sqrt{3}\hat{i}_1+2\sqrt{3}\hat{i}_2\cos(\psi+\varphi_1-\varphi_2+\pi)}{12} & -\frac{1}{6} \\ \frac{-3\hat{i}_1+2\sqrt{3}\hat{i}_2\cos(\psi+\varphi_1-\varphi_2+\frac{5\pi}{6})}{12} & \frac{-\sqrt{3}\hat{i}_1+2\sqrt{3}\hat{i}_2\cos(\psi+\varphi_1-\varphi_2-\frac{2\pi}{3})}{12} & -\frac{1}{6} \end{bmatrix} \cdot \begin{bmatrix} P_{\mathrm{comp}} \\ \hat{i}_{\mathrm{cir},\omega 1,\alpha} \\ \hat{i}_{\mathrm{cir},\omega 1,\beta} \\ \hat{v}_{\mathrm{st},\omega 1,\alpha} \\ \hat{v}_{\mathrm{st},\omega 1,\beta} \\ P_1 \end{bmatrix} \cdot$$

g e

(INNWIND. EU. Deliverable 3.32, Converter designs based on new components and modular multilevel topologies)

The matrix in this equation depends on the phasing between the two systems and does not have a full rank for all operating points. Thus, the branch energies of the Hexverter are not controllable in all operating point. As a consequence, the Hexverter topology should not be used continuously with equal system frequencies.

The number of degrees of freedom for the branch energy control of the MMMC is reduced as well. In general, a branch energy control for equal frequencies should be possible, but no previous publication addresses this problem. [9] only presents the additional branch currents lowering the branch energy variation but does not investigate the necessary changes for a complete branch energy control. A detailed investigation of the branch energy control for equal frequencies is necessary for the component design and control of the converter. Such an investigation would go beyond the scope of this report. This is why the MMMC is not considered for operation with equal frequencies as well.

3.2 Component design

In this section an estimation of the values for the relevant converter components is presented. Based on this estimation the topologies are compared. The parameters for the comparison are the installed capacity for the DC-link of the modules, the installed inductance for the branch inductors, the number of modules and the switching power of the modules' semiconductor switches. Besides, the maximum branch current and the maximum branch voltage are given.
In total, there are six different scenarios. For the generator of the wind turbine system three different nominal electric frequencies are used:

- 2.5 Hz
- 25 Hz
- 50 Hz.

A nominal electric frequency of 2.5 Hz represents a superconducting direct drive generator. For representing a pseudo direct drive generator, 50 Hz are used. In addition, an electric frequency of 25 Hz is also considered.

For all three nominal electric generator frequencies, two nominal active powers are investigated:

- 10 MW
- 20 MW.

The minimum power factor range on the grid-side is from 0.95 leading to 0.95 lagging, which is chosen as an example according to the Federal Energy Regulatory Commission (FERC, USA).

Depending on the nominal electric generator powers, different nominal voltages for the generator and grid-side are used:

- 3.3 kV (for 10 MW)
- 6.6 kV (for 20 MW).

The voltages are given as rms-values of the line to line voltage. The grid-side voltage is identical to the nominal generator voltage, because a grid-side transformer is assumed to transform the voltage to the collection grid level. This grid-side transformer is equal for the different topologies and is not part of the comparison of the different topologies.

In summary, the six scenarios for the comparison of the topologies are given in Table 3-1:

Table 3-1. Generator scenarios

Scenario	Maximum power in MW	Nominal generator voltage in kV	Nominal generator frequency in Hz
1	10	3.3	2.5
2	10	3.3	25
3	10	3.3	50
4	20	6.6	2.5
5	20	6.6	25
6	20	6.6	50

For both topologies, the same constraints for the DC-link of the modules are chosen. IGBTs with 1700 V blocking voltage are used for the modules. In normal operation, the DC-link voltage is restricted to a minimum of 800 V for a single module. Due to the lifetime of the IGBTS, the maximum DC-link voltage is restricted to 1100 V. The setpoint for the DC-link voltage is chosen at 962 V, so that in positive and negative direction, the same amount of differential energy can be accommodated within the voltage limits. Additionally, the voltage variation in normal operation is restricted to 96.2 V (10 % of the set point DC-link voltage).
As described in section 3.1.3, operation of the Hexverter and the MMMC with equal system frequencies is not considered. For this reason, suitability of both topologies for scenarios 3 and 6 cannot be judged without further investigations and therefore no component design is done. For reducing the capacity demand in case of low frequencies in system 2, the MMMC is operated with the method presented in [8].

3.2.1 Number of modules

The number of modules of a modular multilevel converter indicates the mechanical complexity of the system. A higher number of modules results in a larger volume of the converter and a higher cost for the mechanical construction.

For this simplified comparison, the number of necessary modules is calculated based on stationary operation. The number of modules per branch is defined by the minimum DC-link voltage and the maximum branch voltage. In a worst case scenario, all modules in a branch only have the allowed minimum DC-link voltage. These modules must still be able to synthesise the maximum branch voltage, otherwise the converter currents would not be controllable any more.

The upper limit of the branch voltage of the Hexverter can be calculated using the equivalent circuit in Fig. 3-3. Each branch voltage consists of one phase voltage of system 1, one phase voltage of system 2 and the star point voltage. Accordingly, the upper limit for the branch voltage of the Hexverter is

$$v_{\mathrm{b,max}} = \hat{v}_{1,\mathrm{max}} + \hat{v}_{2,\mathrm{max}} + v_{\mathrm{st,max}} \,.$$

The resulting number of modules per branch for the Hexverter is

$$n_{\mathrm{mpb}} = \frac{\hat{v}_{1,\mathrm{max}} + \hat{v}_{2,\mathrm{max}} + v_{\mathrm{st,max}}}{V_{\mathrm{mod,min}}} \,.$$

The total number of modules for the Hexverter topology for all scenarios is calculated based on this equation, and the results are given in Table 3-2.

Table 3-2. Total number of modules for the Hexverter topology

Scenario	1	2	3	4	5	6
Number of modules	48	48	-	96	96	-

For the MMMC, the upper limit of the branch voltages is calculated based on the equivalent circuit in Fig. 3-6. As described above, the star point voltage of the MMMC can always be chosen to zero. For this reason, the upper limit of the branch voltage of the MMMC is

$$v_{\mathrm{b,max}} = \hat{v}_{1,\mathrm{max}} + \hat{v}_{2,\mathrm{max}}$$

and the number of modules per branch is

$$n_{\mathrm{mpb}} = \frac{\hat{v}_{1,\mathrm{max}} + \hat{v}_{2,\mathrm{max}}}{V_{\mathrm{mod,min}}} .$$

It is obvious, that the number of modules per branch is lower for the MMMC. However, the MMMC has nine branches, but the Hexverter has only six branches. For the considered scenarios, the total number of modules of the MMMC is higher compared to the Hexverter. It is presented in Table 3-3.

Table 3-3. Total number of modules for the Modular Multilevel Matrix Converter

Scenario	1	2	3	4	5	6
Number of modules	63	63	-	126	126	-

3.2.2 Switch Power

The switching power of the modules' semiconductor switches can be used as an indicator for the weighed chip size. Thus the switching power is also a cost indicator. The switching power of a single switch is defined by the product of its blocking voltage and the maximum current. The total switching power of a converter is the sum of the switching power of all switches.

The six Hexverter branches with modules comprising four switches lead to a minimum switching power

$$P_{\mathrm{sw,min}} = 6 \cdot 4 \cdot n_{\mathrm{mpb}} \cdot \frac{v_{\mathrm{b,max}}}{n_{\mathrm{mpb}}} \cdot i_{\mathrm{b,max}} = 6 \cdot 4 \cdot v_{\mathrm{b,max}} \cdot i_{\mathrm{b,max}} ,$$

[2]. This minimum switching power is calculated without considering any safety margins and is only used for the comparison. For the calculation of the switching power the maximum branch voltage and the maximum branch current are relevant. The upper limit for the branch voltage is already given, the upper limit for the branch current can be given with

$$i_{\mathrm{b,max}} = \frac{\hat{i}_{1,\mathrm{max}} + \hat{i}_{2,\mathrm{max}}}{\sqrt{3}} + i_{\mathrm{cir,max}} .$$

As a consequence, the switching power depends on the maximum star point voltage and on the maximum circulating current. Both are used to create the adjacent compensating power (see section 3.1.1). For the same adjacent compensating power, different combinations of star point voltage and circulating current are possible. The switching power of the converter can be minimised by using

$$\xi = \frac{V_{\mathrm{st}}}{I_{\mathrm{cir}}} = \pm\sqrt{3} \cdot \frac{\hat{v}_{1,\mathrm{max}} + \hat{v}_{2,\mathrm{max}}}{\hat{i}_{1,\mathrm{max}} + \hat{i}_{2,\mathrm{max}}} ,$$

[2]. For all calculations, the star point voltage and circulating current are chosen with regard to this minimum. The resulting switching power of the Hexverter for all scenarios is given in Table 3-4.

Table 3-4. Total switching power of the Hexverter

Scenario	1	2	3	4	5	6
Switching power in MW	494	494	-	988	988	-

Analogue to the calculations for the Hexverter, the switching power of the MMMC can be determined. With nine branches with modules comprising four switches, the minimum switching power of the MMMC is

$$P_{\mathrm{sw,min}} = 9 \cdot 4 \cdot n_{\mathrm{mpb}} \cdot \frac{v_{\mathrm{b,max}}}{n_{\mathrm{mpb}}} \cdot i_{\mathrm{b,max}} = 9 \cdot 4 \cdot v_{\mathrm{b,max}} \cdot i_{\mathrm{b,max}} \,.$$

The upper limit for the branch voltage of the MMMC can be found in section 3.2.1, the upper limit for the branch current is

$$i_{\mathrm{b,max}} = \frac{\hat{i}_{1,\mathrm{max}} + \hat{i}_{2,\mathrm{max}}}{3} \,.$$

This upper limit for the branch current does not contain any circulating current, because no equivalent to the adjacent compensating power of the Hexverter is necessary, which could cause higher circulating currents. For normal operation, circulating currents are only used for the complete branch energy control. This branch energy control needs only to handle small energy shifts caused by component differences. Thus, these circulating currents are small and will be neglected for all estimations. The switching power of the MMMC in all scenarios is presented in Table 3-5.

Table 3-5. Switching power of the Modular Multilevel Matrix Converter

Scenario	1	2	3	4	5	6
Switching power in MW	497	328	-	994	657	-

For Scenario 2 and 5 (25 Hz), the higher branch voltages (caused by the star point voltage) and the higher branch currents of the Hexverter result in a higher switching power compared to the MMMC, even with a lower number of modules. For the low frequency scenarios, the additional circulating currents used for the MMMC lead to a slightly higher switching power compared to the Hexverter.

3.2.3 Installed Capacity

Besides the semiconductor switches, the capacitors in the modules' DC-link are one of the main cost factors of modular multilevel converters. The DC-link capacitors are designed based on the DC-link voltage variation restriction. The voltage variation is caused by the energy variation in the modules. For the simplified comparison, it is assumed that the branch energy variation is distributed equally between all modules in a branch. Besides that, the energy stored in the branch inductors is neglected because it is small compared to the energy stored in the DC-link capacitors.

The branch energy variation is calculated based on the equivalent circuits in Fig. 3-3 and Fig. 3-6. Ideal system voltages and system currents are used to calculate the branch voltages and branch currents. The resulting branch powers lead to the branch energy. The maximum branch energy variation results from these branch energy curves. A high number of system periods are investigated and calculations with different phasing between the two systems in the beginning are done, for ensuring to calculate the maximum branch energy variation as accurate as possible.

For the Hexverter topology, the calculation of the maximum branch energy variation leads to the results shown in Table 3-6. The results for the maximum branch energy variation of the MMMC are given in Table 3-7.

Table 3-6. Maximum branch energy variation for the Hexverter topology

Scenario	1	2	3	4	5	6
Maximum branch energy variation in kJ	357.5	42.9	-	714.9	85.7	-

Table 3-7. Maximum branch energy variation of the Modular Multilevel Matrix Converter

Scenario	1	2	3	4	5	6
Maximum branch energy variation in kJ	20.5	13.3	-	41.0	26.5	-

The maximum branch energy variation is used to design the DC-link capacitors. With the constraints for the maximum DC-link voltage $v_{\mathrm{mod,max}}$, minimum DC-link voltage $v_{\mathrm{mod,min}}$, and the maximum DC-link voltage variation Δv_{mod} the capacitor can be determined by

$$C_{\mathrm{mod}} = \frac{\Delta e_{\mathrm{branch,max}}}{n_{\mathrm{mpb}}} \cdot \frac{2}{\Delta v_{\mathrm{mod}} \cdot \sqrt{2 \cdot {v_{\mathrm{mod,min}}}^2 + 2 \cdot {v_{\mathrm{mod,max}}}^2 - {\Delta v_{\mathrm{mod}}}^2}}.$$

For this equation, the minimum and maximum energy of a module is expressed with the minimum and maximum DC-link voltage. Then the mean energy is calculated, which leads to a mean DC-link voltage. The capacitor is chosen for a DC-link voltage variation around this mean DC-link voltage. The total capacity of the converter results from this DC-link capacitor and the total number of modules of the converter. Table 3-8 shows the total capacity of the Hexverter and Table 3-9 shows the total capacity of the MMMC. It is important to notice, that these values are not directly comparable to the total capacity of the 2-level and 3-level converters, because the DC-link voltages differ.

Table 3-8. Total capacity of the Hexverter topology (with 1100 V maximum DC-link voltage)

Scenario	1	2	3	4	5	6
Total capacity in F	23.2	2.8	-	46.4	5.6	-

Table 3-9. Total capacity of the Modular Multilevel Matrix Converter (with 1100 V maximum DC-link voltage)

Scenario	1	2	3	4	5	6
Total capacity in F	2.0	1.3	-	4.0	2.6	-

It can be seen, that the higher branch energy variation of the Hexverter leads to a higher capacity demand compared to the MMMC, even with a lower number of branches.

3.2.4 Installed Inductance

The branch inductors in modular multilevel converter ensure a continuous branch current. The current ripple caused by the switching events of the series-connected branch modules must be limited by the branch inductor. This requirement is the basis for designing the inductance of the branch inductors.

For the comparison of the topologies worst case scenarios without consideration of optimised modulation methods are assumed. These worst case scenarios mean that simultaneous switching events in all branches can occur at the same moment. However, it is still assumed that only one module in each branch changes its switching state.

The maximum change of a voltage drop across a branch inductor is calculated based on the equivalent circuit, neglecting any resistors and the two systems. Without the two systems, the voltage drop across the inductor in branch 1 of the Hexverter is

$$\Delta v_{\mathrm{Lb}} = L_{\mathrm{b}} \frac{\partial i_{\mathrm{b},1}}{\partial t} = \frac{1}{6} \cdot \left(v_{\mathrm{b,s1}} + v_{\mathrm{b,s2}} + v_{\mathrm{b,s3}} + v_{\mathrm{b,s4}} + v_{\mathrm{b,s5}} + v_{\mathrm{b,s6}} \right) .$$

As a result, the maximum change in the voltage drop across a branch inductor with simultaneous switching events in all branches is

$$\Delta v_{\mathrm{Lb,max}} = \frac{1}{6} \cdot 6 \cdot V_{\mathrm{mod,max}} = V_{\mathrm{mod,max}} .$$

This result is identical for the voltage drops across all branch inductors of the Hexverter.

Under the same assumptions, the voltage drop across the inductor of branch 1 of the MMMC is

$$\begin{aligned} \Delta v_{\mathrm{Lb}} &= L_{\mathrm{b}} \frac{\partial i_{\mathrm{b},1}}{\partial t} \\ &= -\frac{4v_{\mathrm{b,s1}} - 2v_{\mathrm{b,s2}} - 2v_{\mathrm{b,s3}} - 2v_{\mathrm{b,s4}} + v_{\mathrm{b,s5}} + v_{\mathrm{b,s6}} - 2v_{\mathrm{b,s7}} + v_{\mathrm{b,s8}} + v_{\mathrm{b,s9}}}{9} . \end{aligned}$$

Simultaneous switching events in all branches of the MMMC lead to the maximum voltage drop across a branch inductor:

$$\Delta v_{\mathrm{Lb,max}} = \frac{16}{9} \cdot V_{\mathrm{mod,max}} .$$

The apparent switching frequency of each module is 600 Hz (300 Hz for each switch), according to the apparent switching frequency for each M²LC module. The apparent switching frequency of the branch voltage results from this module switching frequency and the number of modules per branch. The maximum branch current ripple is demanded to be lower than 10 % of the maximum branch current. With the maximum voltage drop across the branch inductors in case of a switching event, the apparent switching frequency of the branch voltages, and the demanded branch current ripple, the necessary branch inductance can be calculated. For the Hexverter it is

$$L_{\mathrm{b}} = \frac{\Delta v_{\mathrm{Lb,max}}}{2 \cdot f_{\mathrm{sw,app}} \cdot \Delta i_{\mathrm{b,max}}} = \frac{V_{\mathrm{mod,max}}}{2 \cdot f_{\mathrm{sw,app}} \cdot \Delta i_{\mathrm{b,max}}}$$

and for the MMMC it is

$$L_{\mathrm{b}} = \frac{\Delta v_{\mathrm{Lb,max}}}{2 \cdot f_{\mathrm{sw,app}} \cdot \Delta i_{\mathrm{b,max}}} = \frac{8 \cdot V_{\mathrm{mod,max}}}{9 \cdot f_{\mathrm{sw,app}} \cdot \Delta i_{\mathrm{b,max}}} .$$

These equations show that the branch inductance of the Hexverter is smaller than the branch inductance of the MMMC. Besides, the number of branches of the MMMC is higher. Nevertheless

the maximum branch current of the Hexverter is higher, which also influence size and cost of the inductor. The resulting total inductance and the maximum stored energy (calculated with the maximum branch current) for the six scenarios are presented in Table 3-10 for the Hexverter and Table 3-11 for the MMMC.

Table 3-10. Total inductance and maximum stored energy of the Hexverter topology

Scenario	1	2	3	4	5	6
Total inductance in mH	1.0	1.0	-	0.5	0.5	-
Maximum stored energy in kJ	5.6	5.6	-	2.8	2.8	-

Table 3-11. Total inductance of the Modular Multilevel Matrix Converter

Scenario	1	2	3	4	5	6
Total inductance in mH	2.7	4.1	-	1.4	2.1	-
Maximum stored energy in kJ	8.8	5.9	-	4.6	3.0	-

3.2.5 Summary

All results of the component design are shown in Table 3-12. Additionally, the maximum branch currents and maximum branch voltage are given. The results show, that the MMMC has advantages regarding the semiconductor and capacitor demand. The total inductance of the Hexverter is lower, but it is problematic to compare these results, because the maximum branch currents through the inductors are different. The maximum stored energy of the branch inductors shows that the branch inductors of the Hexverter will be clearly cheaper for the scenarios 1, 4 and slightly cheaper for the scenarios 2, 6. The number of modules of the MMMC is higher than the number of modules of the Hexverter.

Which topology is most advantageous for a scenario depends on the ratio between semiconductor and capacitor costs and the modules offset cost (driver, electronics, etc.) and the cost for mechanical construction. For high power with higher semiconductor and capacitors costs, the MMMC is the preferable topology. In case of lower power, for which mechanical costs and module offset cost have a higher influence, the Hexverter can be advantageous.

Table 3-12. Component design results (H: Hexverter, M: Modular Multilevel Matrix Converter)

Scenario	1,H	1,M	2,H	2,M	3,H	3,M	4,H	4,M	5,H	5,M	6,H	6,M
Maximum branch voltage in kV	6.15	5.39	6.15	5.39	-	-	12.30	10.78	12.30	10.78	-	-
Maximum branch current in kA	3.35	2.56	3.35	1.69	-	-	3.35	2.56	3.35	1.69	-	-

Maximum rms branch current in kA	1.53	0.95	1.54	0.85	-	-	1.53	0.95	1.54	0.85	-	-
Number of modules	48	63	48	63	-	-	96	126	96	126	-	-
Switching power in MW	494	497	494	328	-	-	988	994	988	657	-	-
Total capacity in F	23.2	2.0	2.8	1.3	-	-	46.1	4.0	5.6	2.6	-	-
Total inductance in mH	1.0	2.7	1.0	4.1	-	-	0.5	1.4	0.5	2.1	-	-
Maximum stored energy (inductance) in kJ	5.6	8.8	5.6	5.9	-	-	2.8	4.6	2.8	3.0	-	-

3.3 Efficiency

The estimation of the losses is done based on ideal branch voltages and branch currents, analogue to section 3.2.3. Only conducting losses and switching losses of the semiconductors are considered. At first, the ideal branch voltages and branch currents are used to calculate a mean duty cycle for the modules in each branch. Next, mean turn on and turn off times for the four switches of the modules are determined. These times and the datasheet parameters (scaled for the correct maximum current) lead to the conducting losses. Furthermore, the datasheet parameters and the modules' switching frequency are used to estimate the switching losses. As already mentioned in section 3.2.4, an apparent switching frequency of the modules of 600 Hz is assumed.

With these assumptions, the losses of all modules are assumed to be equal. As long as the converter is operated with a pulse width modulation concept and turned on and turned off modules are swapped regularly, these assumptions provide acceptable results. For nominal active power and without reactive power, the efficiency is given in Table 3-13 and Table 3-14.

Table 3-13. Efficiency for nominal active power and without reactive power of the Hexverter topology

Scenario	1	2	3	4	5	6
Efficiency	97.8 %	97.8 %	-	97.8 %	97.8 %	-

Table 3-14. Efficiency for nominal active power and without reactive power of the Modular Multilevel Matrix Converter

Scenario	1	2	3	4	5	6
Efficiency	98.4 %	98.3 %	-	98.4 %	98.3 %	-

Additional reactive power influences the Hexverter and the MMMC differently, because of the additional adjacent compensating power of the Hexverter. This effect is shown in Fig. 3-8 – Fig. 3-11 for the scenarios 1, 2, 4, and 5.

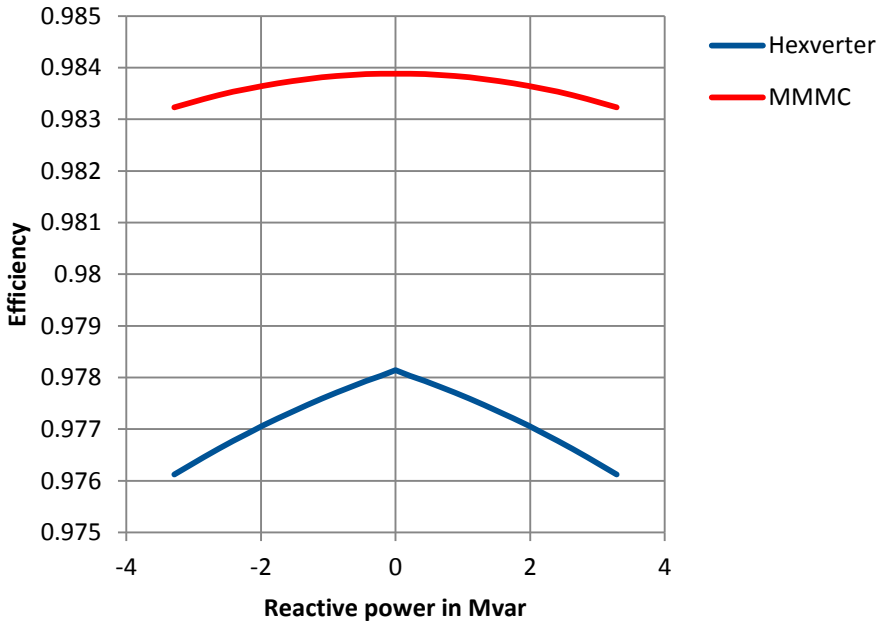

Fig. 3-8. Efficiency for nominal active power and varying reactive power of the Hexverter topology (blue) and the Modular Multilevel Matrix Converter (red) for Scenario 1.

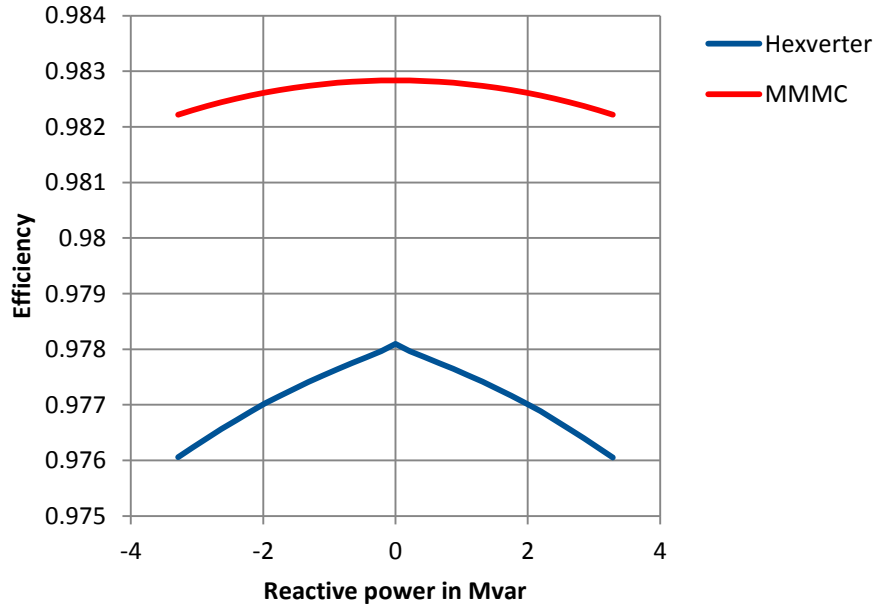

Fig. 3-9. Efficiency for nominal active power and varying reactive power of the Hexverter topology (blue) and the Modular Multilevel Matrix Converter (red) for Scenario 2.

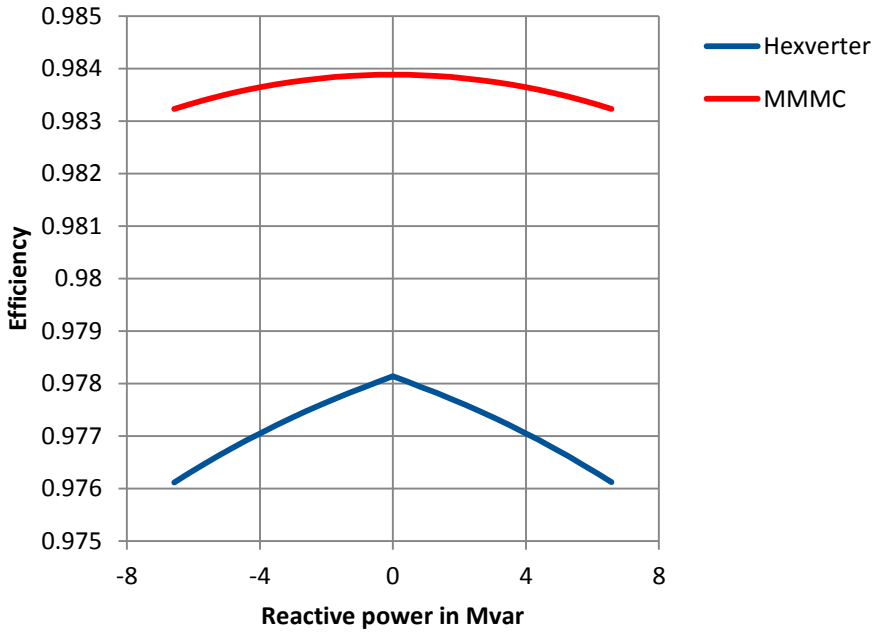

Fig. 3-10. Efficiency for nominal active power and variing reactive power of the Hexverter topology (blue) and the Modular Multilevel Matrix Converter (red) for Scenario 4.

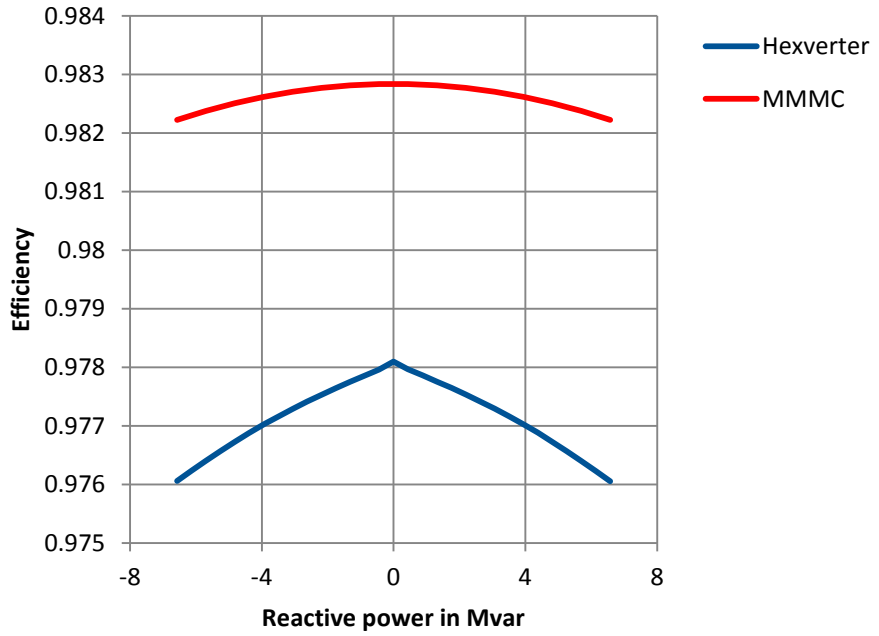

Fig. 3-11. Efficiency for nominal active power and varying reactive power of the Hexverter topology (blue) and the Modular Multilevel Matrix Converter (red) for Scenario 5.

As expected, the efficiency decrease is higher for the Hexverter, caused by the additional circulating current.

For wind energy system, the efficiency at partial load is very important. The investigation for partial load leads to Figs. 3-12 – Fig. 3-15. Reactive power is set to zero and active power, frequency on generator side, and generator voltage are varied for the calculations.

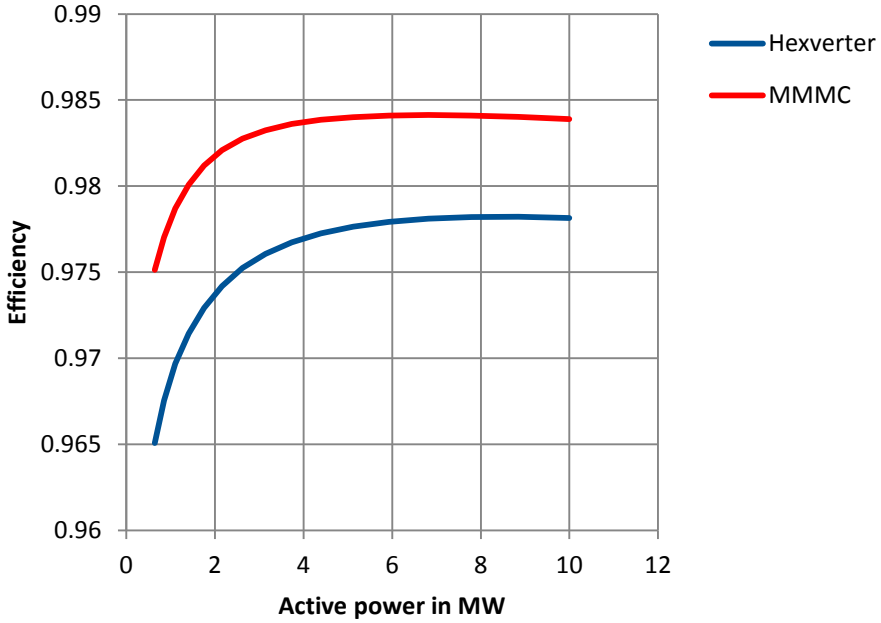

Fig. 3-12. Efficiency for varying active power (and generator voltage) and without reactive power of the Hexverter topology (blue) and the Modular Multilevel Matrix Converter (red) for Scenario 1.

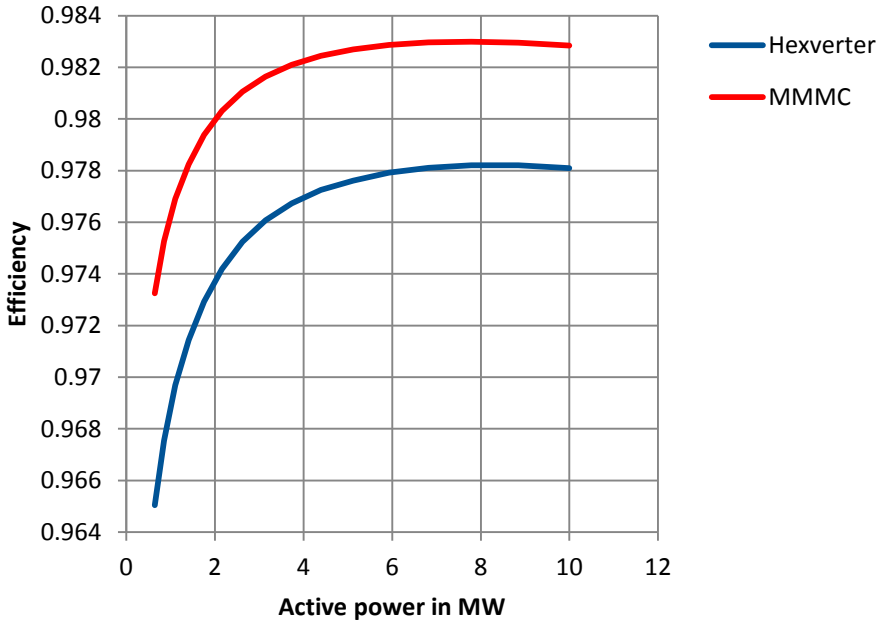

Fig. 3-13. Efficiency for varying active power (and generator voltage) and without reactive power of the Hexverter topology (blue) and the Modular Multilevel Matrix Converter (red) for Scenario 2.

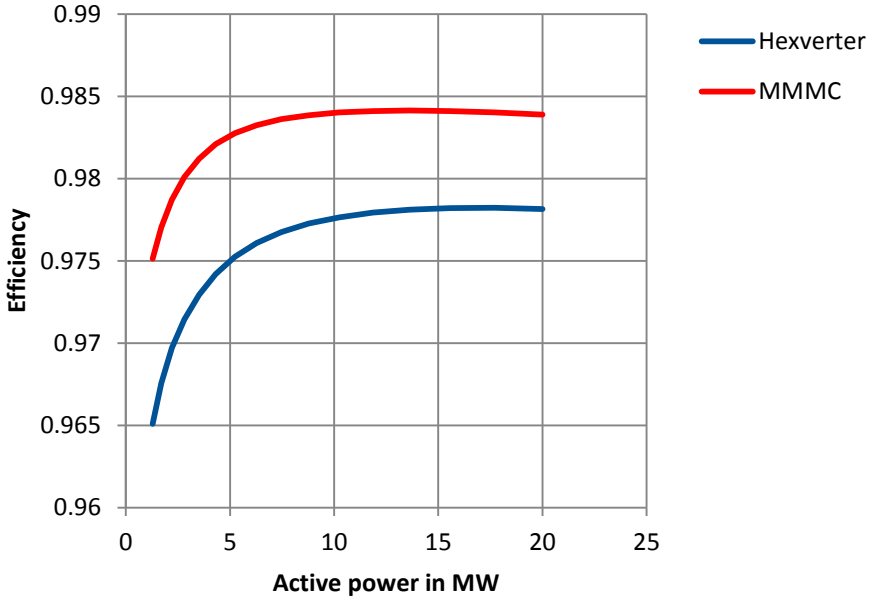

Fig. 3-14. Efficiency for varying active power (and generator voltage) and without reactive power of the Hexverter topology (blue) and the Modular Multilevel Matrix Converter (red) for Scenario 4.

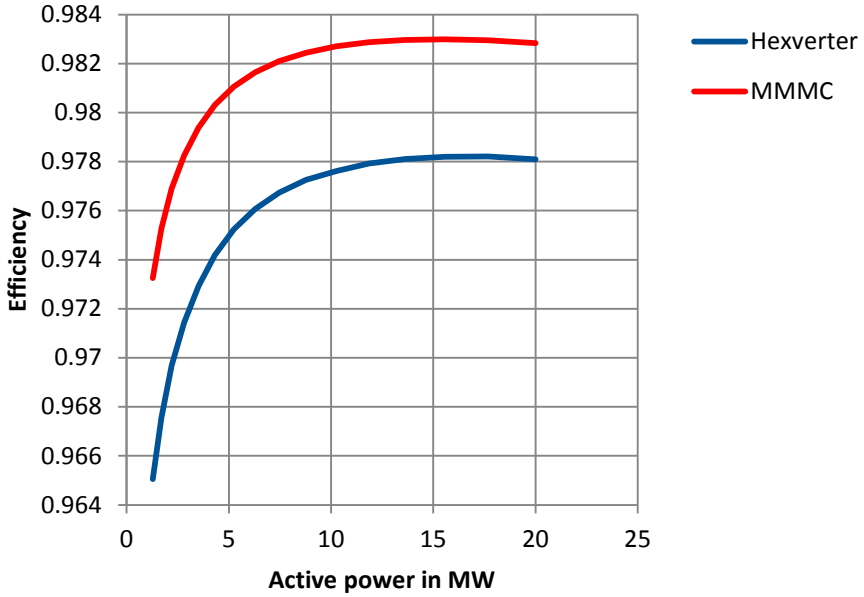

Fig. 3-15. Efficiency for varying active power (and generator voltage) and without reactive power of the Hexverter topology (blue) and the Modular Multilevel Matrix Converter (red) for Scenario 5.

The efficiency for partial load changes slightly for the upper half of the power range. Only for low power the efficiency drops distinguishable. For all partial load operating points, the MMMC has a higher efficiency than the Hexverter.

In total, the MMMC is superior to the Hexverter according efficiency for the chosen scenarios. This conclusion applies for efficiency for nominal power, for partial load and for the influence of additional reactive power on the losses.

3.4 Cost estimation

The cost of the converter is one of the performance indicators that is used to compare the different topologies. The cost of the modular multilevel direct AC/AC converters is estimated based on the designs from section 3.2. Besides the cost for semiconductors, capacitors and inductors, the mechanical cost is estimated based on the number of modules.

The necessary semiconductors are chosen based on the maximum branch current and the maximum DC-link voltage of the modules. Thermal design will be considered for the more detailed converter design for deliverable 3.31. As switches IGBTs with 1700 V blocking voltage are chosen. For the cost estimation, the prices of multiple Infineon IGBTs (with different rated currents; for a quantity of 5; from the same distributor, Mouser Electronics [10]) are used. Based on these prices, a linear approximation is made, Fig. 3-16. The linear approximation prevents jumps in the prices depending on the rated current.

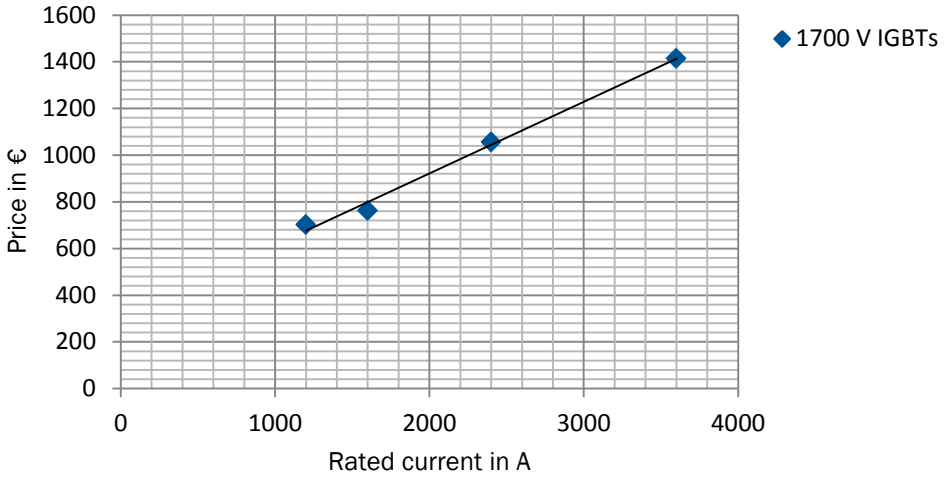

Fig. 3-16. 1700 V IGBT price.

The necessary rated current is calculated with the maximum rms branch current with a safety margin of 2.5. The resulting total cost for semiconductors for the different scenarios based on the linear approximation in Fig. 3-16 are given in Table 3-15 for the Hexverter and in Table 3-16 for the MMMC.

Table 3-15. Semiconductor cost of the Hexverter topology

Scenario	1	2	3	4	5	6
Semiconductor cost in k€	284	286	-	568	573	-

Table 3-16. Semiconductor cost of the Modular Multilevel Matrix Converter

Scenario	1	2	3	4	5	6
Semiconductor cost in k€	262	243	-	524	486	-

The difference in semiconductor costs between Hexverter and MMMC correlates with the results for the switching powers of the two converter systems.

The DC-link capacitors of both modular multilevel direct AC/AC converters have the same maximum DC-link voltage of 1100 V. For estimating the capacitor costs, the price for one reference 1100 V capacitor is used. Multiple of these capacitors are connected in parallel to realise the necessary DC-link capacity. The parameters of the reference capacitor are:

- Maximum DC voltage: 1150 V
- Maximum rms current: 57 A
- Capacity: 530 µF
- Price (Quantity of 50, distributor Mouser Electronics): 92.16 €.

The estimation of the total capacitor cost based on the chosen capacitor leads to the results in Table 3-17 for the Hexverter and Table 3-18 for the MMMC.

Table 3-17. Capacitor cost of the Hexverter topology

Scenario	1	2	3	4	5	6
Capacitor cost in k€	4036	484	-	8072	968	-

Table 3-18. Capacitor cost of the Modular Multilevel Matrix Converter

Scenario	1	2	3	4	5	6
Capacitor cost in k€	347	225	-	694	449	-

The higher capacity demand of the Hexverter, especially for Scenarios 1 and 4 with low generator frequencies, result in significant higher capacitor costs.

The branch inductors are not available as mass produced products by any distributors. To avoid several, detailed requests for these inductors at manufacturers, the copper and iron core volume are estimated. With these volumes, and cupper and iron sheet prices the cost of material is calculated. For representing manufacturing costs and profit margins, the cost of material is multiplied by the factor 4 to get an estimated inductor price.

For the estimation of the volumes, several assumptions are made:

- Maximum current density in the windings: 5 A/mm²
- Filling factor for the windings: 0.4
- Maximum magnetic flux density: 1.2 T

The assumed prices for copper and iron are 9.0 €/kg and 1.5 €/kg. The number of windings is varied to minimise the total cost of material, which results in the costs (considering manufacturing costs and profit margins factor) in Table 3-19 for the Hexverter and Table 3-20 for the MMMC.

Table 3-19. Inductor cost of the Hexverter topology

Scenario	1	2	3	4	5	6
Inductor cost in k€	54.0	54.0	-	32.2	32.2	-

Table 3-20. Inductor cost of the Modular Multilevel Matrix Converter

Scenario	1	2	3	4	5	6
Inductor cost in k€	84.2	61.8	-	51.4	37.4	-

Compared to the capacitor and semiconductor costs, the inductor costs are negligible. Even with a higher factor for manufacturing costs and profit margin the influence on the total cost is small.

The cost for the cooling system is estimated based on the maximum losses of the converters. A cost per losses of 0.8 €/W is assumed (2.9 Appendix. A). The resulting cooling system costs are listed in Table 3-21 and Table 3-22.

Table 3-21. Cooling system cost of the Hexverter topology

Scenario	1	2	3	4	5	6
Cooling system cost in k€	174.8	174.8	-	350.8	350.8	-

Table 3-22. Cooling system cost of the Modular Multilevel Matrix Converter

Scenario	1	2	3	4	5	6
Cooling system cost in k€	129.2	137.2	-	258.2	274.2	-

The mechanical costs and cost for other components are estimated by a module offset cost and the number of modules. The module offset cost is chosen as 40 % of the mean module cost (based on semiconductor and capacitor costs, without Hexverter for 2.5 Hz). This approach leads to a module offset cost of approximately 4 k€ per module (Table 3-23 and Table 3-24), which is added to the total costs of the converters.

Table 3-23. Mechanical costs and cost for other components of the Hexverter topology

Scenario	1	2	3	4	5	6
Mechanical cost in k€	192	192	-	384	384	-

Table 3-24. Mechanical costs and cost for other components of the Modular Multilevel Matrix Converter

Scenario	1	2	3	4	5	6
Mechanical cost in k€	256	256	-	504	504	-

The estimated total costs of the Hexverter and the MMMC as performance indicators are shown in Table 3-25 and Table 3-26. It is worth mentioning, that the absolute values for the total costs can deviate considerably from the real cost of these converters. Changes in different assumptions of this cost estimation can lead to different results, especially compared to other topologies. Several factors are not considered (or only roughly considered within the costs for other components) in this estimation, e.g. mechanical contactors, measuring devices, connecting bars, cubicles, the grid-side transformer and manufacturing costs. Besides, the costs of the mechanical construction and inductors are only roughly estimated and the prices for semiconductors and capacitors do not consider a proper quantity discount. Nevertheless, it is almost certain, that the MMMC is superior to the Hexverter topology according costs for these nominal powers.

Table 3-25. Estimated total cost of the Hexverter topology

Scenario	1	2	3	4	5	6
Total cost in k€	4740.8	1190.8	-	9407.0	2308.0	-

Table 3-26. Estimated total cost of the Modular Multilevel Matrix Converter

Scenario	1	2	3	4	5	6
Total cost in k€	1074.4	919	-	2031.6	1750.6	-

3.5 Size and weight estimation

Without planning the converter and all necessary additional components in detail, a size estimation of the physical is very inaccurate. For avoiding this problem, the size of the two modular multilevel direct AC/AC converters is estimated based on an existing modular multilevel converter for medium voltage drive applications. The only M²LC for medium voltage drive applications on the market is the Siemens SINAMICS PERFECT HARMONY GH150. It consists of a number of cubicles

for different tasks, e.g. for the control system, the branch inductors, the modules and the cooling system. There are two version of the SINAMICS PERFECT HARMONY GH150 available. As a reference the 6SL3825-3AF41-2AA0-Z V12 is used, the relevant parameters are:

- Power rating: 13.3 MVA
- Output voltage: 6.6 kV
- Output Current: 1.16 kA
- Number of cells (two half bridge modules each): 36
- Input diode rectifier: 24-pulse
- Control cubicle: 1.2 m x 2.4 m x 1.275 m
- Diode rectifier cubicle: 1.2 m x 2.81 m x 1.275 m
- Two M²LC cubicles: 1.2 m x 2.81 m x 1.275 m each
- Branch inductor cubicle: 0.9 m x 2.81 m x 1.275 m
- Cooling system cubicle: 1.2 m x 2.4 m x 1.275 m
- Total weight: 8440 kg

The control cubicle and the branch inductor cubicle are assumed to be the same size. The diode rectifier cubicle does not exist for the Hexverter and the MMMC. For the 10 MW converters one cooling system cubicle is used, for the 20 MW converter two cooling system cubicles are assumed. The M²LC cubicles are used as a reference, based on the number of modules in one cubicle, which is 36. Furthermore, it is assumed that modules of one branch must not be split up between cubicles for connecting reasons. The number of cubicles that is needed for the different scenarios is presented in Table 3-27 for the Hexverter and Table 3-28 for the MMMC.

Table 3-27. Number of necessary cubicles for modules (rounded) of the Hexverter topology

Scenario	1	2	3	4	5	6
Number of cubicle for modules	2	2	-	3	3	-

Table 3-28. Number of necessary cubicles for modules (rounded) of the Modular Multilevel Matrix Converter

Scenario	1	2	3	4	5	6
Number of cubicle for modules	2	2	-	5	5	-

Using the known data for the SINAMICS PERFECT HARMONY GH150, the estimated total volume and total floor area for the Hexverter and MMMC are given in Table 3-29 and Table 3-30. As already mentioned, the grid-side transformer is neglected for all estimations. In addition, the size of the single modules, depending highly from the DC-link capacitors, cannot be considered in this approach.

Table 3-29. Floor area and volume for the cubicles of the Hexverter topology

Scenario	1	2	3	4	5	6
Total floor area of the converters' cubicles in m²	7.27	7.27	-	8.80	8.80	-
Total volume of the converters' cubicles in m³	19.17	19.17	-	23.47	23.47	-
Total weight of the converters' cubicles in kg	8440	8440	-	9908	9908	-

(INNWIND. EU. Deliverable 3.32, Converter designs based on new components and modular multilevel topologies)

Table 3-30. Floor area and volume for the cubicles of the Modular Multilevel Matrix Converter

Scenario	1	2	3	4	5	6
Total floor area of the converters' cubicles in m²	7.27	7.27	-	11.86	11.86	-
Total volume of the converters' cubicles in m³	19.17	19.17	-	32.06	32.06	-
Total weight of the converters' cubicles in kg	8440	8440	-	12843	12843	-

As expected, the higher number of modules for the MMMC leads to a higher volume of the converter for 20 MW. Due to rounding, the volume is equal for 10 MW. Table 3-29 and Table 3-30 also included an estimation of the weight based on the number of cubicles needed. As the weight distribution between the cubicles of the reference converter is unknown, a high error for this estimation is probable. Therefore, the estimated weight should not be used to compare the different topologies and can be seen as a rough indicator.

3.6 Simulation results

The converter design is verified with a Matlab/Simulink simulation model. This model is used to get the maximum THD of the system currents and generator currents as well. Only steady state operation is considered and the generator is modelled with sinusoidal voltage sources with constant frequency, series-connected with a resistor and an inductor. The used parameters for the equivalent circuit of the generator in steady state operation and the grid are chosen according to the inductances for the simulations in chapter 2 and are shown in Table 3-31.

Table 3-31. Parameters for the equivalent circuit of the generator at steady state operation and the grid

Scenario	1	2	3	4	5	6
Generator side inductance in mH	14	1.4	-	28	2.8	-
Generator side resistance in mΩ	22	22	-	44	44	-
Grid side inductance in µH	144	144	-	288	288	-
Grid side resistance in mΩ	0	0	-	0	0	-

Controllers based on section 3.1.1 and 3.1.2 are used. The branch voltages and currents, the grid and generator side currents, the circulating current, and the star point voltage of the Hexverter for Scenario 1, 2, 4 and 5 are presented in Fig. 3-17 – Fig. 3-20. The THD for grid currents and generator currents is always lower than the limit of 5 % and 3.5 %, Table 3-32.

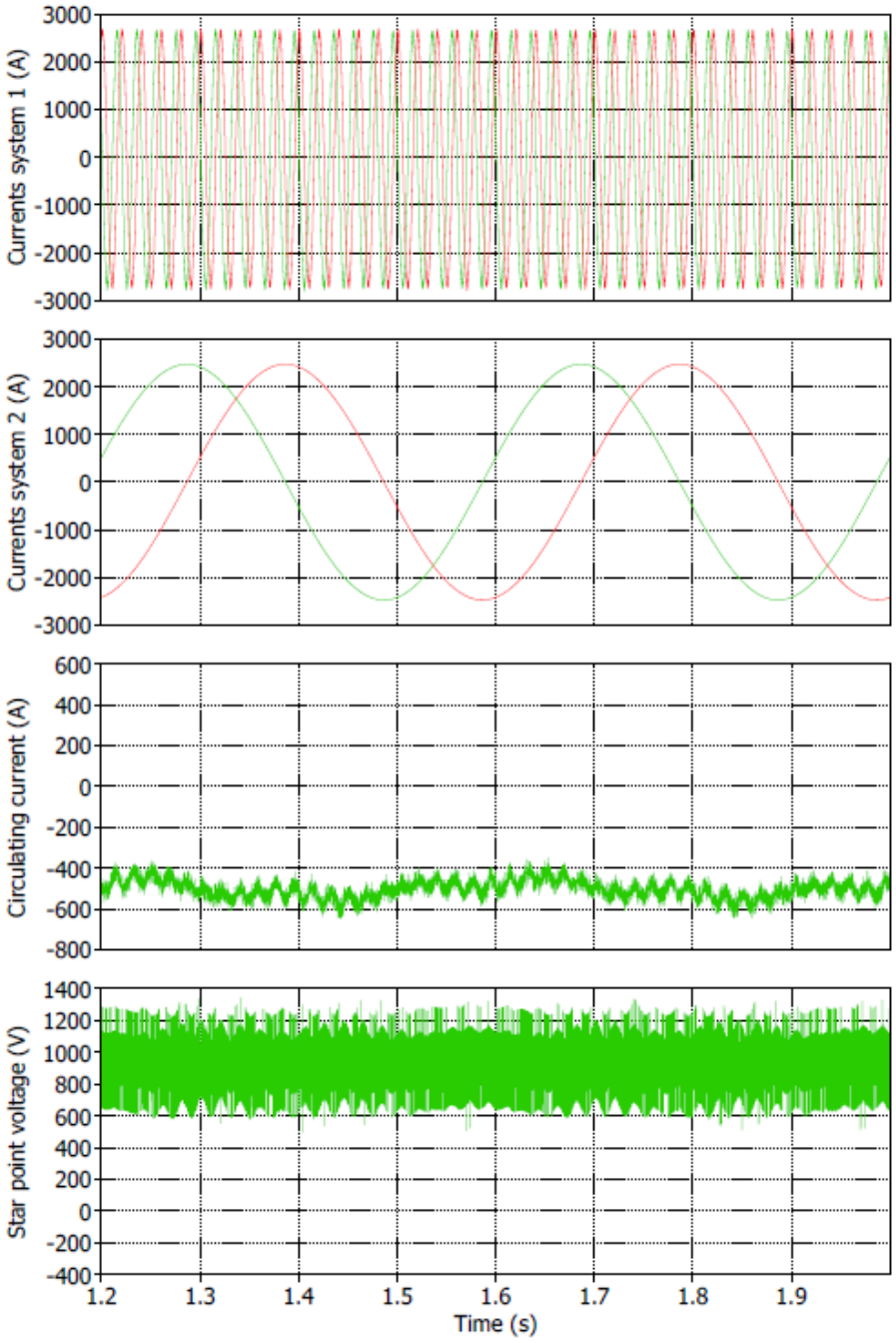
Currents system 1 (A)
3000
2000
1000
0
-1000
-2000
-3000
Currents system 2 (A)
3000
2000
1000
0
-1000
-2000
-3000
Circulating current (A)
600
400
200
0
-200
-400
-600
-800
Star point voltage (V)
1400
1200
1000
800
600
400
200
0
-200
-400
1.2
1.3
1.4
1.5
1.6
1.7
1.8
1.9
Time (s)

(a)

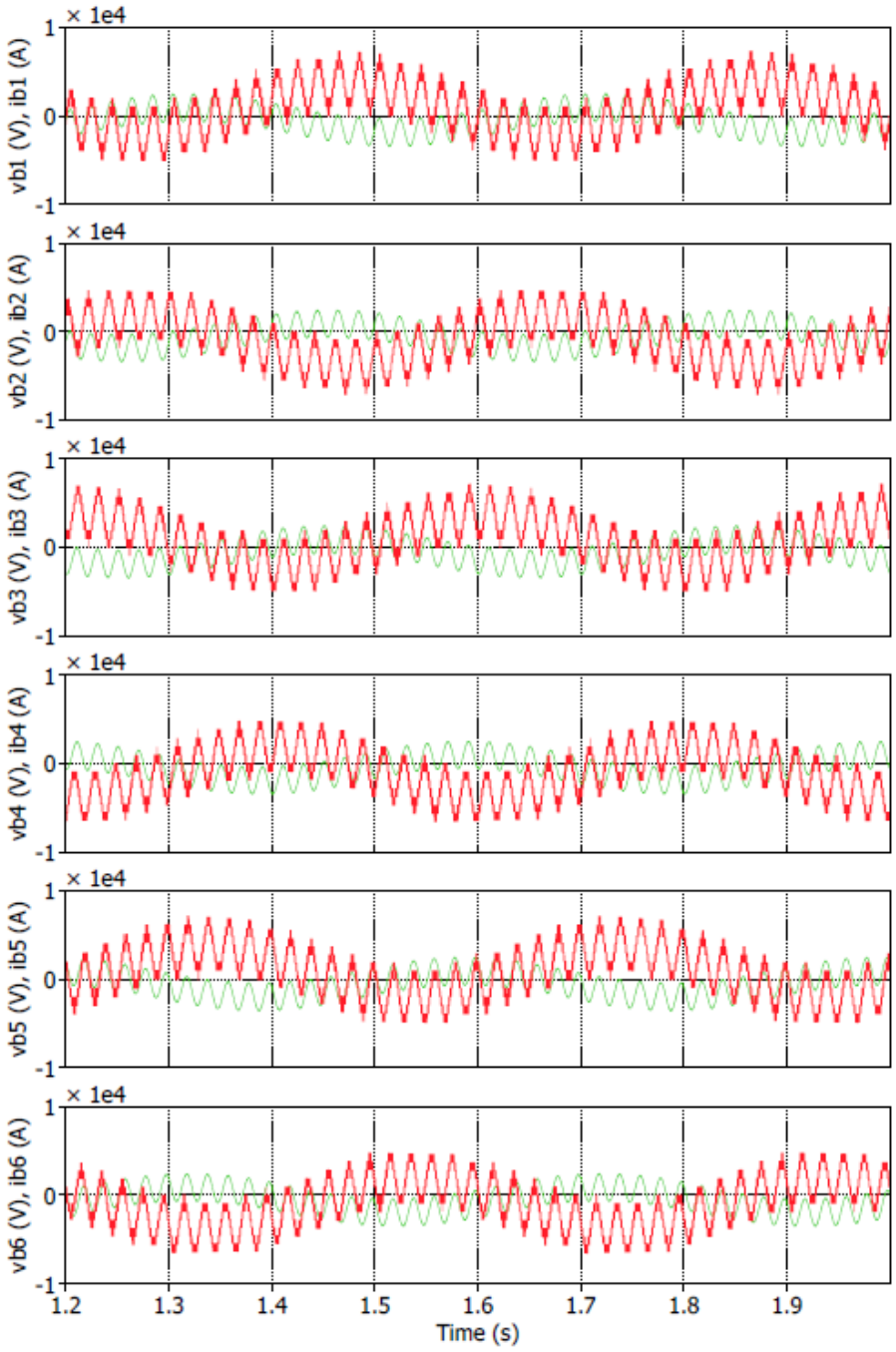

(b)

Fig. 3-17. (a) System currents (in αβ-components), circulating current and star point voltage of the Hexverter topology for Scenario 1; (b): Branch modules' output voltages (red) and branch currents (green) of the Hexverter topology for Scenario 1.

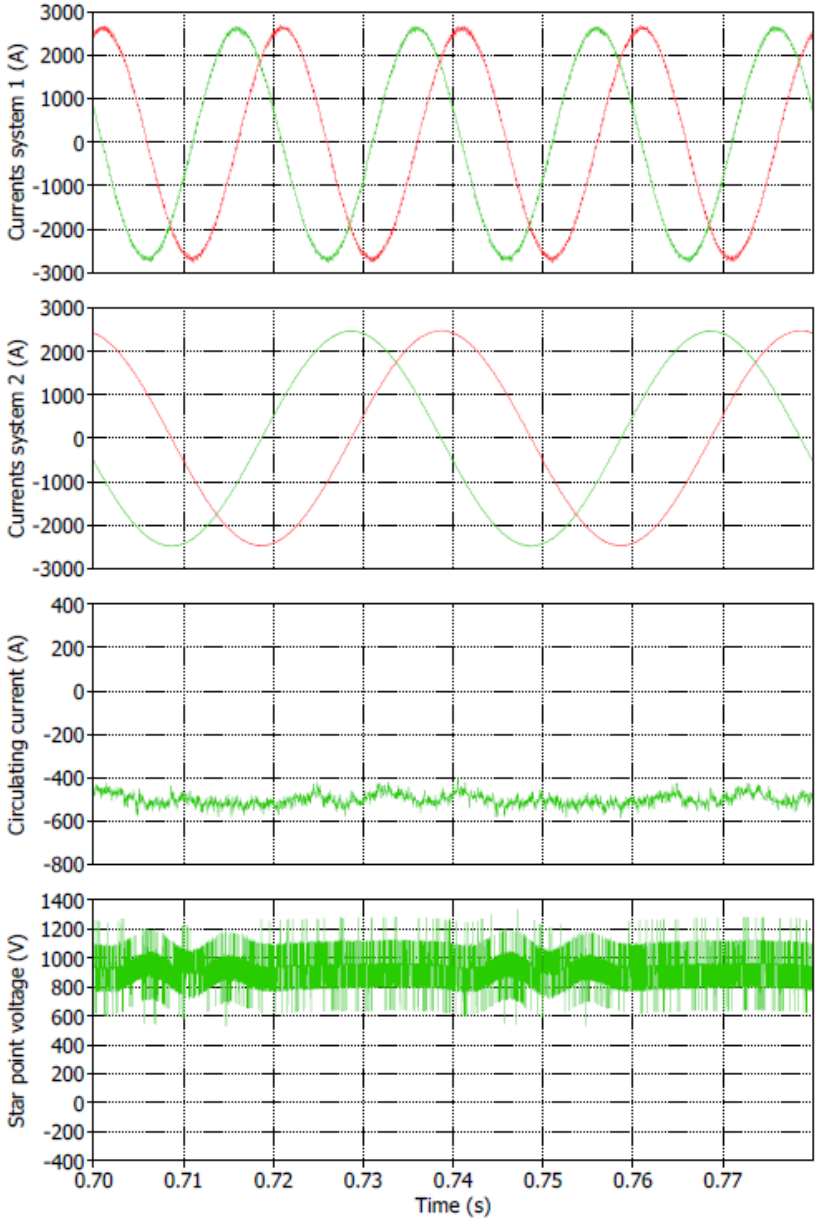
Currents system 1 (A)
3000
2000
1000
0
-1000
-2000
-3000
Currents system 2 (A)
3000
2000
1000
0
-1000
-2000
-3000
Circulating current (A)
400
200
0
-200
-400
-600
-800
Star point voltage (V)
1400
1200
1000
800
600
400
200
0
-200
-400
0.70
0.71
0.72
0.73
0.74
0.75
0.76
0.77
Time (s)

(a)

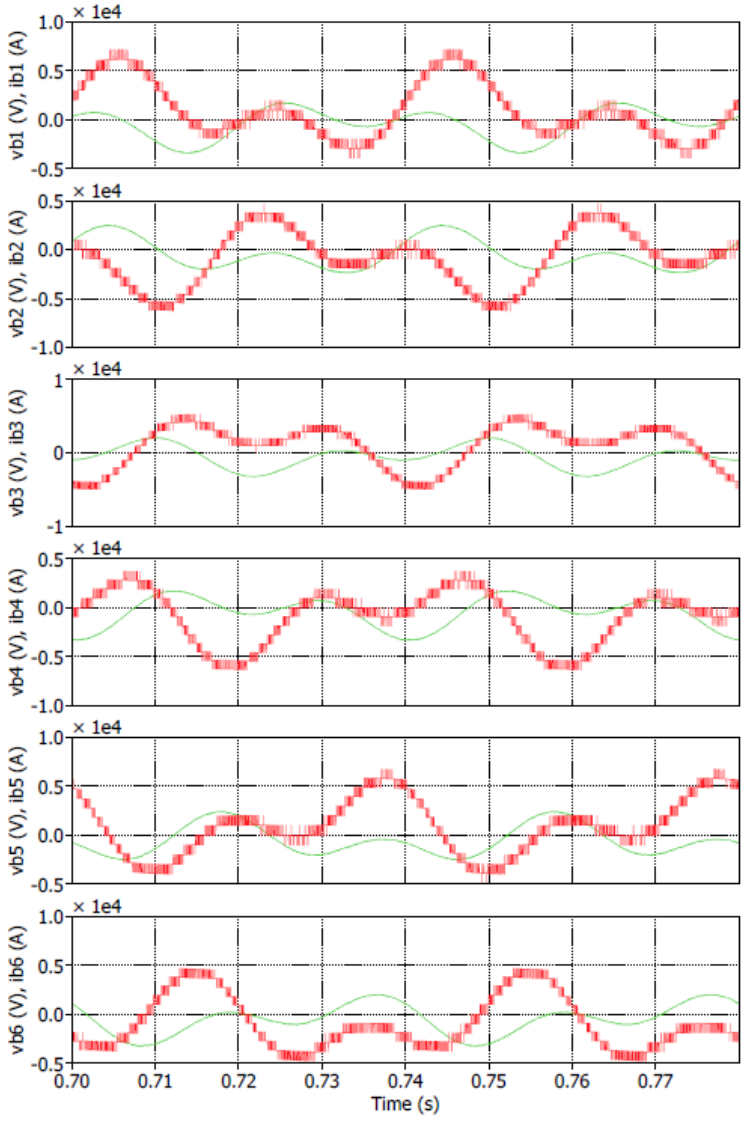

(b)

Fig. 3-18. (a) System currents (in αβ-components), circulating current and star point voltage of the Hexverter topology for Scenario 2; (b) Branch modules' output voltages (red) and branch currents (green) of the Hexverter topology for Scenario 2.

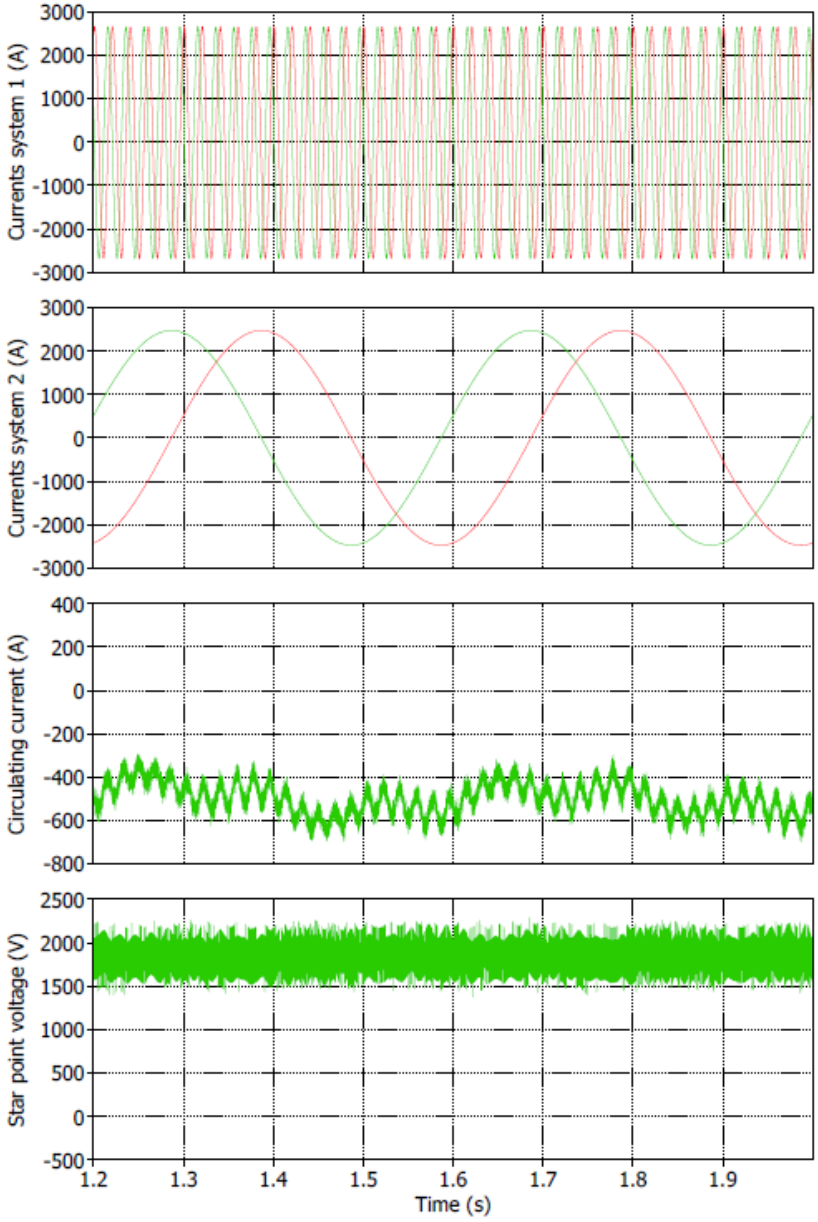
Currents system 1 (A)
3000
2000
1000
0
-1000
-2000
-3000
Currents system 2 (A)
3000
2000
1000
0
-1000
-2000
-3000
Circulating current (A)
400
200
0
-200
-400
-600
-800
Star point voltage (V)
2500
2000
1500
1000
500
0
-500
1.2
1.3
1.4
1.5
1.6
1.7
1.8
1.9
Time (s)

(a)

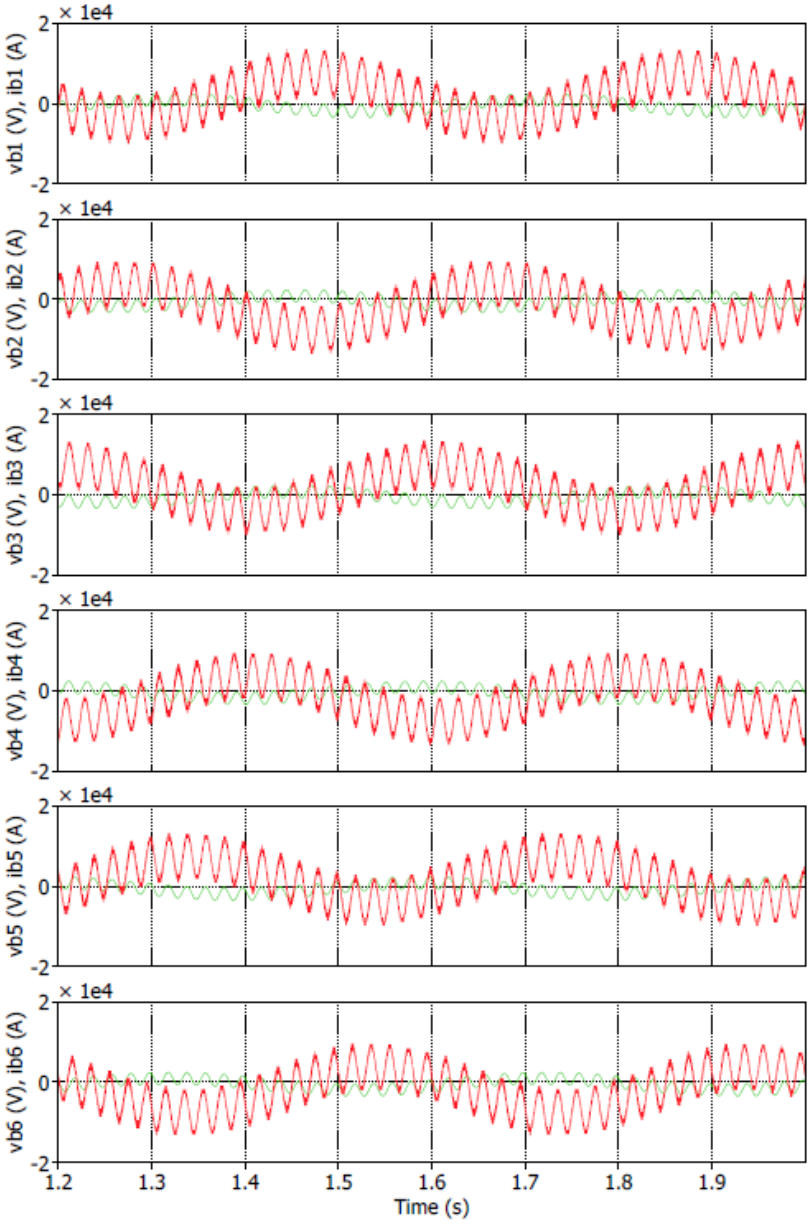

(b)

Fig. 3-19. (a) System currents (in αβ-components), circulating current and star point voltage of the Hexverter topology for Scenario 4; (b) Branch modules' output voltages (red) and branch currents (green) of the Hexverter topology for Scenario 4.

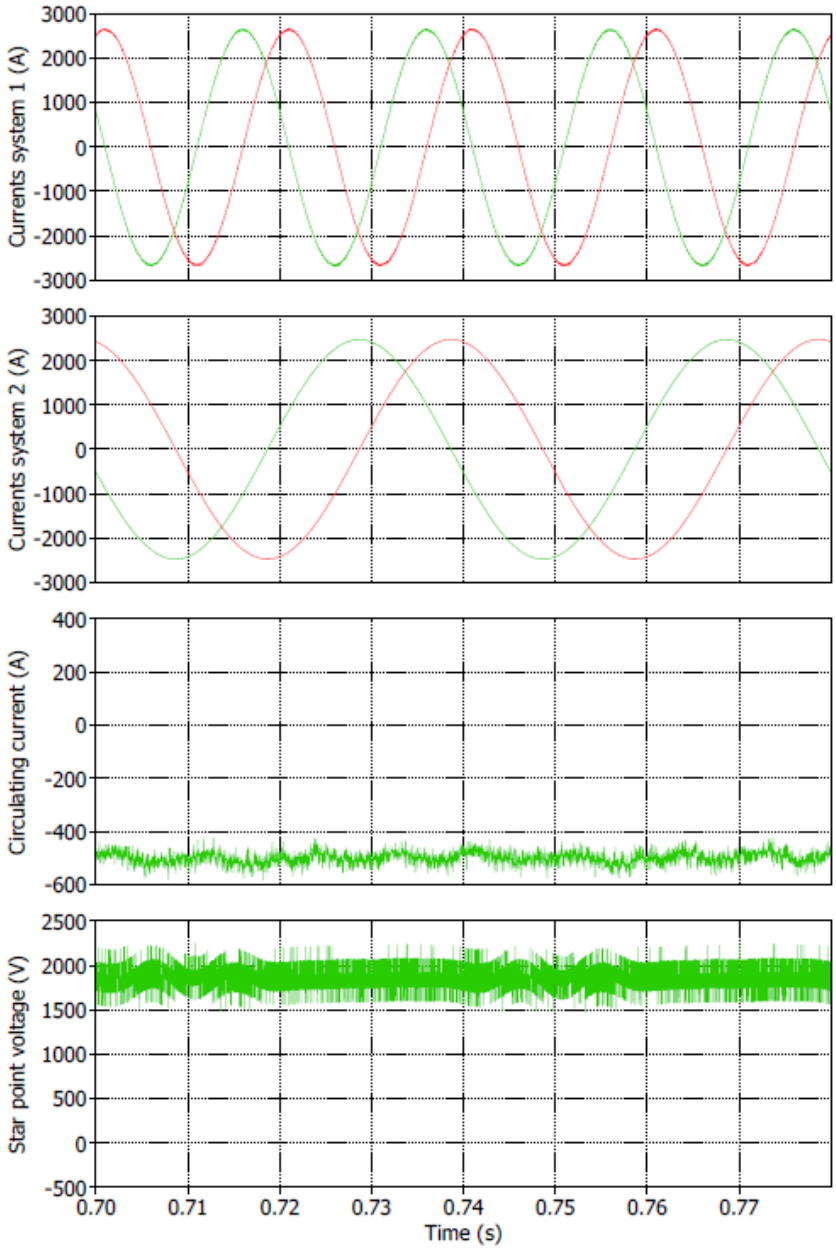
Currents system 1 (A)
3000
2000
1000
0
-1000
-2000
-3000
Currents system 2 (A)
3000
2000
1000
0
-1000
-2000
-3000
Circulating current (A)
400
200
0
-200
-400
-600
Star point voltage (V)
2500
2000
1500
1000
500
0
-500
0.70
0.71
0.72
0.73
0.74
0.75
0.76
0.77
Time (s)

(a)

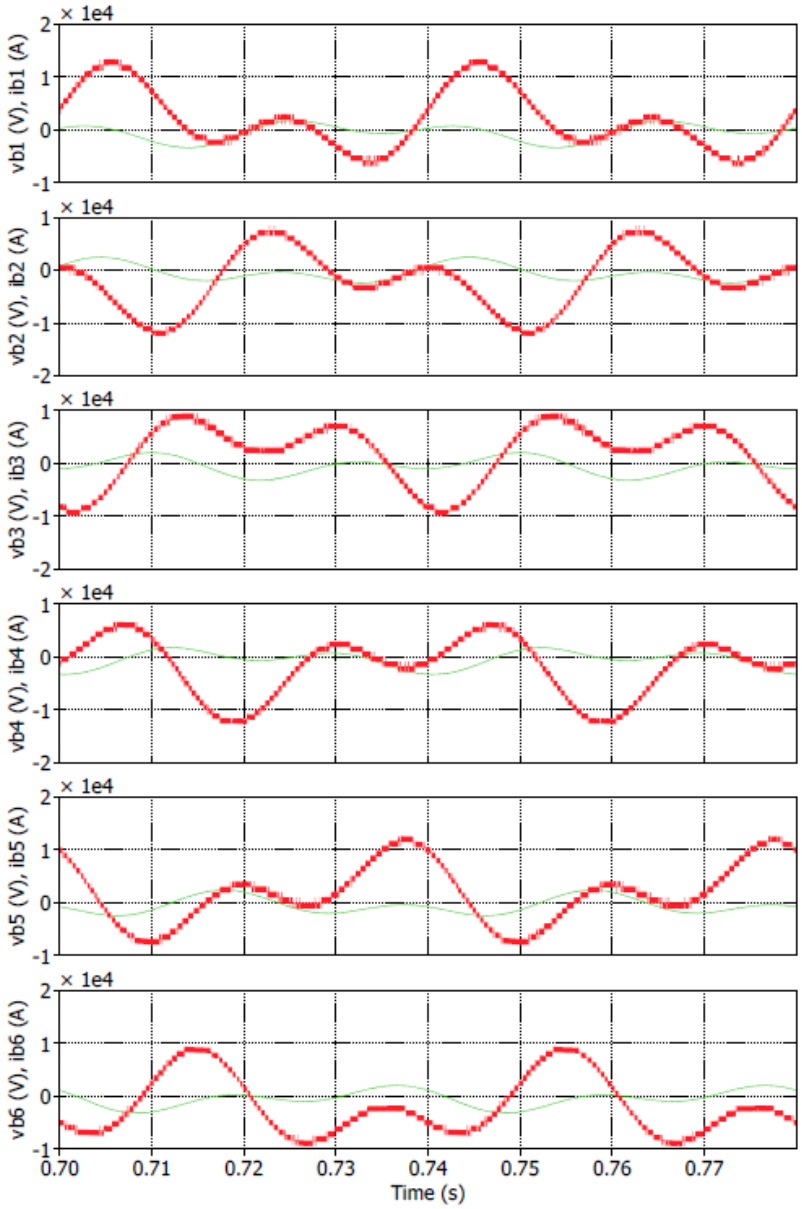

(b)

Fig. 3-20. (a) System currents (in αβ-components), circulating current and star point voltage of the Hexverter topology for Scenario 5; (b) Branch modules' output voltages (red) and branch currents (green) of the Hexverter topology for Scenario 5.

Table 3-32. Total harmonic distortion of the system currents of the Hexverter topology

Scenario	1	2	3	4	5	6
Generator side current THD	0.1 %	0.4 %	-	0.04 %	0.2 %	-
Grid side current THD	2.2 %	2.0 %	-	0.8 %	0.8 %	-

(INNWIND. EU. Deliverable 3.32, Converter designs based on new components and modular multilevel topologies)

The simulation results for the same system parameters for the MMMC are presented in Fig. 3-21 – Fig. 3-24. Instead of one circulating current of the Hexverter, the four circulating currents of the MMMC are displayed. The star point voltage of the MMMC is not shown, because it is always zero.

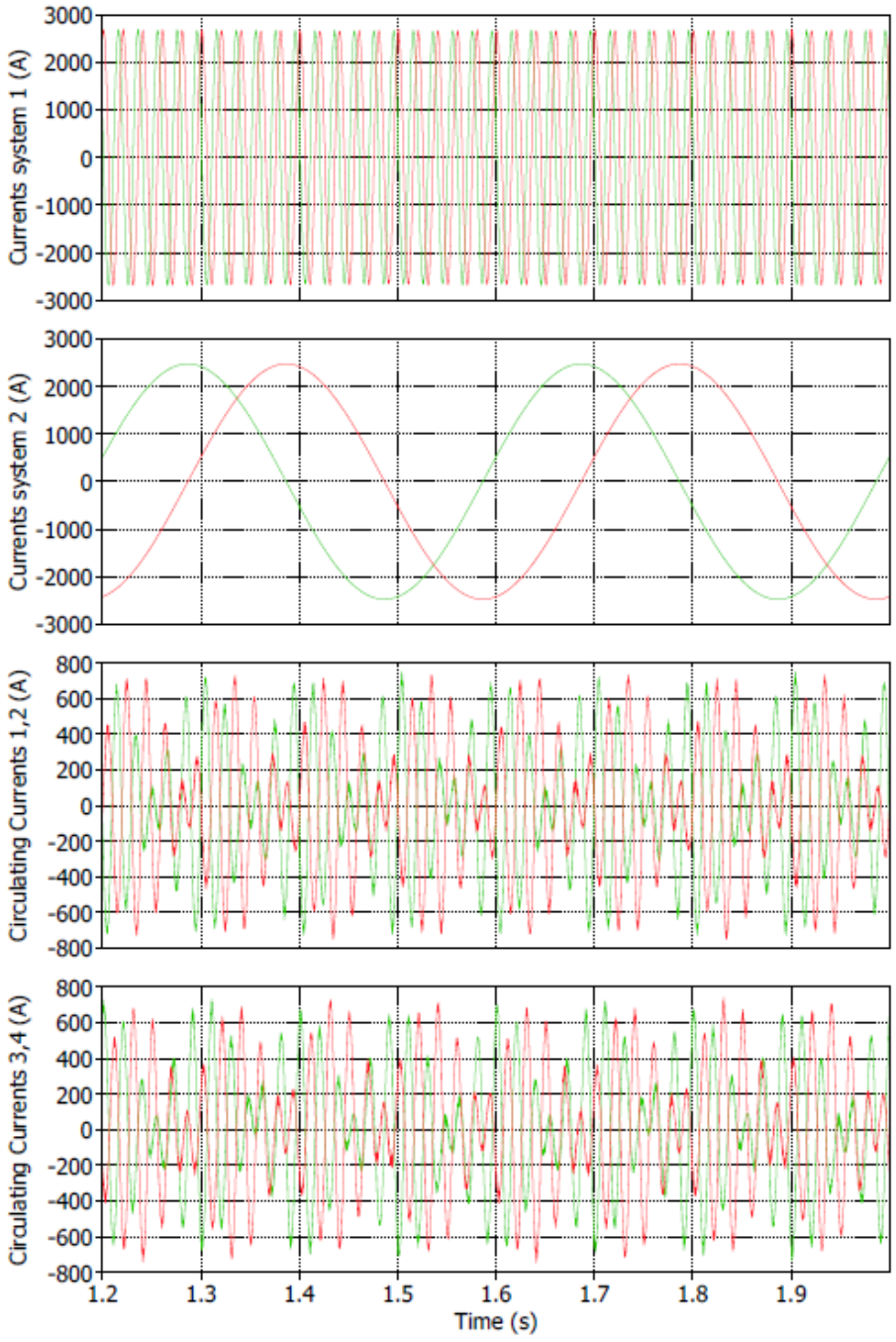
Currents system 1 (A)
3000
2000
1000
0
-1000
-2000
-3000
Currents system 2 (A)
3000
2000
1000
0
-1000
-2000
-3000
Circulating Currents 1,2 (A)
800
600
400
200
0
-200
-400
-600
-800
Circulating Currents 3,4 (A)
800
600
400
200
0
-200
-400
-600
-800
1.2
1.3
1.4
1.5
1.6
1.7
1.8
1.9
Time (s)

(a)

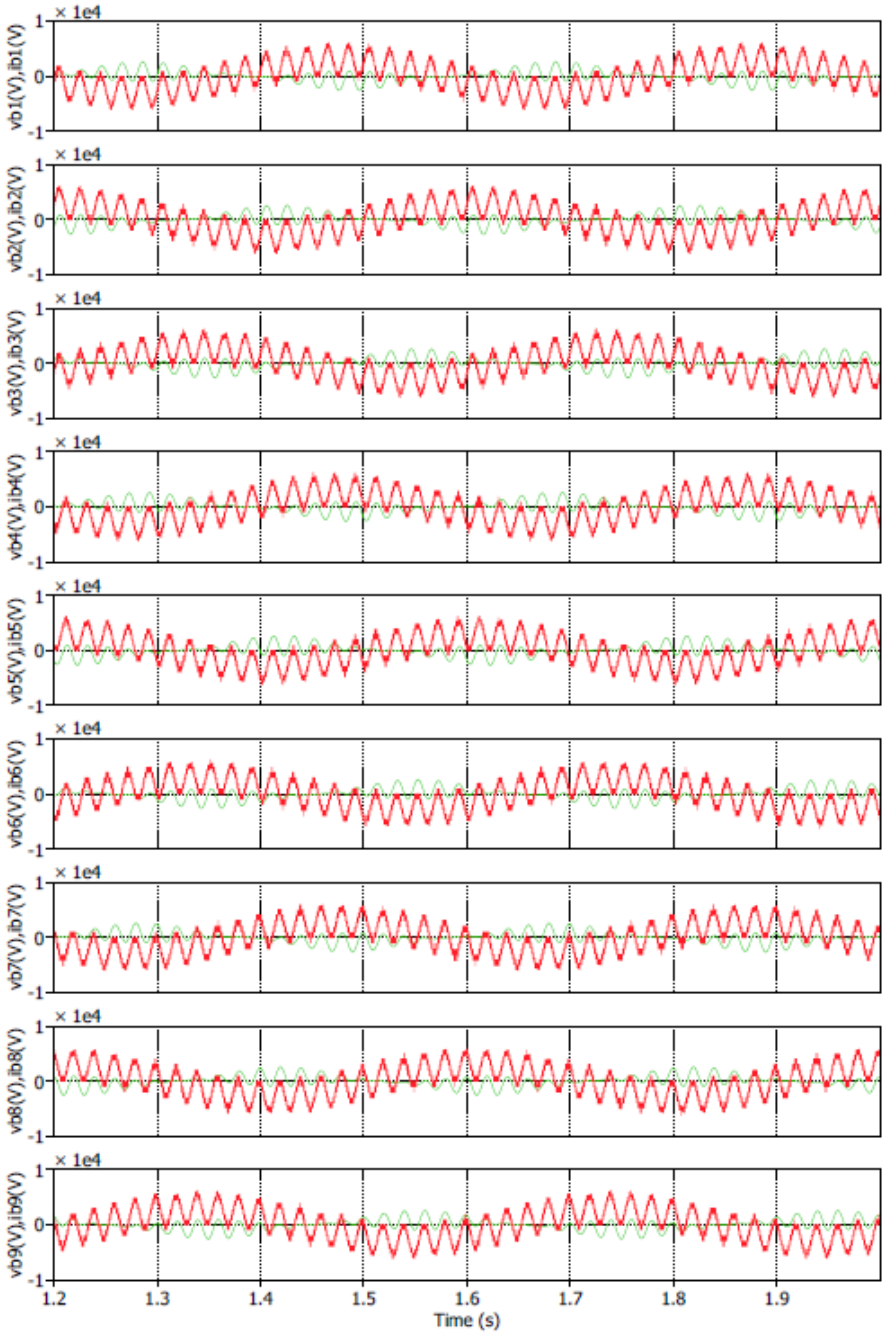

(b)

Fig. 3-21. (a) System currents (in αβ-components) and circulating currents of the Modular Multilevel Matrix Converter for Scenario 1; (b) Branch modules' output voltages (red) and branch currents (green) of the Hexverter topology for Scenario 1.

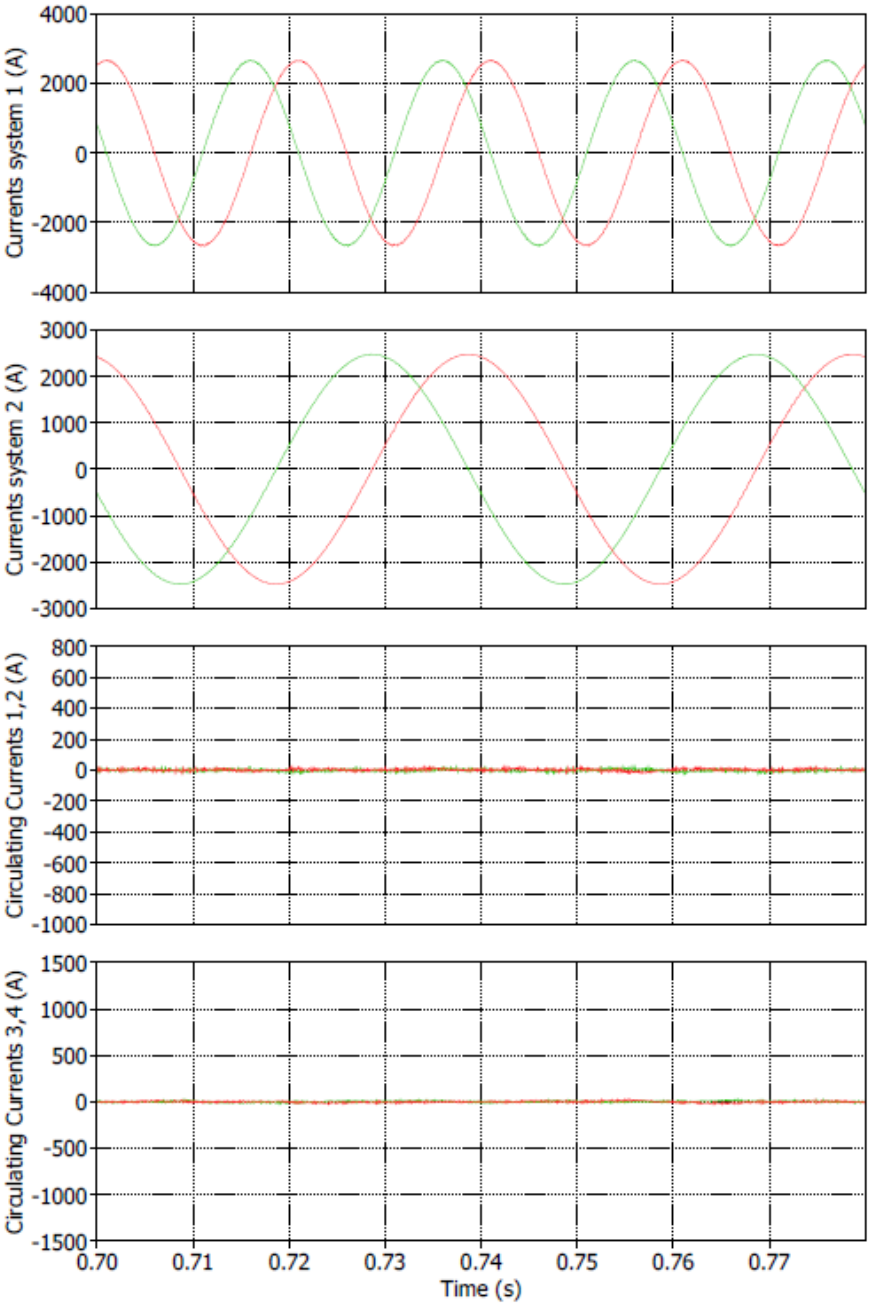
Currents system 1 (A)
4000
2000
0
-2000
-4000
Currents system 2 (A)
3000
2000
1000
0
-1000
-2000
-3000
Circulating Currents 1,2 (A)
800
600
400
200
0
-200
-400
-600
-800
-1000
Circulating Currents 3,4 (A)
1500
1000
500
0
-500
-1000
-1500
0.70
0.71
0.72
0.73
0.74
0.75
0.76
0.77
Time (s)

(a)

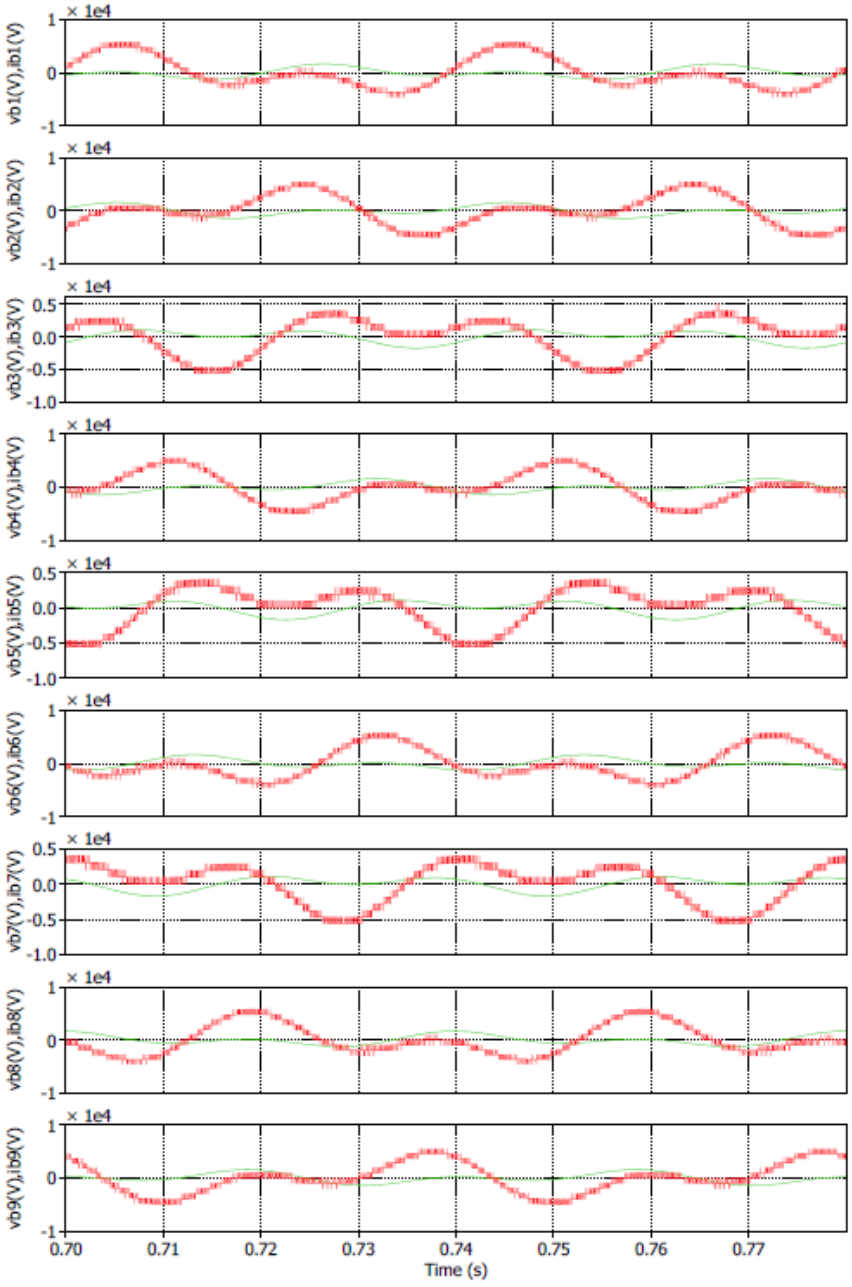

(b)

Fig. 3-22. (a) System currents (in αβ-components) and circulating currents of the Modular Multilevel Matrix Converter for Scenario 2; (b) Branch modules' output voltages (red) and branch currents (green) of the Hexverter topology for Scenario 2.

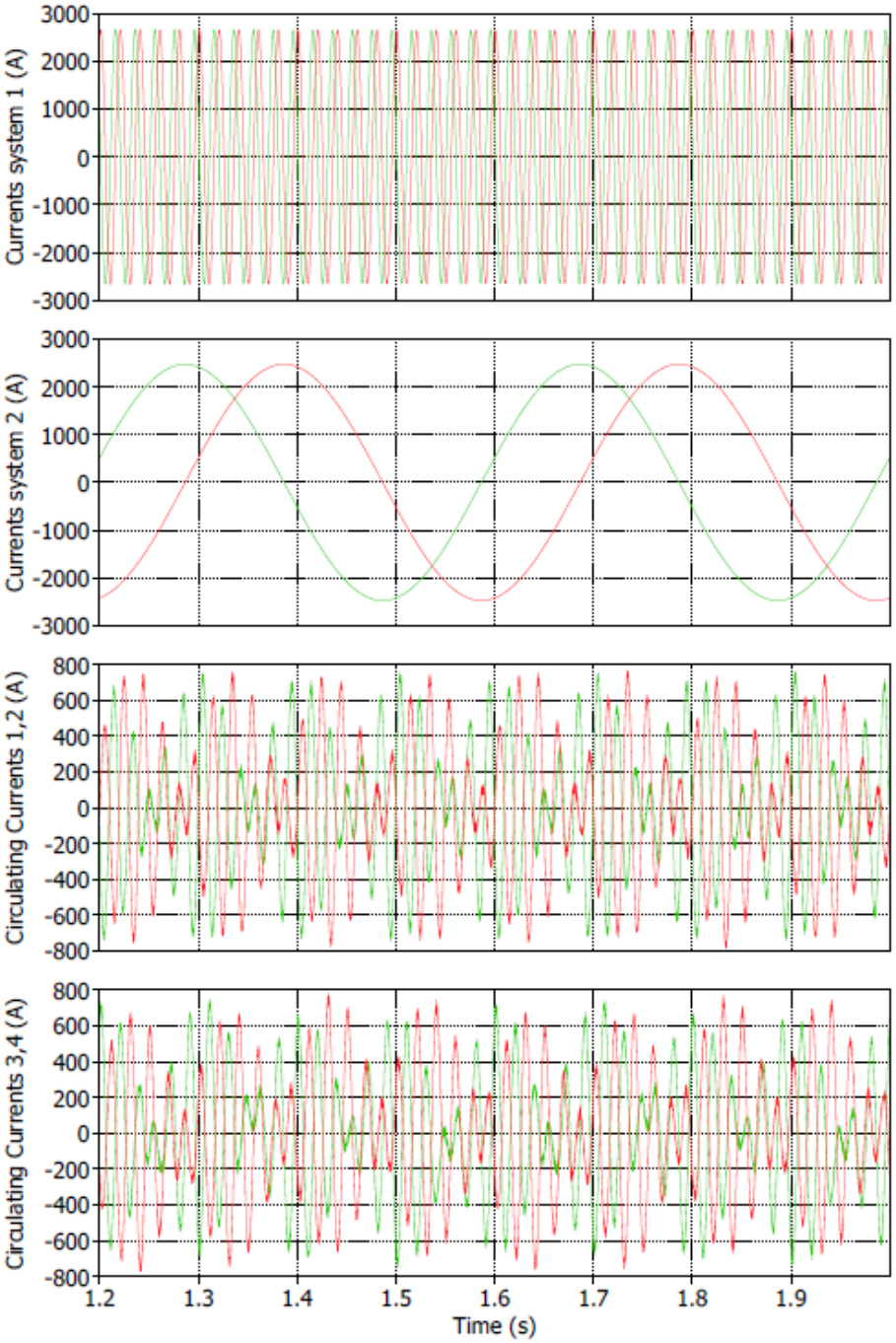
Currents system 1 (A)
3000
2000
1000
0
-1000
-2000
-3000
Currents system 2 (A)
3000
2000
1000
0
-1000
-2000
-3000
Circulating Currents 1,2 (A)
800
600
400
200
0
-200
-400
-600
-800
Circulating Currents 3,4 (A)
800
600
400
200
0
-200
-400
-600
-800
1.2
1.3
1.4
1.5
1.6
1.7
1.8
1.9
Time (s)

(a)

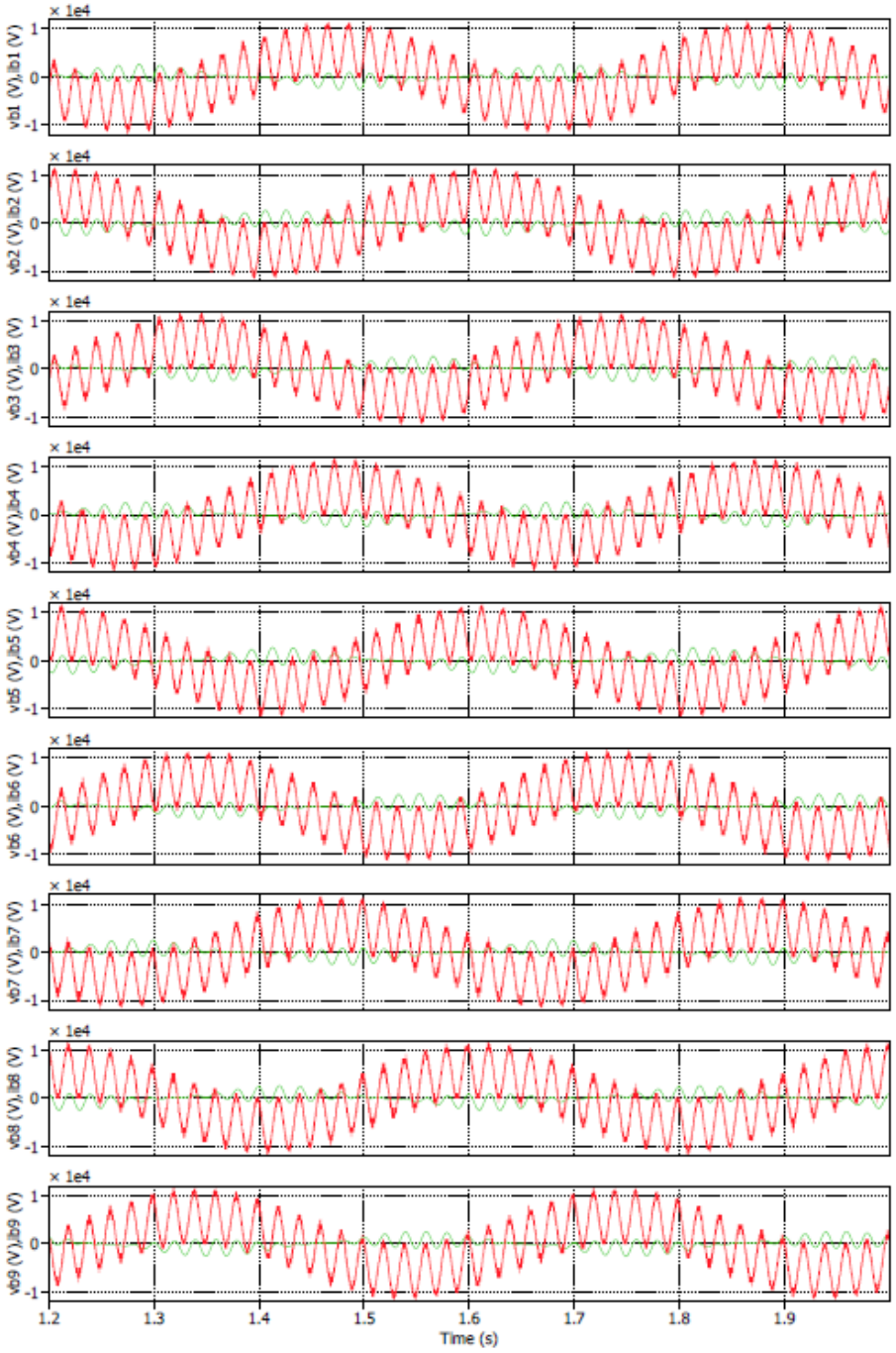

(b)

Fig. 3-23. (a) System currents (in αβ-components) and circulating currents of the Modular Multilevel Matrix Converter for Scenario 4; (b) Branch modules' output voltages (red) and branch currents (green) of the Hexverter topology for Scenario 4.

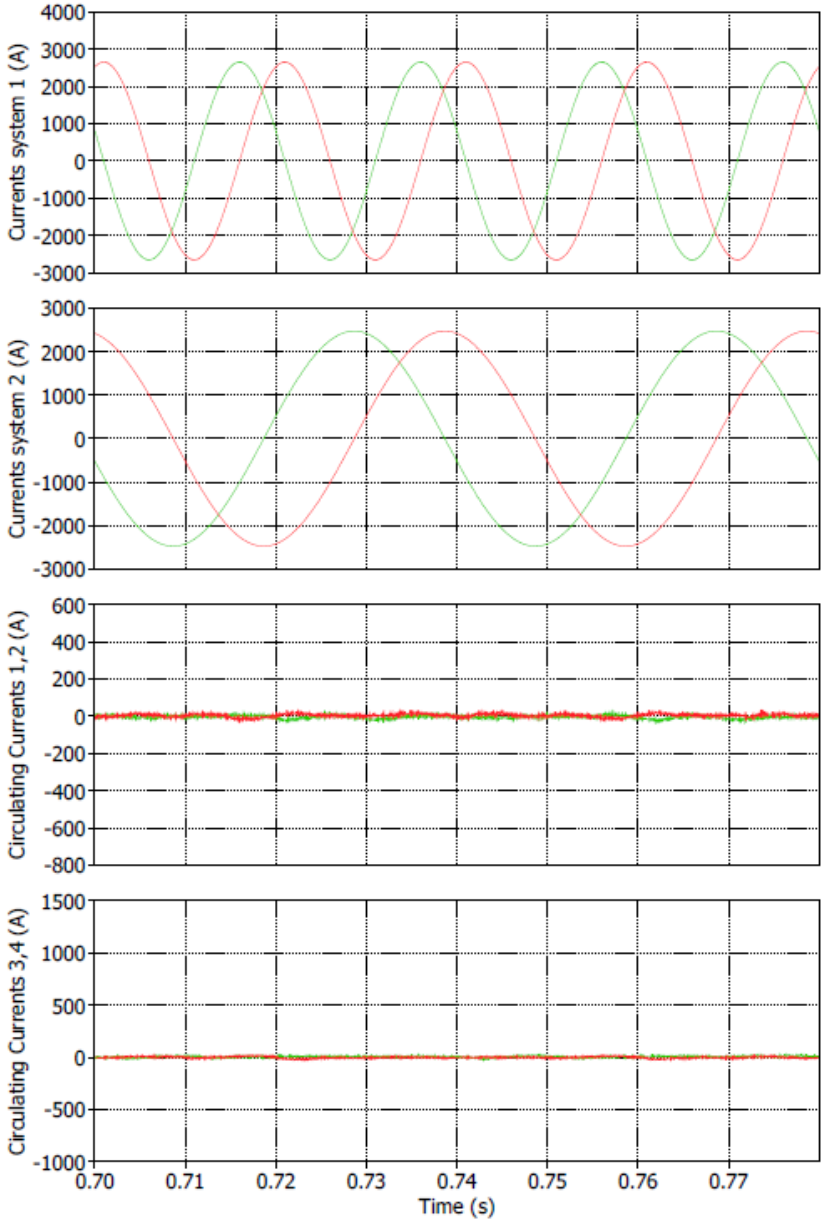
Currents system 1 (A)
4000
3000
2000
1000
0
-1000
-2000
-3000
Currents system 2 (A)
3000
2000
1000
0
-1000
-2000
-3000
Circulating Currents 1,2 (A)
600
400
200
0
-200
-400
-600
-800
Circulating Currents 3,4 (A)
1500
1000
500
0
-500
-1000
0.70
0.71
0.72
0.73
0.74
0.75
0.76
0.77
Time (s)

(a)

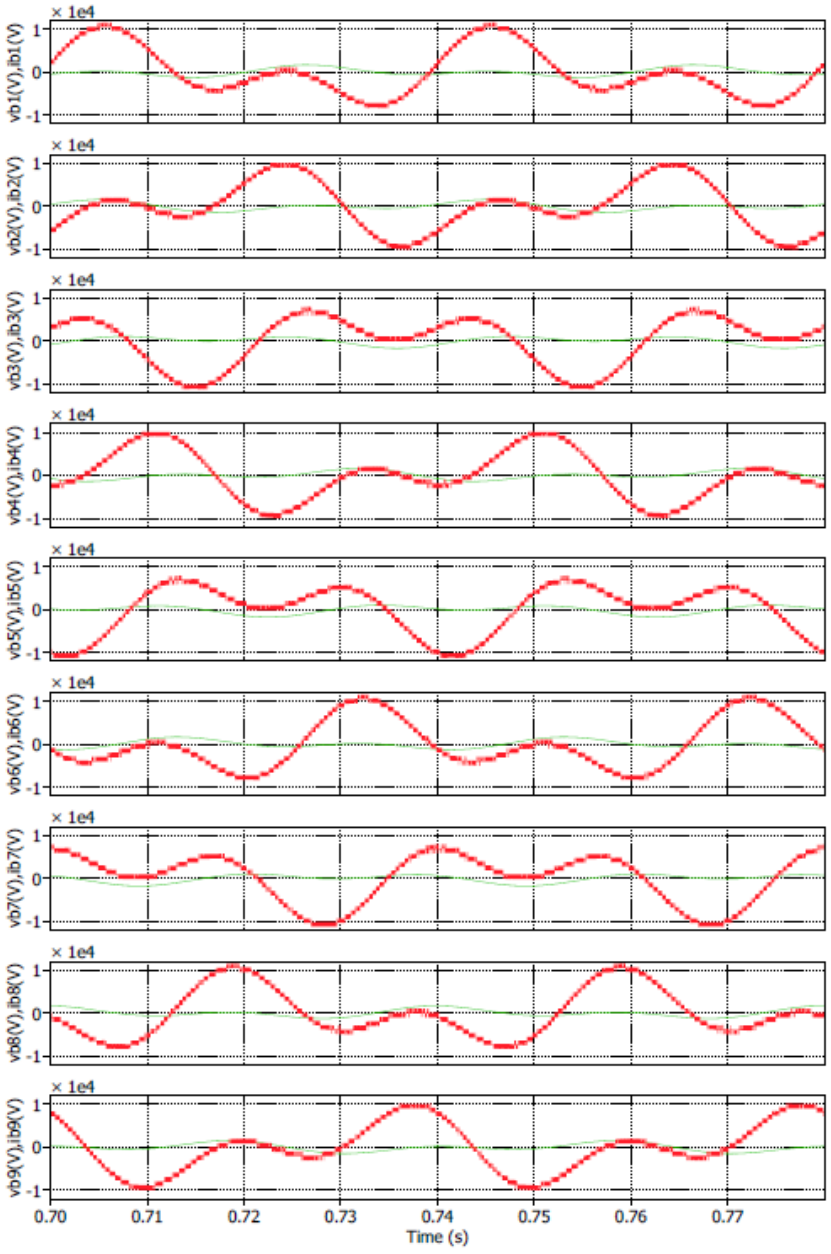

(b)

Fig. 3-24. (a) System currents (in αβ-components) and circulating currents of the Modular Multilevel Matrix Converter for Scenario 5; (b) Branch modules' output voltages (red) and branch currents (green) of the Hexverter topology for Scenario 5.

The THD of the simulated generator and grid side currents is given in Table 3-33. All current THDs are lower than the given limit as well. As a consequence, the Hexverter and the MMMC require no additional filter for the given THD limit. With a lower limit, a filter might be necessary, but will be small compared to the filter required by a 2-level or 3-level converter.

Table 3-33. Total harmonic distortion of the system currents of the Modular Multilevel Matrix Converter

Scenario	1	2	3	4	5	6
Generator side current THD	0.07	0.3	-	0.05	0.1	-
Grid side current THD	0.8	0.7	-	0.3	0.3	-

In conclusion, the simulation results show that a steady state operation of the converters for all considered scenarios is possible with the presented component design.

3.7 Reliability

Like all modular multilevel converters, the Hexverter and the MMMC can be designed for high reliability very easily. This high reliability is achieved by adding additional modules in each branch, which would not be necessary for normal operation. In case of a fault within one of the modules, this module is short circuited and the converter is operated without it. For using this method, fault detection and a short circuit device in each module are needed. As a result, the reliability can be improved by a higher investment in additional modules.

Faults that are not caused by semiconductors or passive components within the modules, e.g. faults of the control system, cannot be handled with this approach and their influence on reliability is similar to their influence on the reliability of 2-level or 3-level converters.
The MMMC has an additional advantage according reliability, which makes it even possible to handle faults in the control systems of the single branches. The basic idea is to operate the MMMC as Hexverter in case of a branch fault of the MMMC, for example caused by an error in the control unit of one branch, by too many failed submodules in one branch, etc.. Fig. 3-25 shows a possible combination of six MMMC branches which can be operated as Hexverter. In total, six combinations of MMMC branches can be used as Hexverter topology.

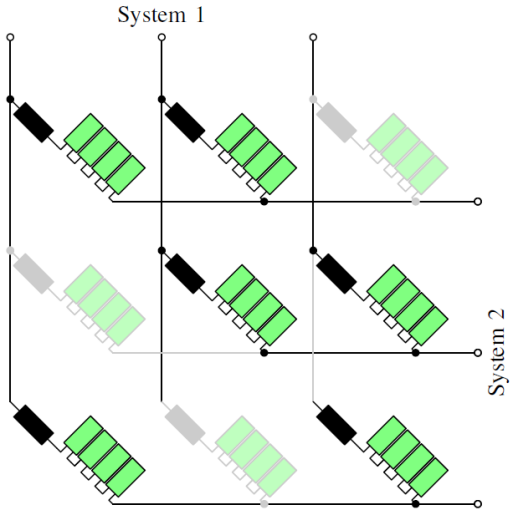

Fig. 3-25. Hexverter topology made up by six Modular Multilevel Matrix Converter branches.

The disadvantage of this approach is the different component design of Hexverter and MMMC branches. The higher branch current, branch voltage and branch energy variation for the Hexverter reduce the maximum power for the MMMC operated as Hexverter. Detailed information on this approach can be found in [11]. For the example in [3-11] the possible maximum active power (without reactive power) in reduced operation is around 56 % of the nominal active power.

According the modular multilevel direct AC/AC converters, the MMMC is advantageous compared to the Hexverter, because of the possibility of operating it as reduced MMMC. In total, the reliability of both topologies can be improved by adding redundant modules, which makes them both to interesting converters for application with high reliability constraints, like offshore wind energy.

3.8 Silicon Carbide (SiC) consideration

The use of SiC for modular multilevel direct AC/AC converters is not investigated in any previous publications. The main advantage of these new semiconductor devices is the possibility of higher switching frequencies. If not operated at these higher switching frequencies, their losses decrease. Looking at the previous results, it can be seen that the advantage of higher switching frequencies for modular multilevel direct AC/AC converters is rather small. The limit for the THD of the system currents is already no problem with the chosen switching frequencies. Only for applications with very high THD requirements, the use of SiC would be an advantage. However, even with very high THD requirements, the use of a higher module number with a lower DC link voltage is an alternative to higher switching frequencies. Using SiC devices with switching frequencies similar to the chosen switching frequencies would improve the efficiency of the system. The disadvantage would be the higher semiconductor costs for SiC device.

Due to the lack of SiC devices with comparable blocking voltages to the chosen Si IGBTs on the market, no calculation of the possible improvement in efficiency and increase in semiconductor cost is done.

3.9 Conclusions

In this Section, the cost, size, efficiency, and reliability of the power converters with different configurations (including Hexverter and MMMCs) are discussed. The MMMCs configurations not only have the higher efficiency but also the low costs in comparison with the Hexverter -based configuration. In addition, the MMMCs size in 2.5 Hz system is a little smaller than Hexverter size and the MMMCs size in 25 Hz system is a little bigger than Hexverter size. The MMMC has an additional advantage according reliability, which makes it even possible to handle faults in the control systems of the single branches. As a consequence, the MMMCs configuration is the better configuration between the two configurations for the given application.

3.10 References

[3-1] S. Rohner, S. Bernet, M. Hiller, and R. Sommer, “Modulation, losses, and semiconductor requirements of modular multilevel converters,” Industrial Electronics, IEEE Transactions on, vol. 57, no. 8, pp. 2633–2642, 2010.

[3-2] L. Baruschka and A. Mertens, “A new three-phase ac/ac modular multilevel converter with six branches in hexagonal configuration,” Industry Applications, IEEE Transactions on, vol. 49, no. 3, pp. 1400–1410, 2013.

[3-3] D. Karwatzki, L. Baruschka, M. v. Hofen, and A. Mertens, “Branch energy control for the modular multilevel converter hexverter,” in Energy Conversion Congress and Exposition (ECCE), 2014 IEEE, accepted for publication, sept. 2014.

[3-4] L. Baruschka, D. Karwatzki, M. v. Hofen, and A. Mertens, “Lowspeed drive operation of the modular multilevel converter hexverter down to zero frequency,” in Energy Conversion Congress and Exposition (ECCE), 2014 IEEE, accepted for publication, sept. 2014.

[3-5] F. Kammerer, J. Kolb, and M. Braun, “A novel cascaded vector control scheme for the modular multilevel matrix converter,” in IECON 2011 - 37th Annual Conference on IEEE Industrial Electronics Society, 2011, pp. 1097–1102.

[3-6] F. Kammerer, J. Kolb, and M. Braun, “Fully decoupled current control and energy balancing of the modular multilevel matrix converter,” in Power Electronics and Motion Control Conference (EPE/PEMC), 2012 15th International, 2012, pp. LS2a.3–1–LS2a.3–8.

[3-7] W. Kawamura and H. Akagi, “Control of the modular multilevel cascade converter based on triple-star bridge-cells (mmcc-tsbc) for motor drives,” in Energy Conversion Congress and Exposition (ECCE), 2012 IEEE, 2012, pp. 3506–3513.

[3-8] A. Korn, M. Winkelnkemper, P. Steimer, and J. Kolar, “Direct modular multi-level converter for gearless low-speed drives,” in Power Electronics and Applications (EPE 2011), Proceedings of the 2011-14th European Conference on, 30 2011-sept. 1 2011, pp. 1 –7.

[3-9] W. Kawamura, M. Hagiwara, and H. Akagi, “A broad range of frequency control for the modular multilevel cascade converter based on triplestar bridge-cells (mmcc-tsbc),” in Energy Conversion Congress and Exposition (ECCE), 2013 IEEE, 2013, pp. 4014–4021.

[3-10] Mouser Electronics. http://dk.mouser.com/

[3-11] D. Karwatzki, M. v. Hofen, L. Baruschka, and A. Mertens, “ Operation of Modular Multilevel Matrix Converters

[3-12] F. Branches,” Industrial Electronics Society, IECON 2013, 2014 IEEE, accepted for publication, sept. 2014.

4 DIODE RECTIFIER, CURRENT SOURCE AND HYBRID VOLTAGE SOURCE CONVERTER – CURRENT SOURCE CONVERTER (VSC-CSC)

4.1 Overview of Topologies

This section covers analysis of converters based around using a passive rectifier and boost converter on the generator side of the converter, and it has also been extended to cover some other current-source topologies with similar characteristics. In INNWIND deliverable report 3.42, *First assessment of performance indicators of Superconducting direct drive and Pseudo magnetic direct drive generators*, it was established that a passive rectifier would not be able to achieve the desired generator harmonic level, and that passive filtering would not be suitable due to the low harmonic frequencies involved and the generator frequency varying with wind speed. Furthermore, the inability of the passive rectifier to supply reactive power to the generator results in higher generator currents and increased losses, in addition to the losses due to the harmonic content. For this reason, it was decided to use an active filter to reduce the harmonics in the generator current, and provide the required reactive power, an example of the tandem inverter [4-1]. The active filter is a power electronic converter which does not transfer real power, and is rated less than half of the main converter rating.

The baseline converter topology, which will be referred to as Boost-Neutral-Point-Clamped (Boost-NPC), is shown in Figure . The active filter is connected to the generator terminals via a small inductance. The diode rectifier is followed by an inductor, and boost converter, which feeds the two voltage levels of a 3-level neutral-point-clamped (NPC) inverter. The inverter is connected to the grid using an LCL filter, to keep the harmonics within those specified by the grid codes. The active switching devices used are Integrated Gate-Commutated Thyristors (IGCTs).

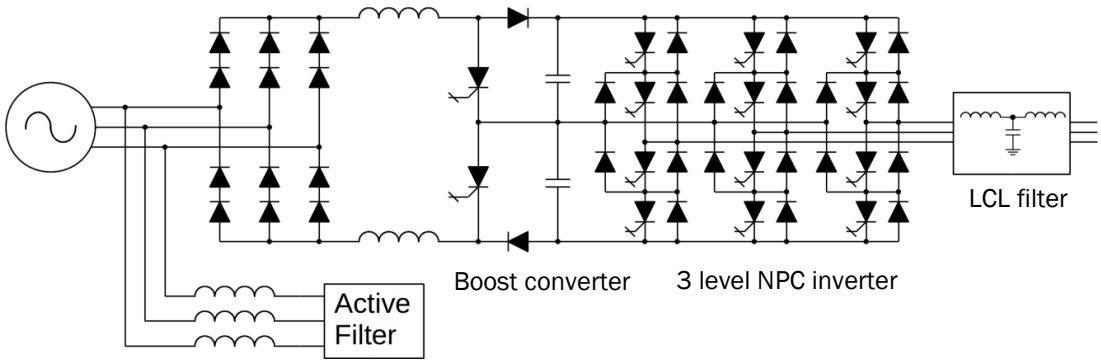

Figure 4-1 Boost-Neutral-Point-Clamped (Boost-NPC) topology consisting of passive rectifier, boost converter, NPC inverter.

An issue with the Boost-NPC topology is that it features three conversion steps, being the rectifier, boost converter and NPC inverter, which leads to greater complexity and potentially lower efficiency. The boost converter is necessary as the DC-link voltage of the NPC converter must always be higher than the peak grid voltage, but at low wind speeds the turbine will be turning slowly and the generator voltage will be low. Hence the boost converter is needed to allow the low generator voltage.

An alternative to the voltage-source NPC inverter is to use a current-source inverter (CSI), using IGCTs with pulsewidth modulated (PWM) switching, in which the DC-link voltage must be lower than the grid voltage. This topology, which will be referred to as CSI, is shown in Figure . In this topology, the diode rectifier is replaced by one based on thyristors – during a grid fault, the grid voltage may drop below the DC-link voltage, while the inverter must remain connected and supplying reactive power. In this case, excessive DC current will flow unless the delay angle on the

generator side rectifier is increased to reduce the DC voltage. The inverter is connected to the grid using an LC filter.

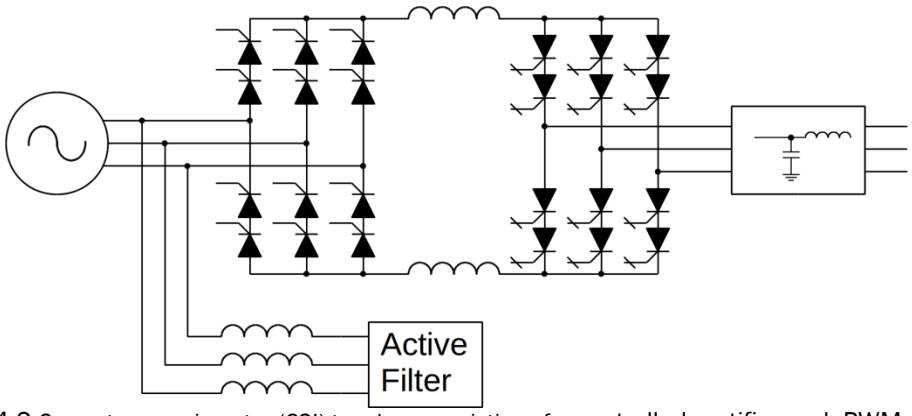

Figure 4-2 Current-source inverter (CSI) topology consisting of a controlled rectifier and PWM current-source inverter.

A third topology, which will be referred to as CSI-Actfilt, is shown in Figure . This uses a thyristor inverter on the grid side, with the current harmonics from the inverter reduced using a second active filter, which also provides power-factor correction to the inverter. The inverter is connected to the grid using a simple inductor, as the active filter results in a low distortion output.

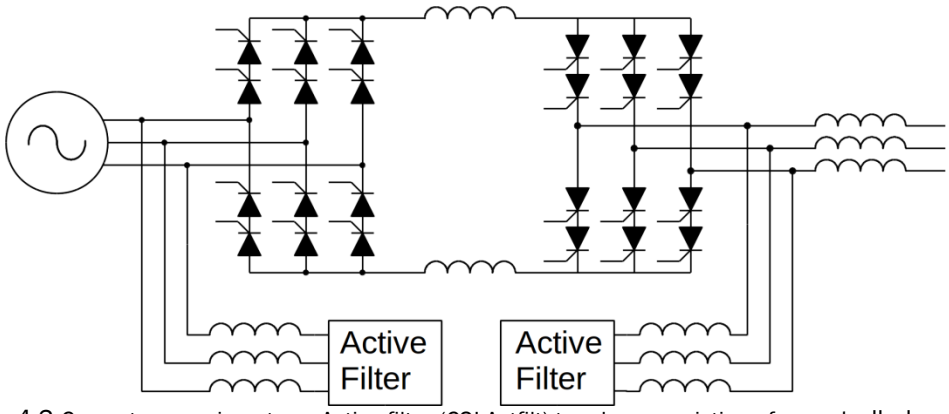

Figure 4-3 Current-source inverter – Active filter (CSI-Actfilt) topology consisting of a controlled rectifier, current-source inverter and an active filter.

The chosen active filter design is shown in Figure , and is based on a modular cascaded multilevel inverter, using cheaper low-voltage IGBTs. As the rectifiers used in all topologies are current-source in nature, a voltage-source shunt active filter must be used [4-2]. This type of converter normally requires isolated voltage sources for each module, but these are not necessary here as the converter is not required to transfer real power [4-3]. The converter voltage rating can be increased by increasing the number of modules, and the converter can also have fault-tolerance or redundancy for increased reliability so long as a method of bypassing the faulted modules is included in the design. In all converters, the converter voltage rating can be increased by increasing the number of series switching devices, and redundancy can be introduced through the same means.

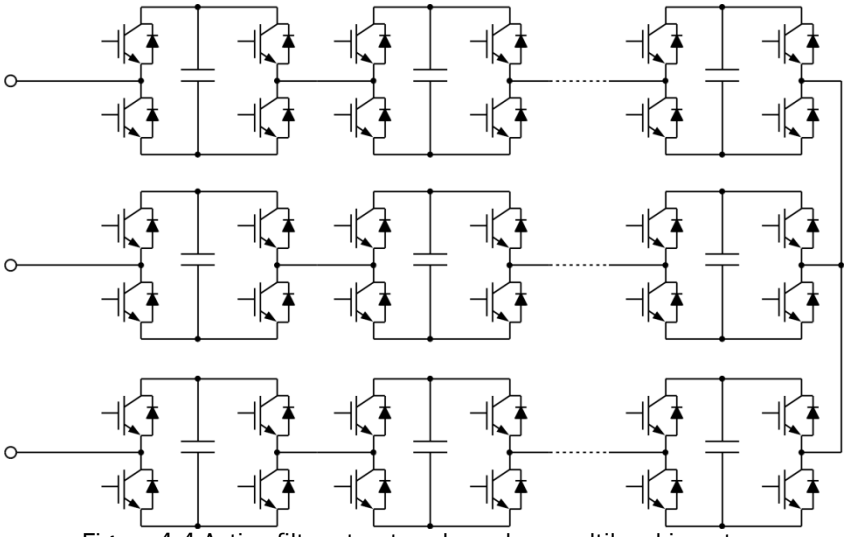

Figure 4-4 Active filter structure based on multilevel inverters

4.2 Principals of Operation

This section will cover the operation of the active filter on its own, based on the connection to the boost-NPC converter, and the operation of the converters themselves separately. Where modifications to the active filter operation for specific converter topologies are necessary, these will be covered along with the operation of the converters.

4.2.1 Active Filter

Control of the active filter follows that of the tandem inverter reported in literature, which uses a thyristor converter with a 2-level shunt filter[4-1]. Differences mainly relate to balancing of the DC-link voltages in the modules of the modular filter, which is ignored in this study. A generalised single-line representation of the generator, rectifier and filter is shown in Figure . The generator produces an EMF e proportional to the generator speed, and has an inductance L_g, with a current i_g flowing, and the generator terminal voltage is v. The active filter has an overall DC-link voltage of V_{DCf}, and supplies a current i_f. It is connected to the generator terminals using a small inductance L_f, which will be ignored in the calculations.

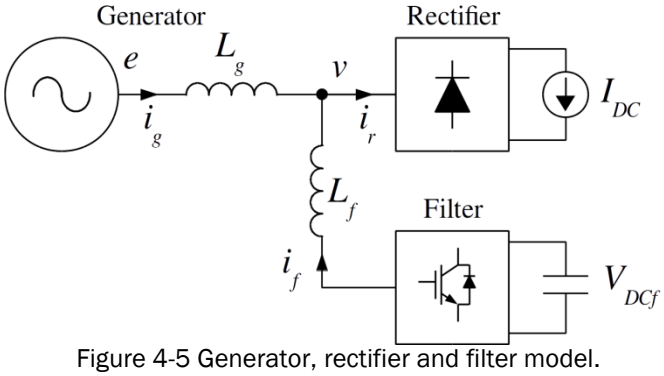

Figure 4-5 Generator, rectifier and filter model.

Preliminary results show that the superconducting generator will have a per-unit inductance of around 0.3. The inductance of the PMDD generator is not known, but it has been stated that this generator is capable of operating through a passive rectifier without an active filter, meaning that it is around 0.4 or lower. A lower inductance will increase the level of current harmonics if no

active filter is used, while a high inductance will increase the reactive power which must be supplied by the filter.

In operation, the current drawn by the passive rectifier can be approximated by a square wave of magnitude I_{DC} and a conduction angle of 120°, given by (4-1), with the fundamental frequency component given by (4-2). For a desired RMS generator current I_g^* with power factor angle δ, the desired generator current is given by (4-3), and this is used to calculate the required DC link current for the converter current controller using (4-4), which is a rearrangement of (4-2). Assuming the active filter is able to force the generator current to follow the desired value, i.e. $i_g = i_g^*$, then the filter current will be given by (4-5).

$$i_r = \begin{matrix} I_{DC} \\ -I_{DC} \\ 0 \end{matrix} \left| \begin{matrix} \pi/6 < \omega t < 5\pi/6 \\ 7\pi/6 < \omega t < 11\pi/6 \\ otherwise \end{matrix} \right. \tag{4-1}$$

$$I_{r,0} = \frac{\sqrt{6}}{\pi} I_{DC} \approx 0.780 I_{DC} \tag{4-2}$$

$$i_g^* = \sqrt{2} I_g^* \sin(\omega t + \delta) \tag{4-3}$$

$$I_{DC}^* = \frac{\pi}{\sqrt{6}} I_g^* \tag{4-4}$$

$$i_f = i_r - i_g^* \tag{4-5}$$

The basic control system for the active filter is shown in Figure . The position of the generator EMF is estimated, and for the given desired d- and q-axis currents the required feedforward voltage at the generator terminals is calculated. This is converted to the fixed reference frame, and over-modulated using 3rd harmonic injection, to maximise the use of the filter DC-link voltage. A proportional controller is used to force the generator currents to follow the desired values – if the feedforward voltages are correct then no steady-stage error will result. The duty cycle for the converter is calculated by dividing by the overall filter DC-link voltage, and the PWM signals for the individual modules are generated using phase-shifted triangular carrier waveforms.

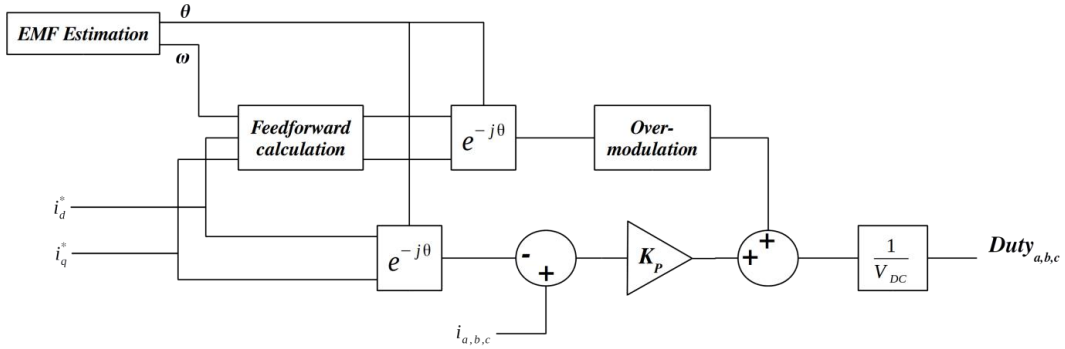

Figure 4-6 Active filter control system block diagram

The system was simulated using Simulink and SimPowerSystems. Due to time constraints, the DC-link voltages of the modules in the active filter were modelled as constant voltage sources. In reality, the overall DC-link voltage would need to be controlled by adjusting the real current demand from the generator in relation to the converter DC-link current. The voltages of the individual modules would need to be balanced, by adjusting the modulation of each module, for which there are several methods reported in literature [4-3 – 4-5]. This could reduce the current control bandwidth of the converter, or require a larger DC capacitance.

Currents in the generator, rectifier and filter are shown in Figure for a 10MW superconducting generator operating at rated power, with a frequency of 2.5Hz. The filter has 4 modules per phase string, switching at 50Hz, each with a DC voltage of 900V. The line-line voltage of the filter is

shown in Figure . The low generator frequency relative to the module switchign frequency, as well as the multilevel nature of the filter, means that the current THD is around 0.4%, well below the specified limit. The module switching frequency could be reduced, but would have minimal effect on the switching losses, and a lower frequency could cause unwanted additional current ripple in the DC-link.

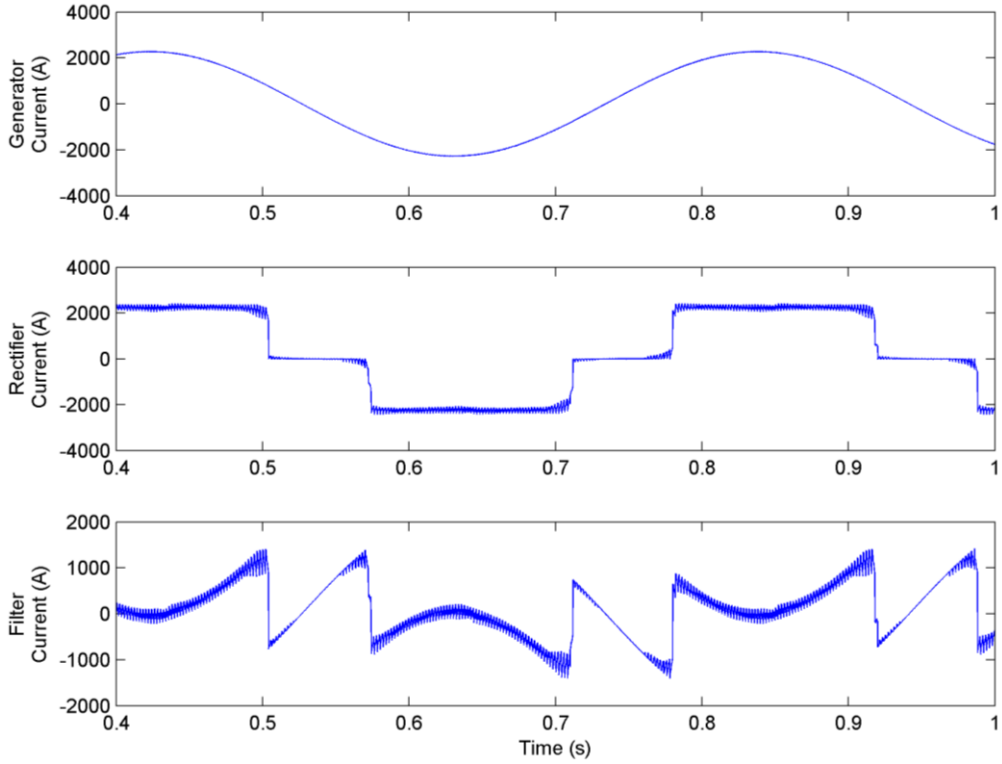

Figure 4-7 Generator, rectifier and filter currents

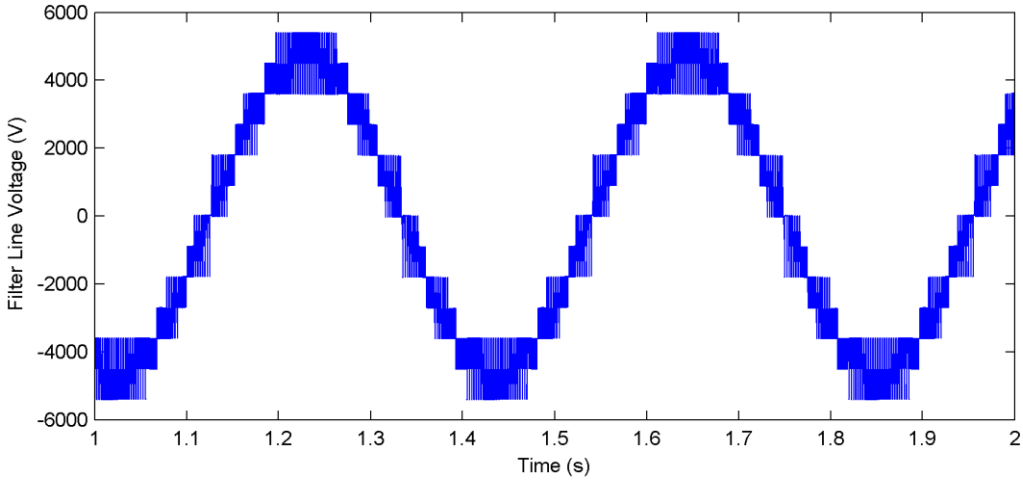

Figure 4-8 Filter line-line voltage

4.2.2 Boost-Neutral-Point-Clamped (Boost-NPC) converter

Operation of this converter is most similar to a conventional converter. Based on the torque demand from the turbine controller, the required generator current is calculated, and a DC current demand calculated according to (4-4), with the DC current being controlled by a simple PI

controller which sets the duty ratio of the boost converter. The switching of the upper and lower boost converters is interleaved to minimise the DC inductor ripple.

The diode rectifier, operating with a current-source DC link as here, will produce a DC voltage ripple at the terminals, according to (4-6), with an average value given by (4-7) [4-6]. This represents a power ripple, which must not be transferred onto the grid, and therefore must be absorbed by storage elements in the converter. To minimise the size requirements for the DC inductors, the DC current in the boost inductor will be held constant by the controller, so the duty cycle will match the ripple given by (4-6), and the energy ripple will be absorbed by the DC link capacitors for the NPC converter.

$$v_{DC} = \sqrt{2}V \cos \omega t \qquad -\frac{\pi}{6} < \omega t < \frac{\pi}{6} \tag{4-6}$$

$$V_{DC} = \frac{3}{\pi}\sqrt{2}V \approx 1.35V \tag{4-7}$$

In simulation, the DC link of the NPC converter was represented as a constant voltage – the NPC converter will be controlled to maintain the DC-link voltage in the conventional manner and this is covered elsewhere. In this implementation, a switching frequency of 500Hz is used for the boost and NPC converters.

The simulated DC-link current and duty cycle of the boost converter from a 10MW converter connected to a superconducting generator are shown in Figure , where the DC-link inductance has been calculated to achieve a 10% peak to peak current ripple. While the boost converter controller is able to reduce the current ripple from the rectifier at 6 times the generator frequency, it cannot eliminate it altogether, due to the rapid reversals in voltage trajectory around $\omega t = \pm {}^{\pi}/_{6}$, leading to an overall ripple exceeding the 10% specification.

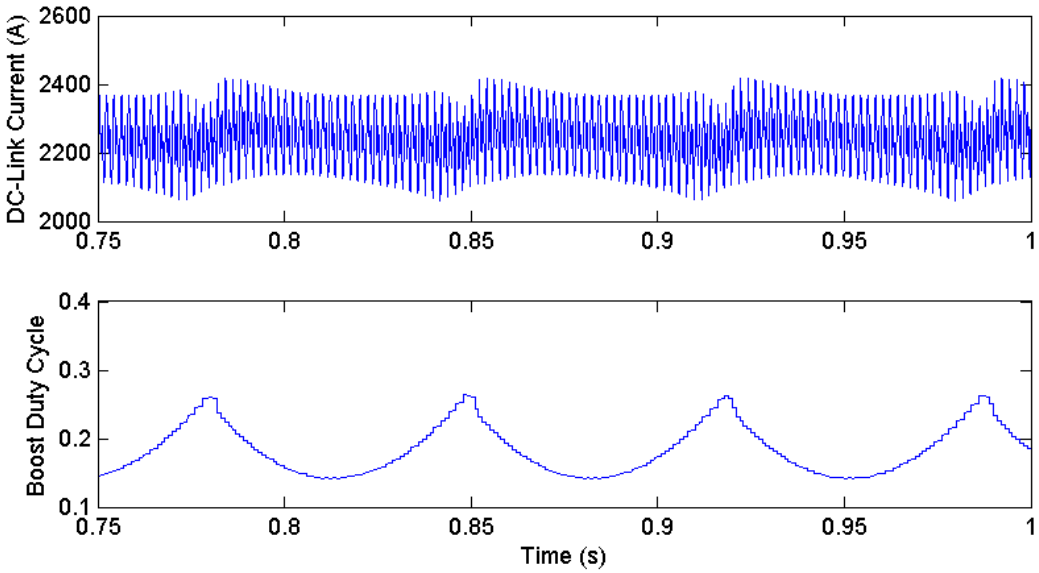

Figure 4-9 Boost-NPC DC-link current and boost converter duty cycle.

4.2.3 Current-source inverter (CSI) topology

The CSI topology is based around a PWM-switched current-source inverter, the control of which differs from a PWM voltage-source inverter in the following ways:

- There must always be one device switched on in the upper and in the lower half of the converter to provide a circular current path.

- The current path cannot divide, so only one device in each of the upper and lower halves can be on at one time.
- Both the upper and lower devices in one leg can be switched on.

Based on these limitations, there are three suitable classes of switching pattern [4-7]:

- Trapezoidal modulation is the simplest method to implement, but harmonic distortion is high.
- Selective harmonic elimination (SHE), which uses a pre-calculated lookup table of switching angles for each modulation depth. It provides the best harmonic content, but the modulation depth is limited to around 0.9, above which harmonic distortion increases.
- Space-vector modulation (SVM), which is similar to the voltage-source version, providing a good range of modulation depths but worse harmonic content.

Selective harmonic elimination was chosen, to give the best possible output waveform and minimal filtering requirements. A full description of the method is given in [4-8], and a brief description will be given here. A switching pattern was chosen which controls the fundamental current magnitude while eliminating 4 harmonics, using 5 controllable angles α_{1-5}, which is shown in Figure . The angles were calculated in order to eliminate the 5th, 7th, 11th and 13th harmonics, and are similar to those shown in Figure . This scheme results in the IGCTs switching at around 500Hz, around the limits of the capability of IGCTs on the market.

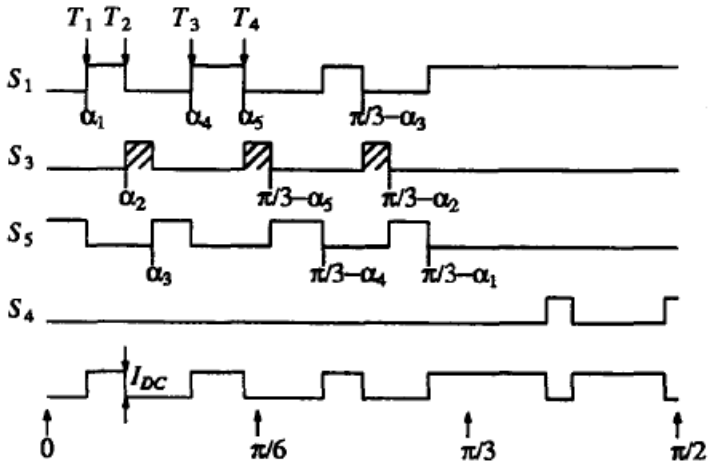

Figure 4-10 SHE-PWM to eliminate 6 harmonics [4-8].

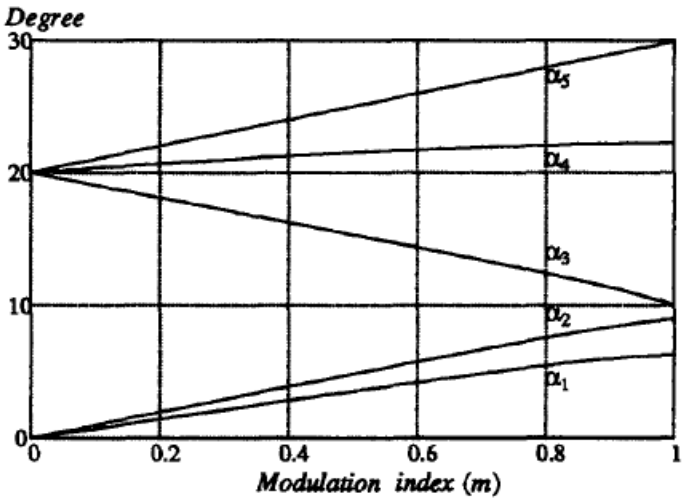

Figure 4-11 Switching angles for the chosen SHE-PWM scheme [4-8]

Grid current and voltage waveforms are shown for the current-source inverter in Figure . The PWM inverter current leads to a sinusoidal inverter voltage with ripple, smoothed by the capacitance at the termninals. The inverter voltage ripple leads to a grid current ripple, determined by the filter inductor. The filter capacitance was set to give a peak-peak voltage ripple of around 20%, and the inductance set to keep the grid current THD below 5%.

The DC link inductor current for the 10MW converter connected to a superconducting generator is shown in Figure , showing the high frequency ripple from the inverter and the low frequency from the generator and inverter.

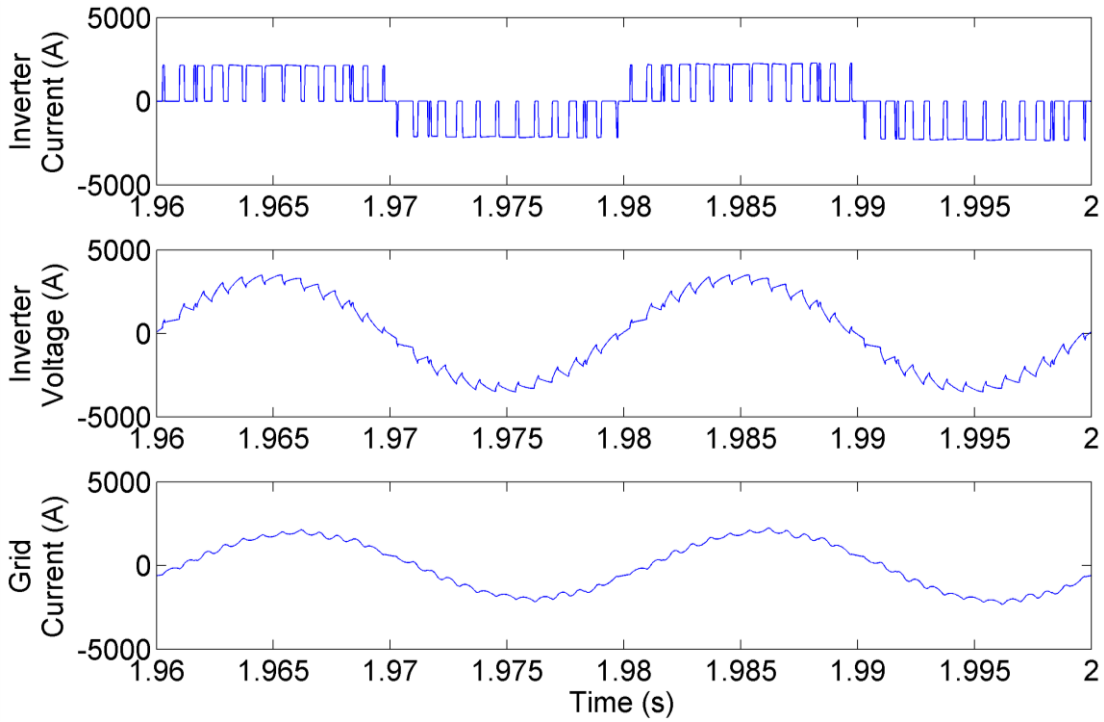

Figure 4-12 PWM current-source inverter voltages and currents.

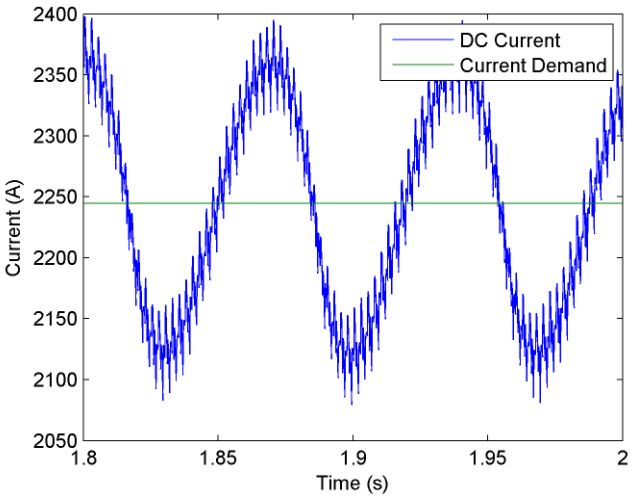

Figure 4-13 CSI DC-link current.

A PI controller is used to regulate the DC current and hence generator torque by adjusting the grid current demand through the modulation depth of the grid converter. This must be fast enough to achieve reasonable torque control bandwidth, but not transfer any of the 6x generator frequency ripple to the grid. There are also potential resonance issues with the grid filter – in the simulations carried out these were damped by adding a resistance in parallel with the grid capacitor, but this wastes energy, and active damping solutions using the inverter controller have been demonstrated [4-9].

An additional control problem is that the grid side capacitor must be provided with reactive power if the converter is to operate at unity power factor, and this is constant at all power levels at around 4.5MVAr for the filter design chosen for the 10MW converter, and double that for 20MW. In order for the inverter to provide this, the DC-link current must be above a certain minimum value. When the generator current is insufficient according to (4-4), a delay angle can be applied to the generator side rectifier, to reduce the generator power factor and increase the current. The resulting reactive power can be provided by the generator itself or the active filter depending on which results in the lowest losses.

A control system implementing this was not developed, but a steady state analysis was carried out in order to calculate device losses and component ratings. Neglecting converter losses, the converter apparent power is a combination of the real power output of the generator P_{Gen} and the reactive power consumed by the filter capacitor Q_{Cap}, as given in (4-8). Combining the formula for 3-phase power with that of the PWM converter output gives the minimum DC current (4-9), where d_{max} is the maximum duty cycle. From (4-4), the minimum rectifier current $I_{r\ min}$ is given by (4-10), which can be used to calculate the reactive current supplied by the active filter.

$$S_{Conv} = \sqrt{P_{Gen}^2 + Q_{Cap}^2} \tag{4-8}$$

$$I_{DC\ min} = \frac{S_{Conv}\sqrt{2}}{d_{max} V_{Grid}\sqrt{3}} \tag{4-9}$$

$$I_{r\ min} = \frac{\sqrt{6}}{\pi} I_{DC\ min} \tag{4-10}$$

Figure shows the minimum and actual DC currents over the variable-speed range of the turbine. For most of the range, the DC current is at the minimum value necessary to supply the reactive power of the output capacitor, and the duty cycle of the CSI will be kept around the maximum of 0.9. In the region between around 7.5 and 11m/s, the current is slightly higher, and the duty cycle will be reduced in order to reduce the grid current.

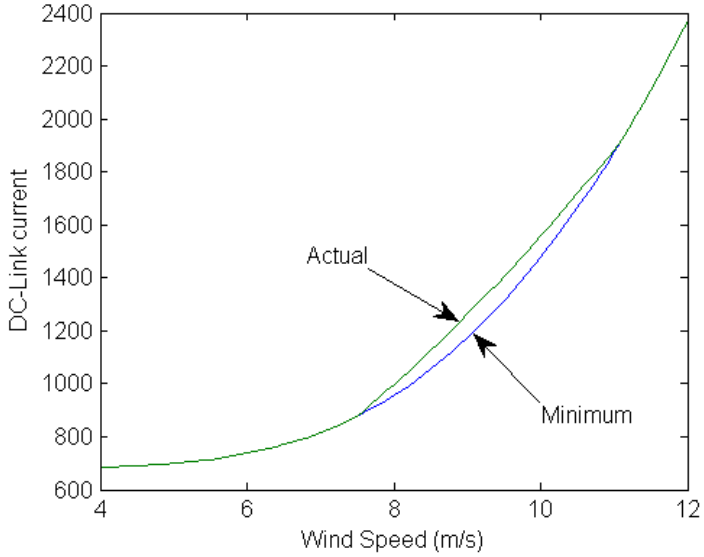

Figure 4-14 CSI minimum and actual DC currents at different wind speeds.

At rated power, the delay angle of the generator side rectifier will be low, and the DC voltage from the rectifier will be close to that given by (4-7), i.e. 4,455 V and 8,910 kV for the 10 and 20MW generators producing 3.3 and 6.6 kV. Given the upper limit on the grid side modulation depth of 0.9, the grid voltage must be at least 3.5 kV and 7 kV for 10 and 20 MW, and grid voltages of 4 kV and 8 kV are chosen, while the generator voltages remain at 3.3 and 6.6 kV.

4.2.4 Current-source inverter – Active filter (CSI-Actfilt) topology

Using an active filter on both the grid and generator sides allows thyristors to be used in both sides of the converter, reducing costs and losses. The generator side converter is normally switched at zero delay angle, with the delay angle only increased when the grid voltage is depressed during a grid fault. The delay angle on the grid side converter is controlled to regulate the DC current, and hence the generator torque. The active filter on the grid side is controlled in the same way as the machine side filter, to maintain unity power factor output and a sinusoidal current, and the switching frequency per module is increased to 300Hz. A grid coupling inductor of 0.1 p.u. is used.

The RMS voltage at the DC terminals of the grid side converter is a function of the grid voltage V_{grid} and the delay angle α, given by (4-11). The voltage across the DC-link inductor V_L, determining the rate of change of current, is found by subtracting (4-11) from (4-7), giving (4-12), where V_r is the rectifier terminal voltage, and this forms the basis of the control system, which controls V_L using α to achieve the required DC current for the torque demand. For the superconducting generator, with a frequency of 2.5Hz, the control system can be set fast enough to react to the 15Hz ripple from the rectifier, transferring it to the grid side where it is absorbed by the grid active filter. This reduces the size of DC-link inductor required to limit the ripple current.

$$V_{DC} = \frac{3}{\pi}\sqrt{2}V_{grid}\cos\alpha \tag{4-11}$$

$$V_L = L_{DC}\frac{di}{dt} = \frac{3\sqrt{2}}{\pi}\left(V_r - V_{grid}\cos\alpha\right) \quad (4\text{-}12)$$

Simulated grid side currents for the converter are shown in Figure . The switching frequency for the active filter modules was set to 300 Hz in order to achieve the specified 5% grid current THD, but it is clear that the ripple current from the switching is relatively low. The bulk of the distortion is due to the spikes around the switching of the thyristors, which cannot be properly compensated for due to the rate of change of filter current being limited by the inductor connecting the filter to the inverter terminals. The inductance had to be relatively high in order for the simulation to be solvable, and could potentially be significantly lower, allowing a lower filter switching frequency.

The DC-link current and inverter firing angle are shown in Figure for the converter connected to a 2.5 Hz generator, with the inverter DC-link current controller compensating for the 15 Hz power ripple from the generator. It is clear that this compensation is only partially successful, limiting the ripple to about equal in magnitude to the higher frequency ripple from the grid side inverter. While the required inductance will be larger than if the ripple were entirely compensated, it will still be significantly smaller than if the ripple had to be absorbed entirely by the inductor, as in the CSI.

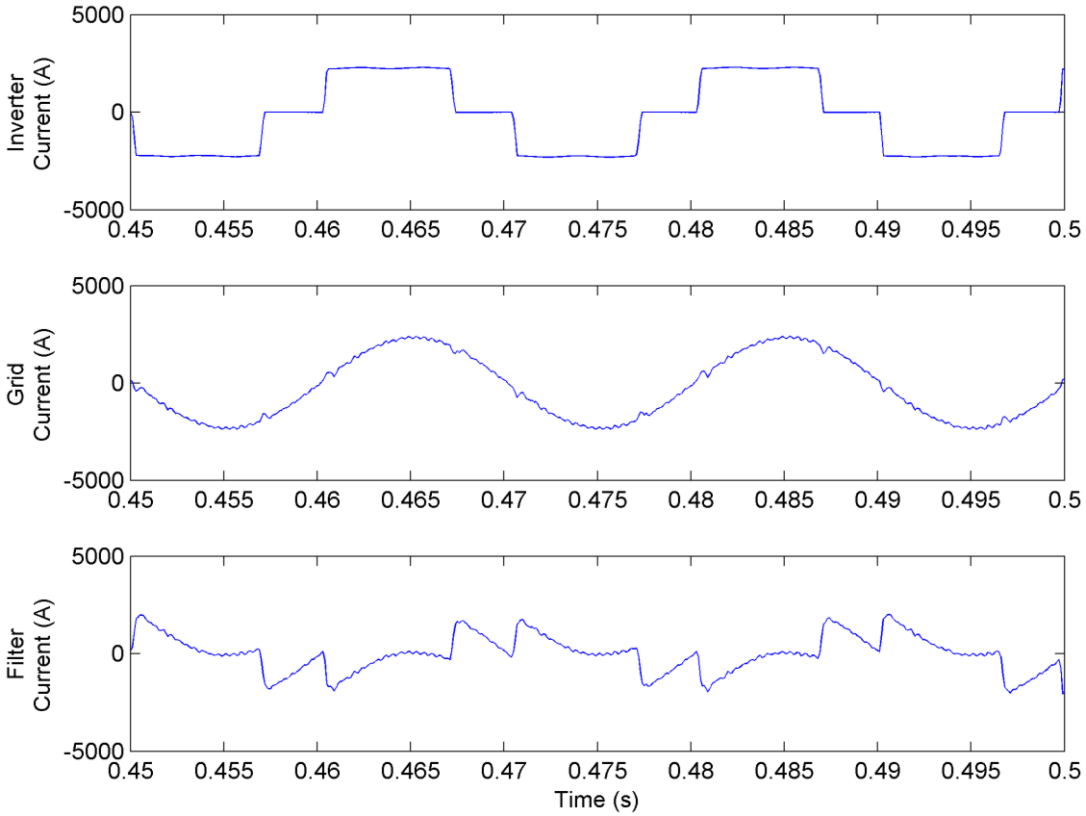

Figure 4-15 Grid side currents for the CSI-Actfilt converter.

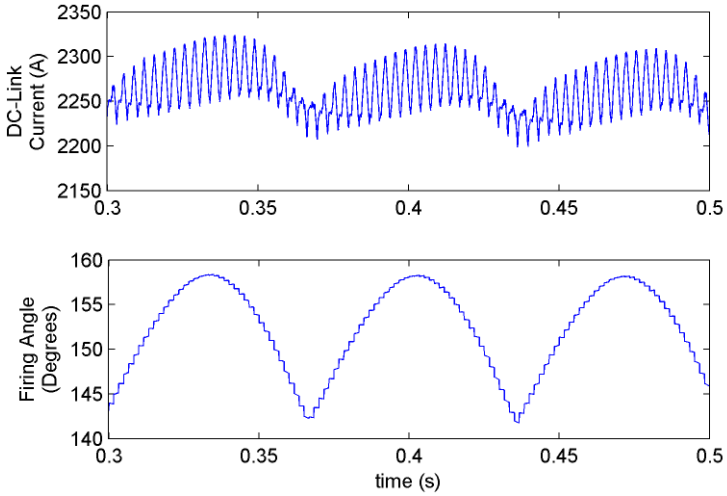

Figure 4-16 CSI-Actfilt DC current and inverter firing angle.

4.3 Component Sizing and Costs

Component sizes are calculated in this section, along with costs. A full breakdown of the converter costs will be given in Section 4.5, as this requires the cooling system cost, which is based on the converter losses calculated in Section 4.4.

4.3.1 Active Filters

The active filter is made up of a number of series modules, with the minimum number of modules determined by the voltage ratings of the switching devices and capacitors. The main components of the active filter are the switching devices and the DC-link capacitor. The switching device is chosen based on keeping the peak current below the DC rating of the transistor – the switching frequency is low so it is assumed that the thermal inertia will not be able to limit the device temperature. A thermal simulation and thermal cycling lifetime analysis would be needed to determine a more accurate rating, but parameters for such an analysis are not available. The transistor choice is listed in Table **4-1**, which are all 1700V devices manufactured by Infineon.

Table 4-1 Active filter switching devices.[3-10]

Transistor	DC current	Cost
FZ3600R17HP4	3600A	€1413.86
FZ2400R17HP4	2400A	€1055.68
FZ1600R17HP4	1600A	€762.29
FZ1200R17HP4	1200A	€702.04

The peak currents and chosen switching devices are shown for the different converters in Table **4-2**, with the peak currents being identical for all generator frequencies and also for both the 10MW and 20MW converters. The CSI has a slightly higher current due to the extra reactive power for supporting the DC-link current, while the grid side filter for the CSI-Actfilt topology has a significantly higher current due to supplying a larger reactive power to compensate for the thyristor converter.

No safety margin is used for the switching devices as it is expected that the actual rating could be much lower due to the thermal inertia of the devices smoothing the current peaks. Avoiding damage due to thermal cycling could mean uprating the switching devices for the 2.5Hz generator, as the lower frequency will result in larger thermal cycle amplitudes.

Table 4-2 Switching devices selected for active filters [3-10]

Converter	Peak Current	Chosen Transistor
Boost-NPC, CSI-Actfilt generator side	1,584A	FZ1600R17HP4
CSI	1,627A	FZ1600R17HP4
CSI-Actfilt grid side	1,839A	FZ2400R17HP4

The chosen DC-link capacitor is listed in Table **4-3**. It is a polypropylene capacitor designed for power factor correction, and has a high RMS current capability, but is used in this case as a DC link capacitor. The filter experiences a current given by (4-1), (4-3) and (4-5), which will cause a ripple in the DC link energy giving a voltage ripple which depends on the capacitance. The energy ripple is determined by integrating (4-5) with respect to time, which was numerically calculated and the peak to peak ripple ΔE recorded. The number of parallel capacitors are selected to give the required capacitance to keep the voltage ripple within specified bounds.

Table 4-3 Active filter capacitor[3-10]

Capacitor	AVX FFL16U0537K
Capacitance	530μF
RMS Current	57A
Maximum Voltage	1100V
Cost	€92.6

The smallest number of series modules n_{min} is given by (4-13), based on the generator voltage V_g and the nominal module DC link voltage $V_{DC\,norm}$, assuming that 12.5% third harmonic injection is used to maximise the voltage utilisation. For a nominal DC link voltage of 950V, the minimum number of series modules will be 3 for the 10MW turbine and 6 for the 20MW. The energy *E* stored in a capacitor is given by (4-14), and the required capacitance is given by (4-15), where the maximum DC-link voltage $V_{DC\,max}$ is the maximum capacitor voltage, 1100V, and the minimum voltage $V_{DC\,min}$ is the peak filter string voltage divided by the number of modules *n*, given in (4-16).

$$n_{min} = \frac{0.875\frac{\sqrt{2}}{\sqrt{3}}V_g}{V_{DC\,nom}} \tag{4-13}$$

$$E = \frac{1}{2}CV^2 \tag{4-14}$$

$$C = \frac{2\Delta E}{V_{DC\,max}^2 - V_{DC\,min}^2} \tag{4-15}$$

$$V_{DC\,min} = \frac{0.875\frac{\sqrt{2}}{\sqrt{3}}V_g}{n} \tag{4-16}$$

It is clear from (4-15) and (4-16) that increasing the number of modules will increase the possible voltage ripple magnitude, which will reduce the required DC capacitance. However, there will also be a minimum capacitance determined by the ripple current requirements. The energy ripple for the different 10MW converter topologies and generator frequencies is given in Table **4-4**, with the ripples for the 20MW converter being double those of the 10MW. The CSI has a higher ripple than the other topologies due to the need to provide reactive power to keep the DC current above the minimum, while the grid side filter of the CSI-Actfilt topology has a higher ripple for the 2.5Hz generator as it must also handle the rectifier ripple passed on to the grid side.

Table 4-4 Active filter DC link energy ripple.

Converter	Generator Frequency	ΔE (J)
Boost-NPC and CSI-Actfilt, generator side	2.5Hz 25Hz 50Hz	62,436 6,244 3,122
CSI, generator side	2.5Hz 25Hz 50Hz	79,278 7,928 3,964
CSI-Actfilt, grid side	2.5Hz 25,50Hz	9,877 5,858

For each of the DC link energy ripples in Table **4-4**, as well as for the 20MW converter, the required DC capacitance was calculated for different numbers of series modules using (4-15) and (4-16), and the required number of parallel capacitors found. The module cost was obtained by adding the total capacitor cost per module to the switch cost and this was multiplied by the number of series modules and the number of phases to obtain the total filter cost.

For the 25Hz and 50Hz generators, as well as the grid side for the CSI-Actfilt topology, the module cost is dominated by that of the switching devices, and the minimum number of modules is the most cost effective. However, it may be desirable to increase the number of modules to provide fault tolerance. For the 2.5Hz generator, the low frequency means that a large capacitance is required, so the capacitor cost dominates.

The variation in the number of capacitors required per module with the number of series modules is shown in Figure , and shows the expected reduction in cost. The total cost is shown in Figure , showing an initial sharp reduction in cost with module number, where the cost is dominated by the capacitor cost, followed by a gentle rise, where the cost becomes more dependent on the switching device cost. While the cost is lowest for 5 modules for 10MW and 9 modules for 20MW, it is expected that additional per-module costs will be added, so the selection of module number should be biased towards a smaller number, with 4 and 8 modules representing a good compromise. The total filter cost for all configurations is given in Table **4-5**.

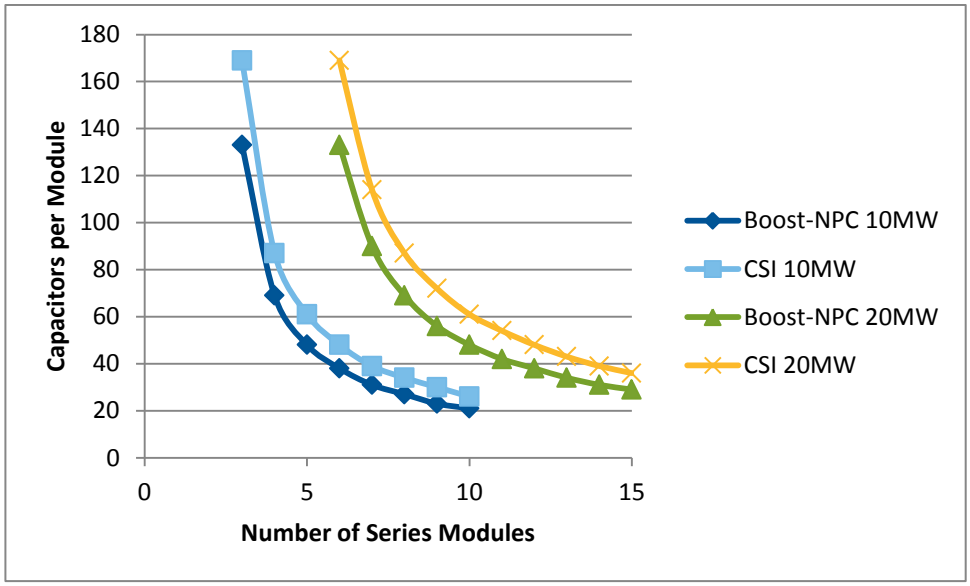

Figure 4-17 Variation in required module capacitors with module number.

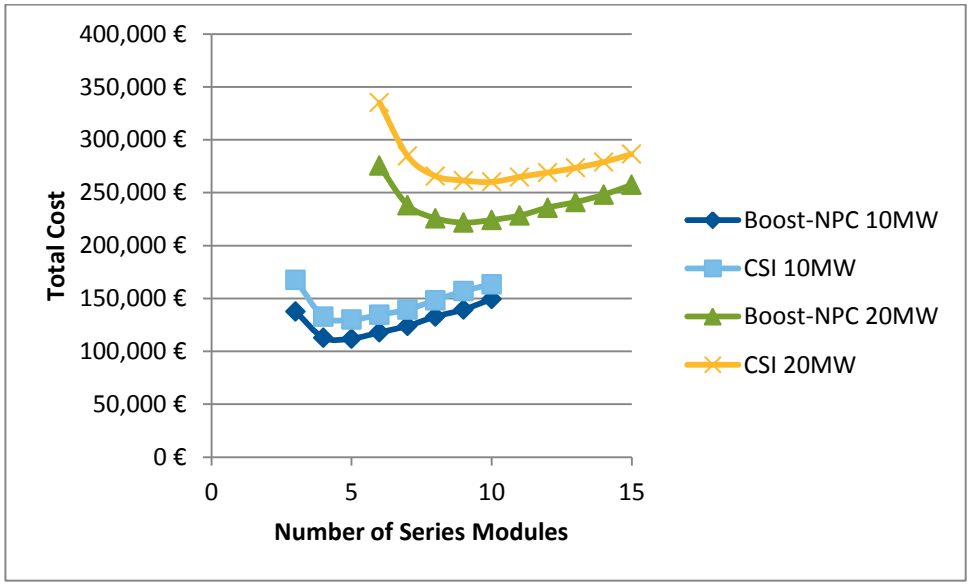

Figure 4-18 Variation in total cost with module number.

Table 4-5 Series modules, capacitors and total costs for all configurations.

Converter	Generator Frequency	Number of Modules per phase		Capacitors per module	Total Cost	
		10MW	20MW		10MW	20MW
Boost-NPC and CSI-Actfilt, generator side	2.5Hz 25Hz 50Hz	4 3 3	8 6 6	69 14 7	€ 112,898 € 39,055 € 33,249	€ 225,797 € 78,110 € 66,498
CSI, generator side	2.5Hz 25Hz 50Hz	4 3 3	8 6 6	87 17 9	€ 132,805 € 41,543 € 34,907	€ 265,610 € 83,086 € 69,814
CSI-Actfilt, grid side	2.5Hz 25, 50Hz	3 3	6 6	21 13	€ 55,423 € 48,787	€ 110,846 € 97,564

4.3.2 Main Switching Devices

The switching devices for the NPC converter are the IGCT and parallel diode shown in Table **4-6**, and these devices are also used for the boost converter and the grid side of the CSI. The 10MW Boost-NPC converter uses 1 series and 1 parallel IGCT, with 2 anti-parallel diodes for the inverter, while the 20MW converter doubles the number of series devices. The boost converter requires two parallel IGCTs – at 500Hz switching frequency the maximum average turn-off current is 1500A, limited by the gate drive thermal rating, and this is exceeded in this case. A slower switching frequency would allow one parallel IGCT, but increase the size and cost of the boost inductor.

The grid side of the CSI, having a 4000V grid voltage, uses two series IGCTs for the 10MW converter and four for the 20MW. For the other devices, the device rating is based on the DC-link current at rated power given in Table **4-7**. The devices are specified by the average current, which in the 6-pulse converters in this study is a third of the DC current, and the average current in Table **4-7** is used to select the devices for 25 and 50Hz operation. For the 2.5Hz generator, the devices are selected to have an average current capability greater than the DC current, as it is expected that the device thermal inertia will not be able to smooth the temperature fluctuations.

Table 4-6 IGCT and diode for NPC and boost converter [4-12]

Device	Model	Voltage rating	Cost each
IGCT	ABB 5SHY 35L4522	4500V	€2195
High speed diode (2 used per IGCT)	ABB 5SDF 20L4520	4500V	€600

Table 4-7 Maximum DC-link currents.

Converter	DC current	Average switch current (50Hz)
Boost-NPC	2211A	737A
CSI	2370A	790A
CSI-Actfilt	2211A	737A

Based on these currents, devices were selected and prices sought, and these are shown in Table 4-8. The devices are manufactured by IXYS-Westcode [4-10], and the prices are based on a pack of 6 devices being bought – in this application they are used in multiples of 6 so this is not a problem. To achieve the required voltage rating, two series devices are used for the 10MW converter and four for the 20MW. The total number of each device and the total switching device cost (excluding those in the active filters) for each converter and frequency is given in Table 4-9.

Table 4-8 Selected diodes and thyristors[4-10].

Device	Model	Av. Current rating	Voltage rating	Cost each
Diode	W2115MC520	2115A	5200V	€190
Thyristor1	K1351VF600	1351A	6000V	€580
Thyristor2	K2359TC600	2359A	6000V	€870

Table 4-9 Total component count and cost for semiconductors.

Converter	Generator Frequency	Number of Devices					Total Cost
		IGCT	HS Diode	Diode	Thyristor 1	Thyristor 2	
Boost-NPC 10MW	All	16	44	12	0	0	€ 68,570
Boost-NPC 20MW	All	32	88	24	0	0	€ 137,140
CSI 10MW	2.5Hz 25, 50Hz	12 12	0 0	0 0	0 12	12 0	€ 36,735 € 33,315
CSI 20MW	2.5Hz 25, 50Hz	24 24	0 0	0 0	0 24	24 0	€ 73,470 € 66,630
CSI-Actfilt 10MW	2.5Hz 25, 50Hz	0 0	0 0	0 0	12 24	12 0	€ 17,370 € 13,950
CSI-Actfilt 20MW	2.5Hz 25, 50Hz	0 0	0 0	0 0	24 48	24 0	€ 34,740 € 27,900

Additionally the thyristors would need a gate drive and snubber circuit, the latter of which would contribute to switching losses, but this has not been designed due to time constraints. It has been suggested by the manufacturer that this might be similar in magnitude to the conduction losses [4-10], but will be lower on the rectifier side for the superconducting generator due to the low frequency.

4.3.3 DC-link Inductors

The inductance of the DC-link inductors was calculated in order to achieve a peak-peak current ripple of 10%. The source of the ripple for the different converters is as follows:

- **Boost-NPC** has the PWM switching of the boost converter.
- **CSI** has the voltage ripple from the generator-side thyristor converter, leading to a current ripple. There is also a high frequency ripple from the PWM inverter, but this is much lower and will be ignored.
- **CSI-Actfilt** has the voltage ripple from both the generator and grid side thyristor converters. For the 2.5Hz generator, the ripple from the generator side is mostly transferred to the grid side filter, so the ripple is around twice that from the grid side converter. For the other generators, the maximum ripple is the sum of the ripples from both converters.

For the Boost-NPC converter, at rated power the inductor current will be 2211A, and the boost converter duty ratio will be 17.5%. The upper and lower converters have their switching interleaved, and it is assumed that the top and bottom inductors will both be part of the same inductor. The relationship between voltage and current across the inductor is given in (4-17). The top and bottom IGCTs are switched on for a period given by (4-18), where d is the duty cycle and f_s is the switching frequency. During this period, the voltage across the inductor is the NPC DC voltage, V_{DC} minus the voltage from the rectifier given by (4-7), and approximating the current as linear during this period, the required inductance is calculated using (4-19).

$$V = L\frac{di}{dt} \tag{4-17}$$

$$T = \frac{1-2d}{2f_s} \tag{4-18}$$

$$L = V\frac{\Delta t}{\Delta i} = \left(V_{DC} - \frac{3\sqrt{2}V}{\pi}\right)\frac{(1-2d)}{2\Delta i f_s} \tag{4-19}$$

For the other converters, the ripple is caused by the voltage ripple from the diode rectifier or thyristor converter. In this analysis it is assumed that the firing angle of the thyristor converter will be close to zero at rated power, so the formulae for the diode rectifier will be used. One side of the converter is considered in isolation, with the inductance calculated and inductances from the different sides added where both sides have a diode or thyristor converter. The exception is the CSI-Actfilt converter with the 2.5Hz generator, where the energy ripple from the rectifier is transferred to the grid side filter. In this case, the required inductance from the grid side thyristor converter is doubled to account for the limitations in the ability to transfer the energy.

In the steady state, the voltage on one side of the inductance is given by (4-6), while the other side could be considered to be the average value given by (4-7). Using (4-6) and (4-7), in conjunction with (4-17), the inductor current is given by (4-20). The current ripple can be found by integrating between the values of time where the integrand is zero, which are $\pm {}^{1}/_{\omega}\cos^{-1}{}^{3}/_{\pi}$, which will be represented as $\pm {}^{a}/_{\omega}$.

The current ripple from the lowest to the highest value is given by (4-21), and solving this gives the current ripple in (4-22), which can be rearranged to find the required inductance for a given voltage and frequency.

$$i = \frac{\sqrt{2}V}{L}\int \cos\omega t - \frac{3}{\pi}dt, \quad \frac{-\pi}{6} < \omega t < \frac{\pi}{6} \tag{4-20}$$

$$\Delta i = \frac{\sqrt{2}V}{L}\int_{-{}^{a}/_{\omega}}^{{}^{a}/_{\omega}} \cos\omega t - \frac{3}{\pi}dt \tag{4-21}$$

$$\Delta i = \frac{2\sqrt{2}V}{\omega L}\left(\sin a - \frac{3}{\pi}\right) \approx \frac{0.02557V}{\omega L} \quad (4\text{-}22)$$

The required inductances are listed in Table **4-10** for the different converters. As these inductors are not available off the shelf, the cost and size was estimated in the same way as for the multilevel matrix converter, by designing inductors and calculating the cost of the iron and copper, and multiplying the resulting cost by 4. The inductors are designed according to the ratios given in [4-6], which give the lowest costs, but where the inductor is too deep for the chosen cabinet depth (1.2m) with 10cm clearance the height ratio is increased to reduce the depth, which was not possible for the 48mH inductor. All inductors were designed for a DC current of 2250A, and the designed inductors are listed in Table **4-11**.

Table 4-10 Required inductances.

Converter	Frequency	Required Inductance		Total Inductance
		Generator side	Grid side	
NPC-Boost 10MW	All	2.8mH	n/a	2.8mH
NPC-Boost 20MW	All	5.6mH	n/a	5.6mH
CSI 10MW	2.5Hz 25Hz 50Hz	24.0mH 2.4mH 1.2mH	n/a n/a n/a	24.0mH 2.4mH 1.2mH
CSI 20MW	2.5Hz 25Hz 50Hz	48.0mH 4.8mH 2.4mH	n/a n/a n/a	48.0mH 4.8mH 2.4mH
CSI-Actfilt 10MW	2.5Hz 25Hz 50Hz	n/a 2.4mH 1.2mH	1.2mH 1.2mH 1.2mH	2.4mH 3.6mH 2.4mH
CSI-Actfilt 20MW	2.5Hz 25Hz 50Hz	n/a 4.8mH 2.4mH	2.4mH 2.4mH 2.4mH	4.8mH 7.2mH 4.8mH

Table 4-11 Inductor designs.

Inductance (mH)	Cost	Mass (kg)	DC Resistance (mΩ)	Width (m)	Depth (m)	Height (m)
48.0	€314,418	19,648	41.7	1.33	1.17	2.17
24.0	€195,759	13,154	25.1	1.12	0.98	1.82
7.2	€74,229	5,842	8.29	1.01	0.89	0.89
5.6	€61,480	5,007	6.99	0.94	0.83	0.83
4.8	€57,160	4,685	6.20	0.92	0.80	0.80
3.6	€46,770	3,953	4.98	0.85	0.74	0.74
2.8	€40,232	3,480	4.18	0.80	0.70	0.70
2.4	€35,262	3,111	3.74	0.76	0.67	0.67
1.2	€23,501	2,203	2.19	0.65	0.57	0.57

4.3.4 DC-link Capacitors

The only DC-link capacitors are those of the NPC inverter in the NPC-Boost topology, and these must absorb the effects of the voltage ripple from the generator-side passive rectifier. The level of energy ripple from the rectifier, assuming a constant current, is found by integrating the DC power between the minima and maxima described in the previous section, which is given by (4-23).

Assuming this ripple is transferred to the DC-link capacitors, the required capacitance can be calculated using (4-15).

$$\Delta E = I_{DC}\int_{-a/\omega}^{a/\omega} v_{DC}dt = \sqrt{2}VI_{DC}\int_{-a/\omega}^{a/\omega} cos\omega t - \frac{3}{\pi}dt = \frac{2\sqrt{2}}{\omega}VI_{DC}\left(\sin a - \frac{3}{\pi}\right) \approx \frac{0.02557VI_{DC}}{\omega} \quad (4\text{-}23)$$

For the DC-link, the same capacitor as for the active filter was selected, with the capacitors placed in series to achieve the required DC voltage rating. These capacitors also have a rated RMS current of 57A each, and the number of parallel capacitors to give the required DC voltage ripple may be insufficient to meet this rating. The RMS capacitor current from the boost converter was calculated, and doubled to take account of the NPC converter. Assuming a DC current of 2211A at rated power, and a boost converter duty cycle of 17.5%, the average current is 1963.5A and the RMS is 860A. Therefore, the capacitors must be capable of handling an RMS current of 1720A, requiring 30 parallel capacitors. The number of capacitors required was calculated based on a 10% ripple voltage requirement, and the resulting capacitor bank parameters are shown in Table **4-12**, which is the total number of capacitors for both the top and bottom halves of the DC link.

Table 4-12 DC-link capacitors for Boost-NPC converter.

Converter rating	Generator frequency	Number of Capacitors					Total cost
		Reg. for I RMS	Req. for ripple	Series	Parallel	Total	
10MW	2.5Hz	30	47	6	47	282	€ 25,989
10MW	25Hz	30	5	6	30	180	€ 16,589
10MW	50Hz	30	3	6	30	180	€ 16,589
20MW	2.5Hz	30	47	12	47	564	€ 51,978
20MW	25Hz	30	5	12	30	360	€ 33,178
20MW	50Hz	30	3	12	30	360	€ 33,178

4.3.5 Filters

Passive filters are used on the grid-side converters to achieve the required current ripple, and consist of an LC filter for the Boost-NPC and CSI converters, and a coupling inductor on the CSI-Actfilt. There are also inductors connecting the active filters to the rectifiers/inverters, but the values of these are determined by whether or not the simulation will run, and are in any case small, so they will be ignored.

The filter parameters for the CSI converters were determined through simulation, with the size of capacitance set to achieve a 20% voltage ripple, and the size of the inductance set to achieve the required 5% grid current THD. The CSI-Actfilt uses an inductance set at 0.1p.u. and the inductance and capacitance for the Boost-NPC converter were calculated to achieve the required 5% ripple with the 500Hz switching frequency. These component values are listed in Table **4-13**.

Table 4-13 Filter component values.

Converter	Inductor		Capacitor	
	10MW	20MW	10MW	20MW
NPC-Boost	1.8mH	2.9mH	170μF	100μF
CSI	389μH	794μH	900μF	450μF
CSI-Actfilt	350μH	700μH	n/a	n/a

Inductors were designed as before, and the cost, size and weight are listed in Table **4-14**.

Table 4-14 Filter inductor sizes and costs.

Converter	Induct-ance	Current Rating (A)	Cost	Mass (kg)	Resistance (mΩ)	Width (m)	Depth (m)	Height (m)
CSI 10MW	389μH	1443	€12,535	607	1.58	0.96	0.37	0.37
CSIAF 10MW	350μH	1650	€15,562	754	1.26	1.04	0.40	0.40
CSI 20MW	794μH	1443	€20,960	1,016	2.60	1.14	0.44	0.44
CSIAF 20MW	700μH	1650	€26,312	1,275	2.08	1.23	0.48	0.48
NPC 10MW	1800μH	1749	€52,069	2,523	4.43	1.55	0.60	0.60
NPC 20MW	2900μH	1749	€73,564	3,565	6.38	1.74	0.68	0.68

Capacitors banks were made up from series and parallel combinations of the capacitor in Table 4-3, and are listed in Table 4-15.

Table 4-15 Filter capacitor costs.

Converter	Capacitance	AC Voltage	Series capacitors	Parallel capacitors	Total capacitors	Capacitor cost
NPC 20MW	100μF	6600V	6	2	36	€3,318
NPC 10MW	170μF	3300V	3	1	9	€829
CSI 20MW	300μF	8000V	7	4	84	€7,741
CSI 10MW	600μF	4000V	4	5	60	€5,530

4.4 Calculation of Efficiency

Losses were calculated across the wind speed range from the cut-in speed of 4m/s to the rated speed of 12m/s using Matlab scripts. For each wind speed, the RMS currents and voltages along with the DC current are calculated, and these are used to calculate the conduction losses in the diode and thyristor components where used, the boost converter switches and the inductors. For the inductors, only the conduction loss is calculated, based on the DC resistance – calculating the AC resistance and iron loss would require a more detailed design than was possible in the time frame. For the DC inductors, the AC conduction loss and iron loss will be very low, while the AC filter inductors are generally small with low losses.

In the loss calculations, the semiconductor devices are represented as a threshold voltage V_T in series with a resistance R. The conduction loss can be calculated using (4-24) for the boost converter (for one IGCT-diode pair), where I is the device current and d the duty cycle, which determines the proportion of the switching cycle which is spent in each conduction path. The switching loss is calculated from the switching frequency f_s and the turn-on and turn-off energies, as well as the reverse recovery losses of the diode, according to (4-25), where I_{SW} is the current at which the losses are specified, assuming the losses vary linearly with current.

$$P_c = dI(IR_{IGCT} + V_{T\,IGCT}) + (1-d)I(IR_{diode} + V_{T\,diode}) \quad (4\text{-}24)$$

$$P_{sw} = f_s\left(\frac{I\left(E_{on\,IGCT} + E_{off\,IGCT} + E_{rr\,diode}\right)}{I_{sw}}\right) \quad (4\text{-}25)$$

A similar method is used for the losses in the active filter IGBTs, the PWM CSI and the NPC converter, except here the currents and duty cycles are calculated across one AC cycle, and the losses according to (4-24) and (4-25) are averaged.

4.4.1 Variation of Efficiency with Wind Speed

Efficiency curves are given for the Boost-NPC converter in Figure , with the converter having identical losses for all generator speeds, and for the CSI and CSI-Actfilt in Figure and Figure . A significant proportion of the Boost-NPC loss is the grid filter inductor, and this leads to a higher loss at high powers, where the grid current is highest, and a reduced efficiency. Moving from 10 to

20MW causes the resistance of the inductor to only increase by around 50%, so the 20MW converter has a slightly higher efficiency.

At low wind speeds, the CSI still requires a significant DC-link current, and this leads to high losses and low efficiency at lower wind speeds. The 20MW converter has a slightly greater efficiency, again due to the scaling of the inductor losses with inductance. Efficiency is lower with the 2.5Hz generator due to the larger DC inductor required to smooth the DC current.

The CSI-Actfilt converter has a similar efficiency for 10 and 20MW. The efficiency for the 2.5Hz generator is higher as the generator-side thyristors are higher rated, due to the assumption that the low frequency will mean the thyristor thermal inertia will not be able to smooth the thermal cycles from the AC waveform. Efficiency is higher for the 50Hz generator than for 25Hz as the DC-link inductance is lower, hence the inductor losses are lower.

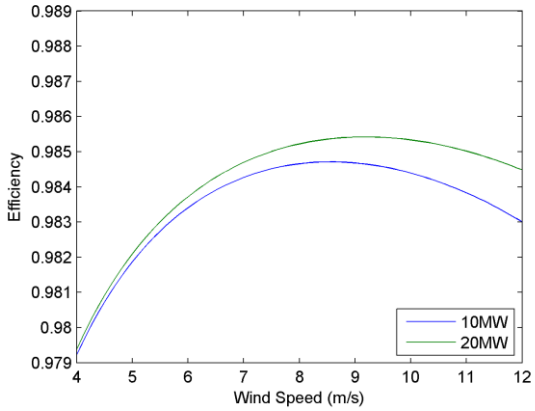

Figure 4-19 Boost-NPC Efficiency (all generators)

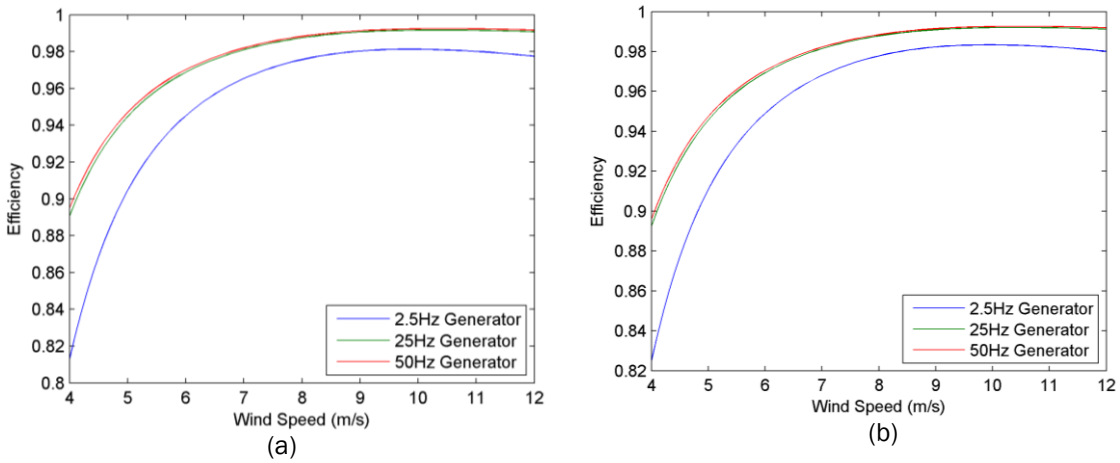

(a) (b)

Figure 4-20 CSI Efficiency, (a) 10MW, (b) 20MW.

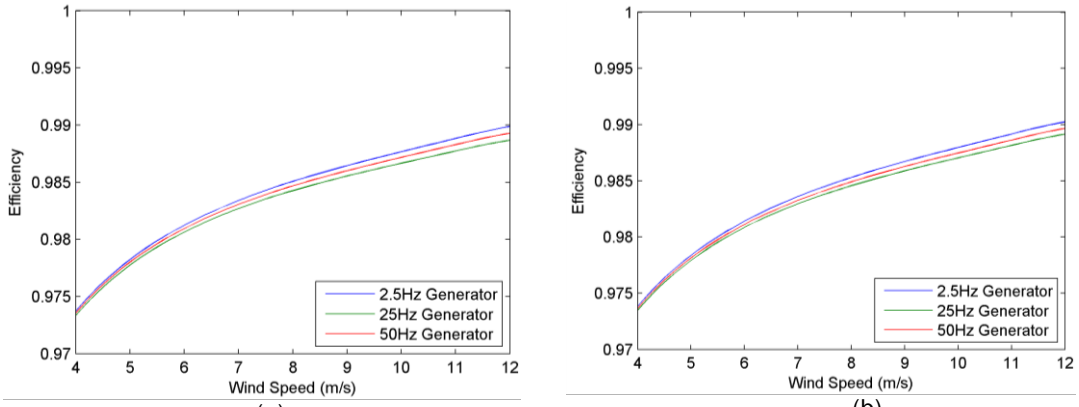

Figure 4-21 CSI-Actfilt Efficiency, (a) 10MW, (b) 20MW.

A comparison between the three converter topologies, for the 10MW 2.5Hz generator, is given in Figure . The CSI is less efficient than the others at all wind speeds, while the Boost-NPC is most efficient at low wind speeds and the CSI-Actfilt most efficienct at high wind speeds. This difference is mainly due to the high grid filter inductor losses in the Boost-NPC at high wind speeds, and the poor power factor of the CSI-Actfilt at low wind speeds leading to a higher compensating current in the active filter.

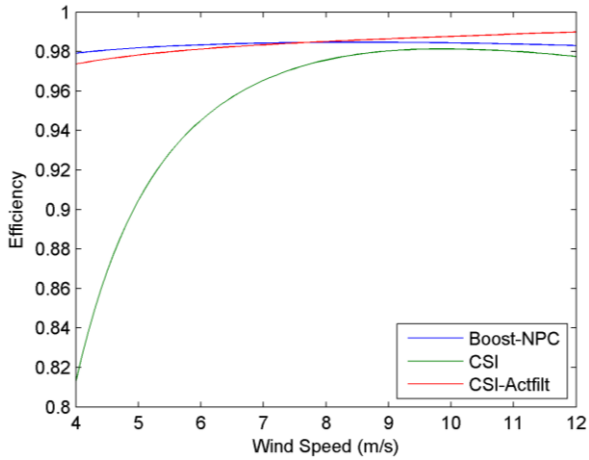

Figure 4-22 Efficiency comparison between converters, 10MW 2.5Hz.

4.4.2 Comparison of Losses

A breakdown of the losses by component for the different converters is shown in Figure for 10MW and Figure for 20MW. What is immediately apparent is the high loss for the CSI system with the 2.5Hz generator, which is due to the size of the DC inductor required to absorb the 6x generator frequency ripple. This ripple is absorbed in the Boost-NPC and CSI-Actfilt in the DC-link capacitors of the NPC converter and grid filter respectively, with significantly lower losses. For the higher frequency generators, the CSI has the lowest losses at rated power, due to the reduced component counts. The Boost-NPC system has high losses due to having both the boost and NPC converters switching at high frequency.

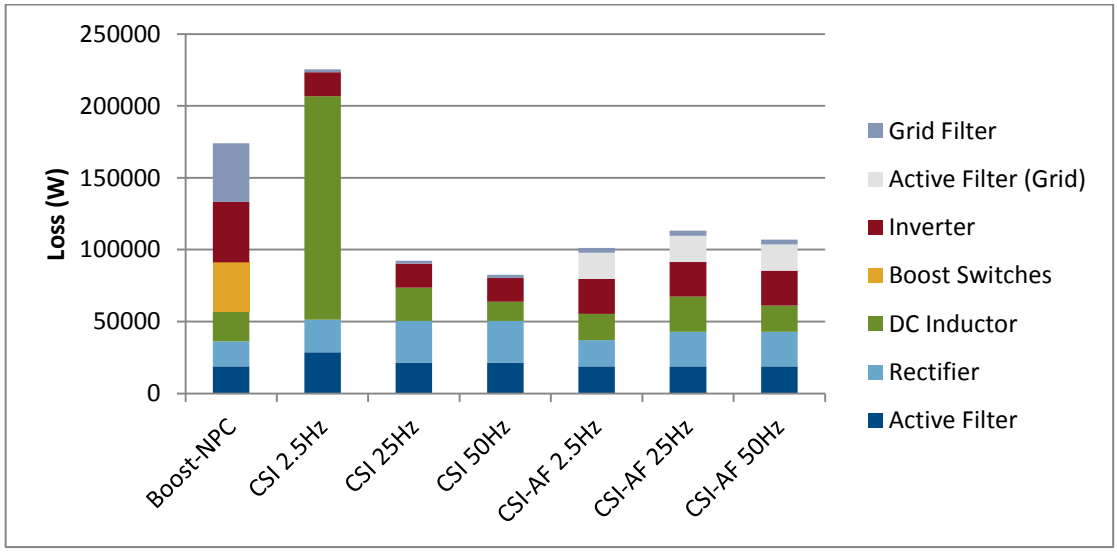

Figure 4-23 Loss comparison at rated power, 10MW converter.

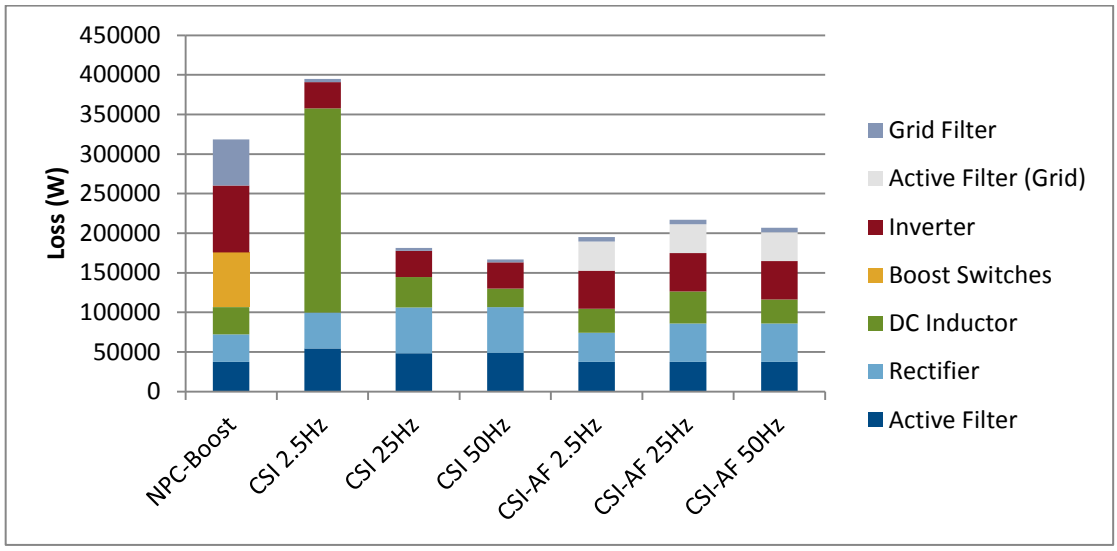

Figure 4-24 Loss comparison at rated power, 20MW converter.

The active filters have a relatively low loss, and potentially the components are over-rated – in this case they are rated at the peak filter current, which is around half the peak AC current, but the RMS current is only about a quarter of the AC RMS current in this type of converter[4-1]. In fact, the grid side active filter for the CSI-Actfilt has a lower loss than the passive filter on the Boost-NPC converter.

4.5 Calculation of Overall Cost

Peak losses are shown in Table **4-16**, and cooling system costs are calculated at €800 per kW (2.9 Appendix. A) of loss as with the other converters. The total cost is listed in Table **4-17**. In general, a low generator frequency increases the cost, due to the increased capacitor size requirement for the active filter. In the case of the CSI, a large DC inductor is required, significantly increasing the cost for 2.5Hz, with the higher losses also leading to an expensive cooling system. In general, the CSI with higher generator frequencies and the CSI-Actfilt have the lowest costs due to the higher efficiency and converter simplicity.

Table 4-16 Peak losses and cooling system cost.

Converter	Gen. Frequency	Peak Losses		Cooling System Cost	
		10MW	20MW	10MW	20MW
Boost-NPC	All	169,940W	296,670W	€135,952	€237,336
CSI	2.5Hz 25Hz 50Hz	225,416W 92,372W 82,411W	394,703W 181,530W 166,839W	€180,333 €73,898 €65,929	€315,763 €145,224 €133,471
CSI-Actfilt	2.5Hz 25Hz 50Hz	101,170W 113,140W 107,060W	194,920W 216,920W 206,700W	€80,936 €90,512 €85,648	€155,936 €173,536 €165,360

Table 4-17 Total converter system cost.

Converter	Gen. Frequency	Cost		Cost per kW	
		10MW	20MW	10MW	20MW
Boost-NPC	2.5Hz 25Hz 50Hz	€435,710 €352,466 €346,660	€787,655 €621,167 €609,554	€43.57 €35.25 €34.67	€39.38 €31.06 €30.48
CSI	2.5Hz 25Hz 50Hz	€563,168 €204,294 €177,930	€996,350 €384,673 €337,750	€56.32 €20.43 €17.79	€49.82 €19.23 €16.89
CSI-Actfilt	2.5Hz 25Hz 50Hz	€317,451 €254,637 €232,458	€610,791 €477,661 €440,804	€31.75 €25.46 €23.25	€30.54 €23.88 €22.04

A breakdown of the costs by subsystem is shown in Figure for 10MW and Figure for 20MW. What is immediately clear is that much of the cost of the CSI topology is made up of the cooling system, due to the low efficiency of this converter. Furthermore, with the 2.5Hz generator, the DC-link inductor also makes up a significant proportion of the cost. The Boost-NPC and CSI-Actfilt topologies make do with a smaller inductor by transferring the ripple to the DC-link capacitors in the NPC converter and grid side active filter respectively, with the capacitors representing a significantly lower cost for a given amount of energy storage.

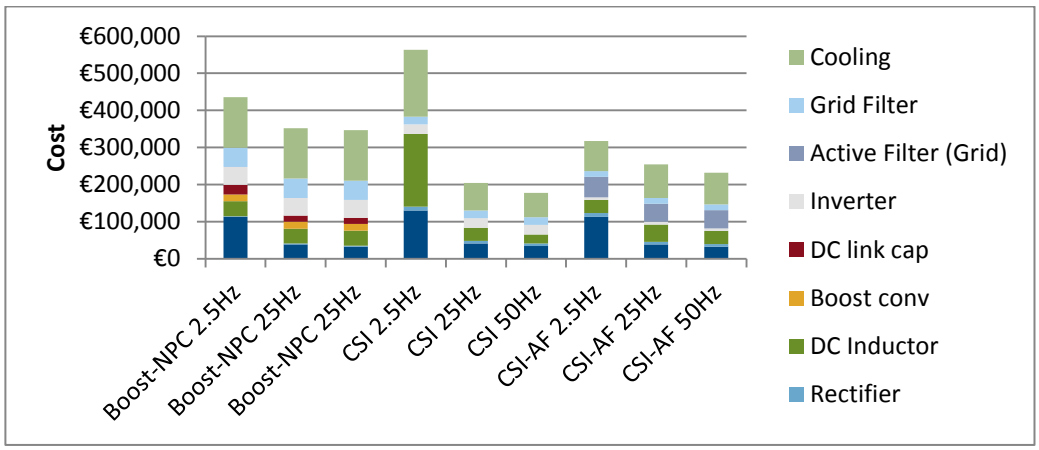

Figure 4-25 Breakdown of costs, 10MW.

For all converters, having a 2.5Hz generator significantly increases the cost of the active filter due to the increased capacitor size requirements. Most other components have a much smaller difference in cost between the 2.5Hz and higher frequency versions, with the exception of the DC inductor in the CSI topology. Overall the CSI topology has the lowest cost for higher frequency

(INNWIND. EU. Deliverable 3.32, Converter designs based on new components and modular multilevel topologies)

generators – this is due to the low losses, leading to a smaller cooling system, and the use of cheaper inverter components and a low component count. For the 2.5Hz generator, the CSI-Actfilt has the lowest cost, due to the reduced inductor size compared with the CSI and cheaper main inverter components compared with the Boost-NPC, which offset cost of a second active filter on the grid side.

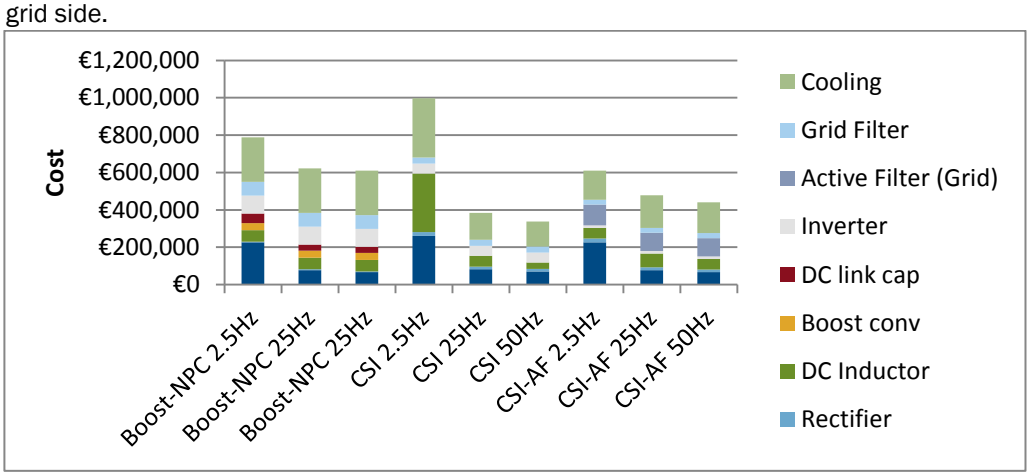

Figure 4-26 Breakdown of costs, 20MW.

4.6 Calculation of Size and Weight

All sizes are based around the need for the converter to fit into a cabinet 1200mm deep by 2450mm high, as used by the ABB PCS6000 medium voltage converter, with the cabinet length adjusted to fit the different components. Components such as the control system and cooling system were not included in the analysis and will add to the size and weight of the converters.

4.6.1 Active Filters

For the active filter, example modules were designed based on the sizes of capacitors and IGBTs, and a cabinet layout calculated. The capacitors are cylindrical, with a height of 150mm and a diameter of 100mm, and an additional 20mm is added to the height to allow for busbars and mounting hardware. The IGBTs are approximately 120mm square. Two types of module have been designed, shown in Figure , with the larger Type 1 used for the 2.5Hz generator where a large number of capacitors are used, and the smaller Type 2 used for the higher frequency applications. For these layouts, the Type 1 filter can have up to 72 capacitors and the Type 2 up to 18, but the number of columns, and hence the module depth, can be changed as necessary subject to the cabinet depth limitations.

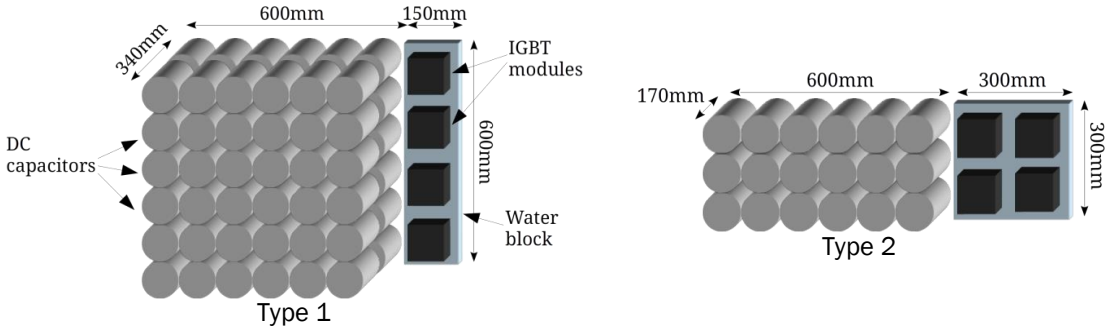

Figure 4-27 Module layouts for the active filters.

The module configurations are listed in Table **4-18**. Cabinet configurations were designed around this, with a clearance of 100mm between the modules and cabinet wall, and between the different phases. A clearance of 30mm was used between modules of the same phase. In total,

four configurations are used: Type 1 modules for 10 and 20MW, with 4 and 8 modules respectively, and Type 2 modules for 10 and 20MW, with 3 and 6 modules. These configurations and their size are shown in Figure .

Table 4-18 Module Configurations

Converter	Generator Frequency	Module Capacitors	Module Type	Capacitor Columns	Total Depth
Boost-NPC, CSI-Actfilt Gen. Side	2.5Hz 25Hz 50Hz	69 14 7	Type 1 Type 2 Type 2	6 5 3	750mm 800mm 600mm
CSI Gen. Side	2.5Hz 25Hz 50Hz	87 17 9	Type 1 Type 2 Type 2	8 6 3	950mm 900mm 600mm
CSI-Actfilt Grid Side	2.5Hz 25, 50Hz	21 13	Type 2 Type 2	7 5	1000mm 800mm

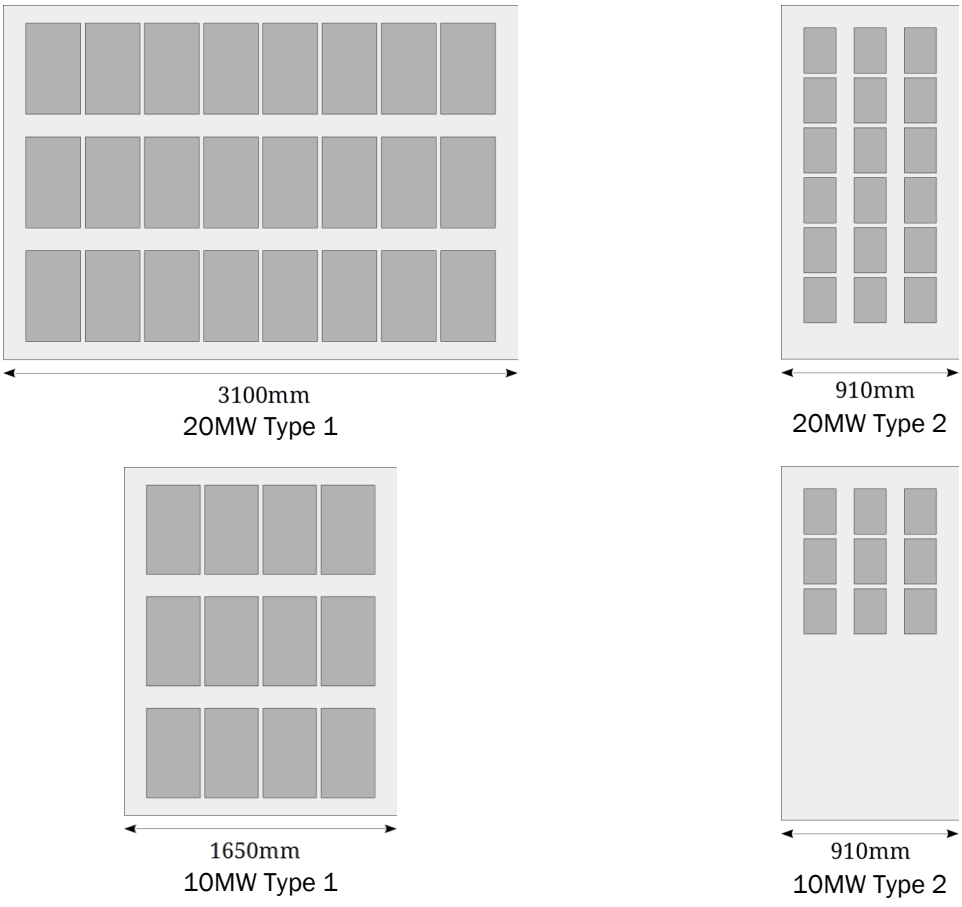

Figure 4-28 Active filter cabinet configurations.

Total mass is estimated by adding the masses of all the active components in the filter. From the datasheets, the IGBTs weigh 1300g each, while the capacitors weigh 1500g. A mass of 2kg has been estimated for the water block. The module and total masses are given in Table **4-19**.

Table 4-19 Active filter module and total weights.

Converter	Generator Frequency	Module Capacitors	Module Mass (kg)	Total Mass (kg)	
				10MW	20MW
Boost-NPC, CSI-Actfilt Gen. Side	2.5Hz 25Hz 50Hz	69 14 7	110.7 28.2 17.1	1,328 254 154	2,657 508 308
CSI Gen. Side	2.5Hz 25Hz 50Hz	87 17 9	137.7 32.7 20.7	1,652 294 186	3,305 589 373
CSI-Actfilt Grid Side	2.5Hz 25, 50Hz	21 13	38.7 26.7	348 240	697 481

4.6.2 Main Switching Devices and DC Links

The main switching devices are arranged in stacks, sandwiched between water blocks, which is similar to the system used in the ABB PCS6000 converter shown in Figure . In this converter, 12 IGCTs and the associated diodes are stacked, with the DC-link capacitors underneath, and the total width of this section is around 1m. The Boost-NPC converter, using IGCTs in a similar configuration, will have a cabinet width of around 1m for the NPC converter for 10MW. For 20MW the number of IGCTs will double, and a cabinet width of 2m will be necessary.

The boost inductors are 800mm and 940mm wide, according to Table **4-11**, giving a cabinet width of 1000mm and 1140mm with 100mm clearance, and the boost IGCTs will be able to fit above them. The passive rectifier will require 1 stack of 12 devices for 10MW and 1 stack of 24 devices for 20MW, which will be around 600mm and 1200mm high respectively. A width of 500mm will be allowed for the rectifier.

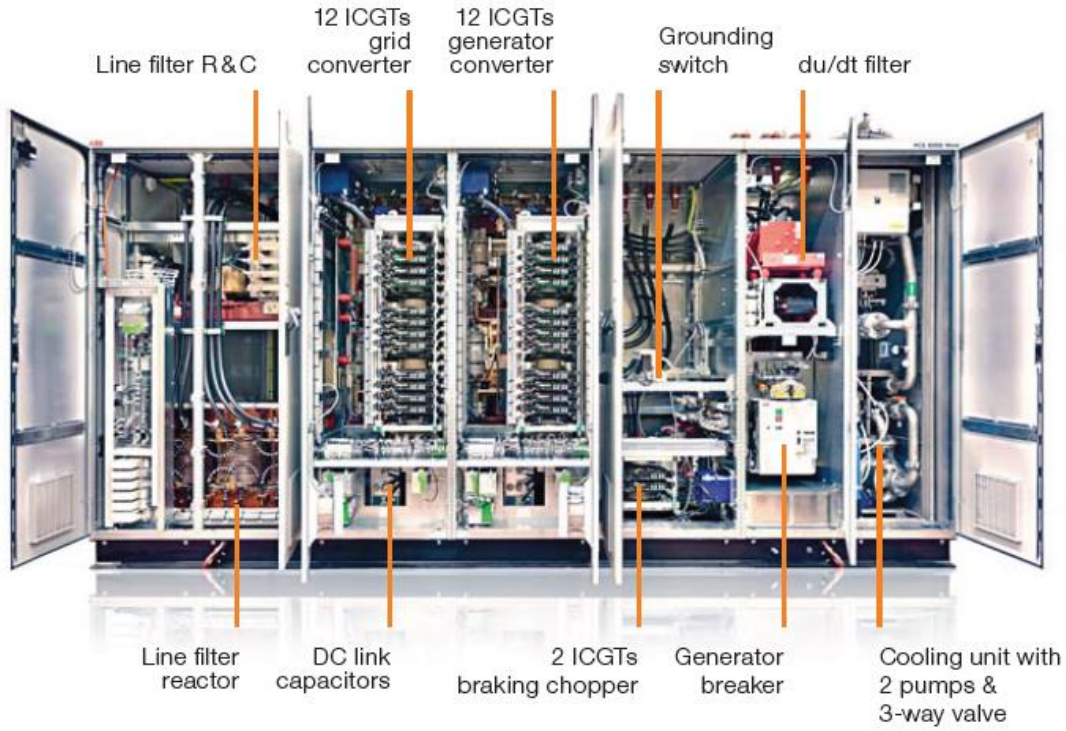

Figure 4-29 ABB PCS6000 cabinet layout [4-11].

A typical current-source inverter is shown in **Error! Reference source not found.**, and the current-source topologies will be based on the same stack arrangement, with 12 devices on a stack and a total width per stack of around 1m including snubbers.

The 10 and 20MW converters, using 12 and 24 IGCTs in the inverter respectively, will use 1 and 2 stacks of 12, and each stack will have a total width of 1m to allow space for snubbers, giving an inverter width of 1m and 2m. The rectifiers have 12 and 24 devices, giving widths of 1 and 2m. The space taken up by the DC inductor is found by taking the inductor width from Table **4-11** and adding 100mm clearance to each side.

The CSI-Actfilt uses 24 or 48 devices in total for 10MW and 20MW, which will be arranged into two or four stacks of 12 devices. Again a total width of 1m will be allowed per stack to provide space for snubbers.

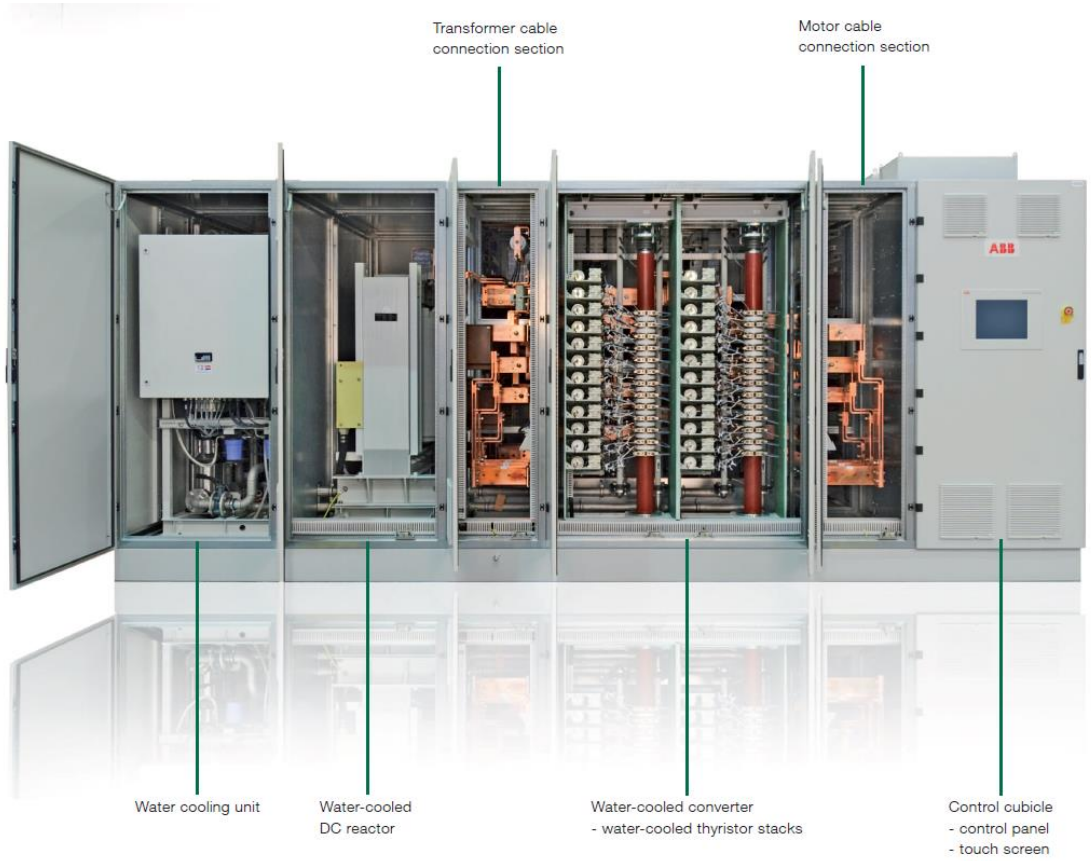

Figure 4-30 ABB Megadrive LCI cabinet layout [4-12]

Inductor masses are given in Table **4-11**, and masses of the switching stacks are estimated by adding together the masses of the components and water blocks, using data from the manufacturer [4-10], and doubling them to take account of the weight of the clamping system and busbars. The IGCT has a mass of 2.9kg and the high speed diode 1.45kg. The smaller thyristor has a mass of 1kg, the larger one 1.7kg, and the diode 530g. A suitable aluminium water block has a mass of 500g. The total mass for the switching device assemblies is given in Table **4-20**.

Table 4-20 Switching device assembly masses.

Converter	Gen. Frequency	Mass (kg)	
		10MW	20MW
NPC-Boost	All	305	610

CSI	2.5Hz 25, 50Hz	134 118	269 236
CSI-Actfilt	2.5Hz 25, 50Hz	89 72	178 144

The mass of the DC-link capacitors for the Boost-NPC converter is found by multiplying the number of capacitors given in Table 4-12 by the capacitor mass of 1.5kg, and the result is given in Table 4-21.

Table 4-21 NPC DC-Link capacitor mass.

Rating	Generator frequency	Number of Capacitors	Mass (kg)
10MW	2.5Hz	282	423
10MW	25, 50Hz	180	270
20MW	2.5Hz	564	846
20MW	25, 50Hz	360	540

4.6.3 AC Filters

The size of the AC filter will generally be determined by the width of the inductors, which are given in Table 4-14, plus the 100mm clearance on each side. The capacitors will be able to fit above the inductors. Total mass and filter width are given in Table 4-22 and are dominated by the inductor mass. For the 10MW CSI-Actfilt, the grid side active filter only takes up half of the cabinet height, so the inductor will be located in the bottom half and the cabinet width will be that necessary to accommodate the inductor.

Table 4-22 Grid filter size and mass.

Converter	Filter Width (m)	Mass (kg)		
		Inductor	Capacitors	Total
Boost-NPC 10MW Boost-NPC 20MW	1.75 1.95	2,523 3,565	13.5 54	2,537 3,619
CSI 10MW CSI 20MW	1.16 1.34	607 1,016	90 126	697 1,142
CSI-Actfilt 10MW CSI-Actfilt 20MW	1.24 1.43	754 1,275	0 0	754 1,275

4.7 Overall Size and Mass

Overall size and mass are given for all the converters and generator frequencies in Table 4-23. Sizes are similar for all converters, with the converters for the 2.5Hz generator having a slightly larger size due to the larger active filter. The CSI and CSI-Actfilt converters have a smaller size than the NPC, due to having fewer switching stages and devices in a more compact layout, allowing a more compact power stage. The CSI has the smallest size, except at 10MW and 2.5Hz where the large DC-link inductor adds size, due to the greater simplicity and lower component count.

Mass in all converters is dominated by the inductor mass, which results in a particularly high overall mass for the CSI when used with a 2.5Hz generator due to the size of the inductor. At higher generator frequencies the CSI actually has the lowest mass of all the topologies, as the grid filter design is based around having a small inductance and large capacitance. If converter mass is a key constraint, then it could be reduced in the NPC-Boost converter by reducing the grid filter inductance while increasing the capacitance. In the CSI-Actfilt, the grid filter inductance could be reduced by increasing the active filter switching frequency.

Table 4-23 Overall converter size and mass.

Converter	Generator Frequency	Total Cabinet Length (m)		Total Active Component Mass (kg)	
		10MW	20MW	10MW	20MW
NPC-Boost	2.5Hz	5.90	8.69	8,073	12,739
	25Hz	5.16	6.50	6,846	10,284
	50Hz	5.16	6.50	6,746	10,084
CSI	2.5Hz	6.13	9.97	15,637	24,364
	25Hz	5.03	7.37	4,220	6,651
	50Hz	4.92	7.21	3,203	4,861
CSI-Actfilt	2.5Hz	5.85	10.56	5,630	9,492
	25Hz	5.20	8.46	5,273	8,250
	50Hz	5.11	8.37	4,431	6,893

4.8 Conclusion

Three different converter topologies based on a diode or thyristor rectifier have been analysed. In order to meet the generator THD constraints, an active filter based on a cascaded multilevel inverter has been used. This allows an extremely low THD, but has a high DC-link capacitance requirement when used with the 2.5Hz generator, although this is lower than that required for a fully-rated MMC-type converter.

A significant problem with the diode or thyristor rectifier is the voltage ripple on the DC-link at 6 times the generator frequency. When a current-source inverter is used this must be absorbed by the DC-link inductor, requiring an extremely large inductor for the 2.5Hz generator, with high losses, a high cost and massive weight. Using a boost converter and voltage-source NPC inverter means that the ripple is absorbed by the DC-link capacitors, with considerably lower cost, losses and weight. If a CSI with an additional grid-side active filter is used, then the second active filter can also absorb this ripple.
For the higher generator frequencies, the PWM-switched CSI without active filter gives the highest efficiency at rated power, and lowest cost and size. However such a converter is difficult to recommend as the efficiency is low at lower wind speeds due to the requirement to supply reactive power to the large grid filter capacitors. The line-commutated CSI with grid-side active filter represents the lowest cost and mass for the 2.5Hz generator, while having a high efficiency over the turbine operating range for all frequencies, and this converter will be used in comparisons with the converters designed in the other chapters.

4.9 References

[4-1] A. Trznadlowski, F. Blaabjerg, J. Pedersen, N. Patriciu, “The Tandem Inverter: Combining the Advantages of Voltage-Source and Current-Source Inverters,” Proc. Thirteenth Annual Applied Power Electronics Conference and Exposition, APEC ’98, pp. 315-320, 1998.

[4-2] F. Peng, “Application Issues of Active Power Filters,” IEEE Industry Applications Magazine, 1998.

[4-3] F. Peng, J. McKeever, D. Adams, “A Power Line Conditioner Using Cascade Multilevel Inverters for Distribution Systems,” IEEE Trans. Indust. Appl., Vol. 34 (6), pp. 1293-1298, 1998.

[4-4] H. Sepahvand, J. Liao, M. Ferdowsi, “Investigation on Capacitor Voltage Regulation in Cascaded H-Bridge Multilevel Converters With Fundamental Frequency Switching”, IEEE Trans. Indust. Elec., Vol. 58 (11), pp. 5102-5111, 2011.

[4-5] J. Leon, S. Kouro, S. Vazquez, R. Portillo, L. Franquelo, J. Carrasco, J. Rodriguez, “Multidimensional Modulation Technique for Cascaded Multilevel Converters,” IEEE Trans. Indust. Elec., Vol. 58 (2), pp. 412-420, 2011.

[4-6] N. Mohan, T. Undeland, W. Robbins, “Power Electronics: Converters, Applications and Design,” John Wiley & Sons, Inc., 2003.
[4-7] B. Wu, “High Power Converters and AC Drives,” Wiley-Blackwell, 2006.
[4-8] H. Karshenas, H, Kojori, S. Dewan, “Generalized Techniques of Selective Harmonic Elimination and Current Control in Current Source Inverters/Converters,” IEEE Trans. Power Electr., Vol. 10 (5), pp. 566-573, 1995.
[4-9] Y. Li, “Control and Resonance Damping of Voltage-Source and Current-Source Converters With LC Filters,” IEEE Trans. Indust. Elec., Vol. 56 (5), pp. 1511-1521, 2009.
[4-10] IXYS Westcode Ltd. (http://www.westcode.com)
[4-11] ABB PCS6000 Wind data sheet, found at: http://www.abb.co.uk/product/seitp322/8cb6b0fde98c9ca6c1256dfa002bcda9.aspx
[4-12] ABB Megadrive LCI datasheet, found at: http://new.abb.com/drives/medium-voltage-ac-drives/megadrive-lci

5 COMPARISONS OF POWER CONVERTERS

Three types of power electronic converters with various configurations are investigated in applications of 10 and 20 MW wind turbine systems in this report including

- Voltage source type BTB converters
- Voltage source type AC/AC converters
- Current source type BTB converters

From Chapters 2-4, the P3L configuration, MMMC configuration, and CSI-Actfilt are respectively the best configuration for the above three type converters, therefore, are selected for the comparison among the different types. The basic parameters for the power converters are listed in Table 5-1 in the wind turbine system.

Table 5-1
Investigated Power Converters

Converter capacity P_n (MW)	AC voltage V_{ll} (kV)	Generator-side nominal AC frequency (Hz)	Grid-side nominal AC frequency (Hz)
10	3.3	2.5	50
20	6.6		
10	3.3	25	
20	6.6		
10	3.3	50	
20	6.6		

5.1 Comparisons of Cost

According to the above analysis, the detailed components and costs of the compared power converters with the different configurations are listed in Table 5-2, Table 5-4, and Table 5-5, respectively.

5.1.1 P3L-based BTB Power Converter

The P3L-based BTB power converter configuration is shown in Fig. 5-1 and the detailed information of the P3L-based BTB power converter is listed in Table 5-2.

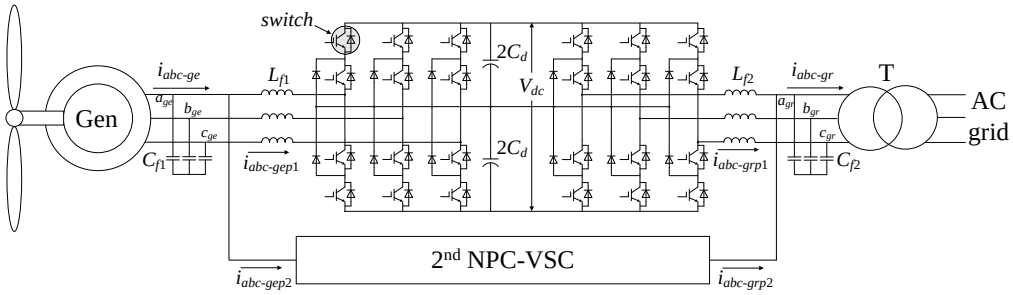

Fig. 5-1 Converter configuration of P3L-based BTB Power Converter.

Table 5-2
P3L-based BTB Power Converters

			2.5 Hz system		25 Hz system		50 Hz system	
Semiconductor	Basic parameters	Rated power (MW)	10	20	10	20	10	20
		AC voltage u_{abc_ge} and u_{abc_gr} (kV)	3.3	6.6	3.3	6.6	3.3	6.6
		AC current peak value i_{abc_ge} and i_{abc_gr} (kA)	2.47					
		Converter current peak value i_{abc_gep1} and i_{abc_gep2} and i_{abc_grp1} and i_{abc_grp2} (kA)	1.235					
		DC-link voltage V_{dc} (kV)	5.4	10.8	5.4	10.8	5.4	10.8
	Switch voltage and current	Switch nominal voltage (kV)	2.7	5.4	2.7	5.4	2.7	5.4
		Switch current with 2.5 RMS nominal value (kA)	2.2					
		Clamping diode nominal voltage (kV)	2.7	5.4	2.7	5.4	5.4	2.7
		Clamping diode current with 2.5 RMS nominal value (kA)	2.2					
	Device type	Switch device type and price	IGBT/DIODE FZ2400R17HP4 (1700V/2400A) 1055.68 €					
		Diode device type and price	DIODE DZ800S17K3 (1700V/800A) 133.83 €					
	Device number	Total IGBT number	144	288	144	288	144	288
		Total Diode number	216	432	216	432	216	432
	Costs	Total IGBT cost (k€)	152	304	152	304	152	304
		Total Diode cost (k€)	29	58	29	58	29	58
		Total semiconductor cost (k€)	181	362	181	362	181	362
Passive components	Generator-side filter	Inductor L_{f1} (mH)	1	2.3	1.5	2.3	2.2	3.5
		Capacitor C_{f1} (mF)	0.8	0.45	0.3	0.15	0.15	0.07
	Grid-side filter	Inductor L_{f2} (mH)	2.2	3.5	2.2	3.5	2.2	3.5
		Capacitor C_{f2} (mF)	0.15	0.07	0.15	0.07	0.15	0.07
	DC-link	Capacitor C_d (mF)	12.5	6.25	12.5	6.25	12.5	6.25
		Capacitor type and price	AVX FFLI6B3007KJE (3000uF/800V) 288.4 €					
		Capacitor number	528	812	528	812	528	812
	Costs	Filter inductor cost (k€)	115	209	133	209	158	252
		Filter Capacitor cost (k€)	11	25	5	11	4	7
		DC Capacitor cost (k€)	152	234	152	234	152	234
		Total passive components costs (k€)	278	468	290	454	314	493
Cooling system	Costs (k€)		143	306	144	317	147	304
Mechanical system	Costs (k€)		184	332	188	326	198	342
Total cost (k€)			786	1468	803	1459	840	1501

The reference price for the filter inductor and filter capacitance are listed below

Table 5-3
Reference Price for Filter

Filter	Type	Price (k€)
Three-phase filter inductor	0.33 mH/2.4 kA	16
	0.50 mH/1.2 kA	9
	0.26 mH/3.2 kA	22
Three-phase filter capacitor	150 uF/3 kV	1.8
	75 uF/6 kV	3.6

5.1.2 MMMC-based AC/AC Converter

The MMMC configuration is shown in Fig. 5-2 and the detailed information of the MMMC is listed in Table 5-4.

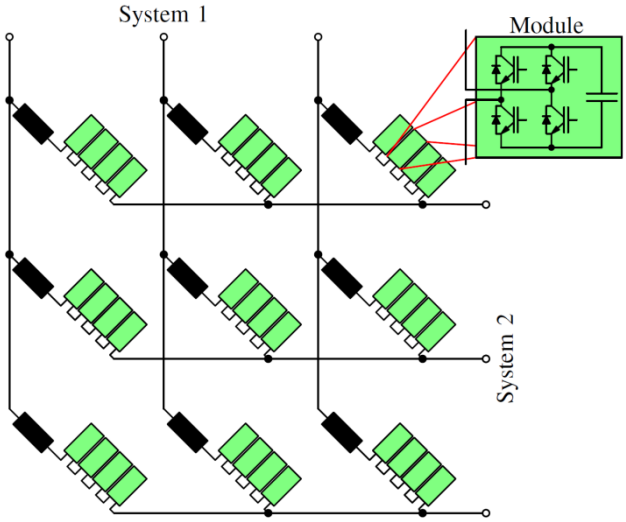

Fig. 5-2 Converter configuration of MMMC.

Table 5-4
MMMC-based AC/AC Converter

			2.5 Hz system		25 Hz system	
Semiconductor	Basic parameters	Rated power (MW)	10	20	10	20
		Voltage of systems 1 and 2 (kV)	3.3	6.6	3.3	6.6
		AC current peak value of systems 1 and 2 (kA)	2.47			
		Arm current peak value for 2.5 Hz (kA)	2.56		1.69	
		Maximum DC-link voltage in each module (kV)	1.1			
	Switch voltage and current	Switch nominal voltage (kV)	1.1			
		Switch current with 2.5 RMS nominal value for 2.5 Hz (kA)	2.38		2.13	
		Number of modules, 4 switches each	63	126	63	126
		Switch device type and price	IGBT/DIODE 1700V, see Fig. 3-16			
	Costs	Total semiconductor cost (k€)	262	524	243	486
Passive components	Arm inductor	Inductance (mH)	0.3	0.46	0.16	0.23
	Module capacitor	Capacity (mF)	31.7	20.6	31.7	20.6
	Costs	Total inductor (k€)	84	51	62	37
		Total capacitor cost (k€)	347	694	225	449
		Total passive components costs (k€)	431	745	287	486
Cooling system	Costs (k€)		129	258	137	274
Mechanical system	Costs (k€)		256	504	256	504
Total cost (k€)			1074	2032	919	1751

(INNWIND. EU. Deliverable 3.32, Converter designs based on new components and modular multilevel topologies)

5.1.3 CSI-Actfilt based Current Source Type Converter

The CSI-Actfilt configuration is shown in Fig. 5-3, with the active filter in Fig. 5-4 and the detailed information is listed in Table 5-5.

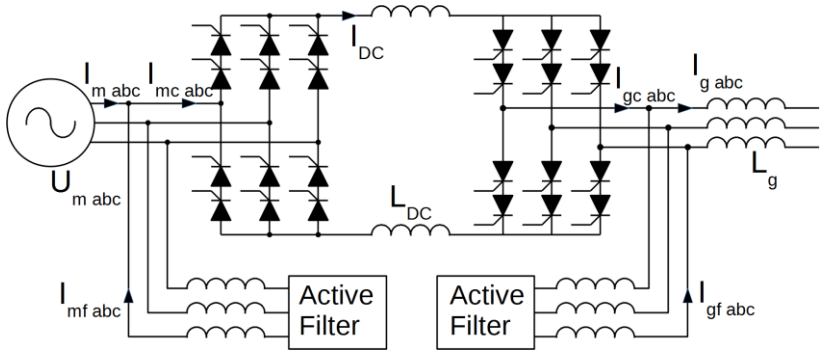

Fig. 5-3 Converter configuration of CSI-Actfilt.

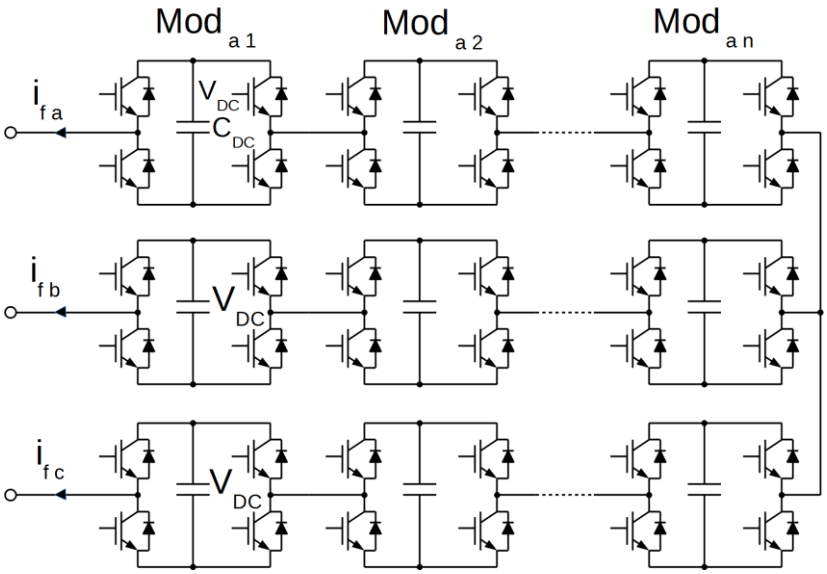

Fig. 5-4 Active filter configuration

Based on the analysis in Chapter 4, the CSI-Actfilt topology, based around a fundamental frequency switched current-source converter with active filters on both the generator and grid side is chosen. While the PWM current source converter has a lower cost and losses for the higher frequency generators at rated power, it has a higher cost for the 2.5Hz generator, and unacceptably high losses at low wind speeds. This is due to the PWM CSI having a large filter capacitance on the grid side, which consumes a constant level of reactive power at all wind speeds, which must be supplied from the converter for unity power factor operation, leading to a minimum DC current requirement resulting in significant losses when the wind speed is low. For the 2.5Hz generator, a large inductance is required for the CSI smooth the ripple from the generator rectifier at 6x the generator frequency, while in the CSI-Actfilt this ripple is transferred to the grid side active filter and absorbed in the filter DC-link capacitance.

Table 5-5
CSI-Actfilt Configuration-based Converters

			2.5 Hz system		25 Hz system		50 Hz system	
Semiconductor	Basic parameters	Rated power (MW)	10	20	10	20	10	20
		AC voltage (gen/grid) (kV)	3.3/3.5	6.6/7	3.3/3.5	6.6/7	3.3/3.5	6.6/7
		AC current i_{m_abc} (kA)	1.75					
		Active filter modules (gen/grid)	4/3	8/6	3/3	6/6	3/3	6/6
		Filtrt DC-link voltage V_{dc} (gen/grid) (kV)	0.85/ 0.95	0.85/ 0.95	0.85/ 0.85	0.85/ 0.85	0.85/ 0.85	0.85/ 0.85
		DC-link current I_{dc} (kA)	2.21					
	Switch voltage and current of Active - Filter	Switch nominal voltage (gen/grid) (V)	850/ 950	850/ 950	950/ 950	950/ 950	950/ 950	950/ 950
		Peak switch current (gen/grid) (kA)	1.58/1.90					
	Switch voltage and current – main converter	Switch nominal voltage (kV)	4.67	9.33	4.67	9.33	4.67	9.33
		Series switches	2	4	2	4	2	4
		Average Switch current (for rating purpose) (gen/grid)	2.2/ 0.74	2.2/ 0.74	0.74/ 0.74	0.74/ 0.74	0.74/ 0.74	0.74/ 0.74
	Device type	Switch device type and price of generator Active filter	IGBT/DIODE FZ1600R17HP4 (1700V/1600A) 762.29 €					
		Switch device type and price of grid active filter	IGBT/DIODE FZ2400R17HP4 (1700V/2400A) 1055.68 €					
		Switch device type and price of main converter 1	Thyristor K2359TD600 (6000V, 2359A) 870 €					
		Switch device type and price of main converter 2	Thyristor K1351VF600 (6000V, 1351A) 580 €					
	Device number	IGBT number (gen/grid)	48/36	96/72	36/36	72/72	36/36	72/72
		Thyristor number (Main converter 1/2)	12/12	24/24	0/24	0/48	0/24	0/48
	Costs	IGBT cost	75	149	65	131	65	131

(INNWIND. EU. Deliverable 3.32, Converter designs based on new components and modular multilevel topologies)

		(k€)						
		Thyristor cost (k€)	17	35	14	28	14	28
		Total semiconductor cost (k€)	92	184	79	159	79	159
Passive components	Grid-side filter	Inductor L_g (mH)	1.2	2.4	1.2	2.4	1.2	2.4
	DC-link – Generator-side Active Filter	Capacitor $C_{DC\,m}$ (mF)	439	878	66.8	133.6	33.4	66.8
		Capacitor type and price	AVX FFL16U0537K (530µF 1100V) 92.60 €					
		Capacitor number	828	1656	126	252	63	126
	DC-link – Grid-side Active Filter	Capacitor $C_{DC\,g}$ (mF)	100	200	62	124	62	124
		Capacitor type and price	AVX FFL16U0537K (530µF 1100V) 92.60 €					
		Capacitor number	189	378	117	234	117	234
	DC-link – main converter	Inductor L_{DC} (mH)	2.4	4.8	3.6	7.2	2.4	4.8
	Costs	Filter inductor cost (k€)	16	26	16	26	16	26
		DC capacitor cost cost (k€)	94	188	23	45	17	33
		DC inductor cost (k€)	35	57	47	74	35	57
		Total passive components costs (k€)	145	271	86	145	68	116
Cooling system	Costs (k€)		81	156	91	174	86	165
Mechanical system	Costs (k€)		87	185	66	122	59	110
Total cost (k€)			317	611	255	478	233	441

5.1.4 Conclusions

According to Tables 5-2 - Table 5-5, the total costs of each converter configuration is listed in Table 5-6.

Table 5-6
Total cost of different power converter

Converter type	Converter configuration	Total cost (k€)					
		2.5 Hz system		25 Hz system		50 Hz system	
		10 MW	20 MW	10 MW	20 MW	10 MW	20 MW
Voltage source type BTB	P3L	786	1468	803	1459	840	1501
Voltage source type AC/AC	MMMC	1074	2032	919	1751	-	
Current source type	CSI-Actfilt	317	611	255	478	233	441

It can be seen that the CSI-Actfilt converter has a reduced number of IGBTs compared with the other converter designs, as these only carry the filter current and not the full converter current. The converter uses thyristors for the main converter path, which are relatively cheap, making the semiconductor cost the lowest out of the converter designs. DC capacitance is high relative to the BTB converter, but low relative to the AC/AC converter, and inductance is also relatively low, and the smooth AC waveform means that like the AC/AC converter AC filter capacitors are not required. In addition, the use of bigger capacitance results in higher cost of the MMMC configuration. As a consequence, the CSI-Actfilt converter has the lower costs for the semiconductors and the passive components in comparison with the P3L configuration and the MMMC configuration, which results in the lower cost of the CSI-Actfilt converter, as shown in Table 5-6. The MMMC configuration has the highest costs among the three configurations.

5.2 Comparisons of Size and Weight

According to the above analysis, the sizes and weights of the power converters with the different configurations are listed in Table 5-7, respectively, where the P3L configuration has the smaller size in the 10 and 20 MW systems due to its compact arrangements in comparison with the MMMC and CSI-Actfilt configurations.

Table 5-7
Comparisons of Size and Weight

Power converters				Volume (m^3)	Weight (kg)
2.5 Hz	10MW	VSC-BTB	P3L	17.1	6411
		VSC-AC/AC	MMMC	19.2	8440
		Current source type	CSI-Actfilt	22.3	5630
	20MW	VSC-BTB	P3L	21.1	8522
		VSC-AC/AC	MMMC	32	12843
		Current source type	CSI-Actfilt	41.6	9492
25 Hz	10MW	VSC-BTB	P3L	17.1	6411
		VSC-AC/AC	MMMC	19.2	8440
		Current source type	CSI-Actfilt	20.6	5273
	20MW	VSC-BTB	P3L	21.1	8522
		VSC-AC/AC	MMMC	32.1	12843
		Current source type	CSI-Actfilt	34.6	8250
50 Hz	10MW	VSC-BTB	P3L	17.1	6411
		VSC-AC/AC	MMMC	-	-
		Current source type	CSI-Actfilt	20.3	4431
	20MW	VSC-BTB	P3L	21.1	8522
		VSC-AC/AC	MMMC	-	-
		Current source type	CSI-Actfilt	35.3	6893

5.3 Comparison of Efficiency

According to the above analysis, the efficiencies of the power converters with the different configurations at the rated power are listed in Table 5-8. It can be seen that the CSI-Actfilt configuration has a higher efficiency in comparison with the P3L and MMMC configurations, which

is partly due to the IGBTs of the active filters potentially being over-rated, and the lack of switching losses for the fundamentally-switched thyristors. This is in line with commercial products, for instance the ABB Megadrive LCI, a thyristor-based current-source converter, claims an efficiency of over 99% at rated power.

Table 5-8
Comparisons of Efficiency

Power converter			Converter configuration	Efficiency at rated power (%)
2.5 Hz	10 MW	VSC-BTB	P3L	98.2
		VSC-AC/AC	MMC	98.4
		Current source type	CSI-Actfilt	99.0
	20 MW	VSC-BTB	P3L	98.1
		VSC-AC/AC	MMC	98.4
		Current source type	CSI-Actfilt	99.0
25 Hz	10 MW	VSC-BTB	P3L	98.2
		VSC-AC/AC	MMC	98.3
		Current source type	CSI-Actfilt	98.9
	20 MW	VSC-BTB	P3L	98.1
		VSC-AC/AC	MMC	98.3
		Current source type	CSI-Actfilt	98.9
50 Hz	10 MW	VSC-BTB	P3L	98.16
		VSC-AC/AC	MMC	-
		Current source type	CSI-Actfilt	98.9
	20 MW	VSC-BTB	P3L	98.1
		VSC-AC/AC	MMC	-
		Current source type	CSI-Actfilt	99.0

5.4 Comparison of Reliability

According to the above analysis, the reliability feature of the power converters with the different configurations is shown in Table 5-9. The P3L configuration has two parallel converter units and the P3L can still work if some fault occurs to one converter unit. The MMMC configuration has extra modules, which can effectively increase system reliability. As to the CSI-Actfilt configuration, the extra module is used for the active filter to increase its reliability but not for the main converter. Redundancy can be included in the main converter by increasing the number of series thyristors, but this will increase the cost and losses. As a consequence, the P3L and MMMC configurations have a higher reliability in comparison with the CSI-Actfilt configuration. The Redundancy of the MMMC is much easier and cheaper achievable with the modular topologies than that of the P3L configuration.

Table 5-9
Reliability Analysis

Converter type	Converter configuration	Reliability
VSC-BTB	P3L	Fault tolerance with two converter units
VSC-AC/AC	MMC	Redundancy with extra modules
Current source type	CSI-Actfilt	Redundancy with extra active filter modules

5.5 Conclusions

According to above analysis, it can be observed that the CSI-Actfilt configuration has the lower cost and the higher efficiency in comparison with the P3L and MMMC configuration. The P3L configuration has the smaller size. Furthermore, the P3L and MMMC configuration have higher reliability than CSI-Actfilt configuration. In addition, the P3L configuration has lower costs and similar efficiency in comparison with the MMMC configurations.

In this comparative study, the requirements of grid operation are not considered, however, the solution has to meet the grid code requirements, such as reactive power regulation, voltage support, fault ride through etc. the performance of the power electronic systems will be further evaluated in these aspects in the subsequence work of the project.

Finally the cost estimates of the different converter designs of this report will be combined with the expected wind resource distribution of the INNWIND.EU turbines and the efficiency estimates to calculate the contribution to the Cost of Energy (CoE). This will be done in coordination with tasks on developing the new generator concepts.

It should be noted the results presented in this report are preliminary and need to be further investigated and proved.